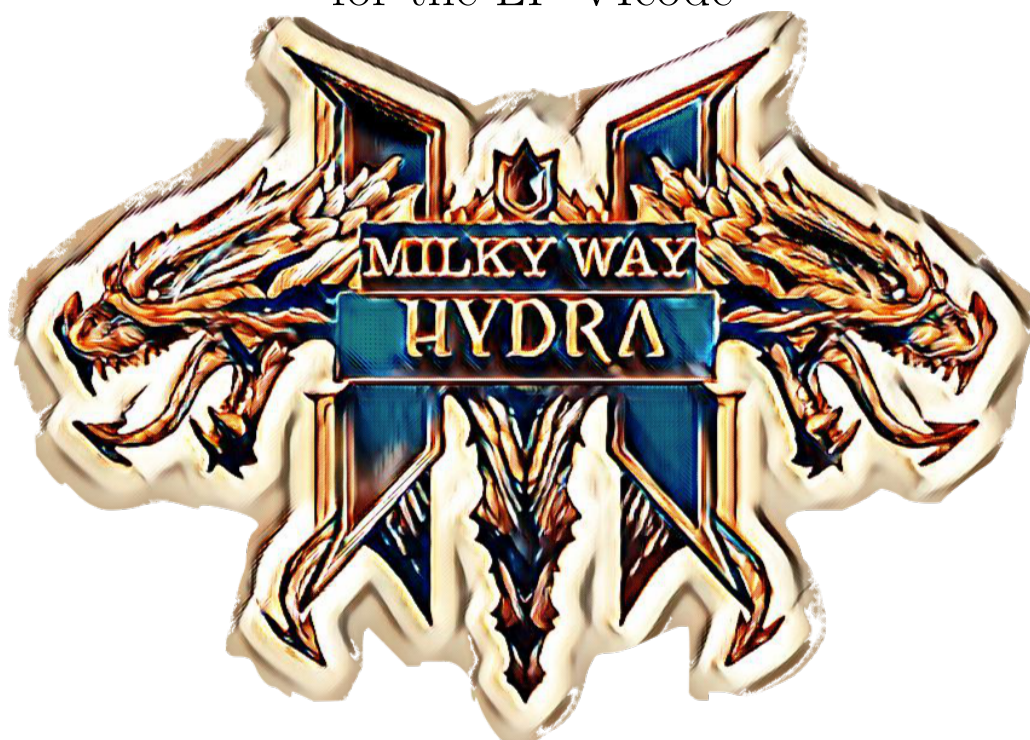# MilkyWayHydra 2.0
A ready-to-use Milky Way-type galaxy potential
Descriptive memory
for the LP-VIcode

Authors

N.P. Maffione, F.A. Gómez & D.D. Carpintero

Facultad de Ciencias Astronómicas y Geofísicas, UNLP, Argentina.
CITECCA, UNRN–Sede Andina, Argentina.
Instituto de Astrofísica de La Plata, UNLP–CONICET, Argentina.
Universidad de La Serena, Chile.

Last update: May 2021

The cover logo is a modified image taken from *Hydra,* the sixth studio album by Dutch symphonic metal band *Within Temptation.*

Contents

Chapter 1

Initiative: the `LP-VIsuite` project

The correct analysis of a given dynamical system rests on the reliable identification of the chaotic or regular behaviour of its orbits. The most commonly used tools for such analyses are based either on the study of the fundamental frequencies of the trajectories, or on the study of the evolution of the deviation vectors, the so–called variational chaos indicators (CIs hereafter). Therefore, it seems very useful to have a software with which one can compute several CIs in an easy and fast way. But, what a about the object to study? Galaxies, as probably the most complex stellar dynamical systems in near–field Cosmology, might be a suitable starting point. Then, besides the software to compute the CIs, a ready-to-use realistic galactic potential is also included in the package. This is the main goal of the `LP-VIsuite` (the acronym for *La Plata–Variational Indicators Suite*).

The current version of the `LP-VIsuite` is composed of three basic elements, (1) the suite's kernel code: the `LP-VIcode` (the acronym for *La Plata–Variational Indicators code*, v. 2.0.2 codename "`CONTROL`" [5, 3]); (2) the automatic differentiation pre-processing slave program: `SMART` (v. 1.2.3) and (3) a ready–to–use realistic Milky Way–type galaxy potential: `MilkyWayHydra` (v. 2.0).

Hereinafter we describe the last element of the `LP-VIsuite`, the galactic potential. For further information about the other elements of the suite, please visit the webpage of the project at:

http://www.fcaglp.unlp.edu.ar/LP-VIcode/

And for references related to the elements of the project, please visit the following:

The suite's kernel code: the `LP-VIcode`
Carpintero, D., Maffione, N. & Darriba, L. 2014, Astronomy and Computing, 5, 19-27. [3]

The suite's automatic differentiation pre-processing slave program: `SMART`
Carpintero, D. & Maffione, N. (submitted to Astronomy and Computing)

The suite's ready–to–use realistic Milky Way–type galaxy potential: `MilkyWayHydra`
Maffione, N., Gómez, F. & Carpintero, D. (in prep. 2021)

Chapter 2

Basics of the `MilkyWayHydra` **2.0**

2.1   Short presentation

The actual version of the `MilkyWayHydra` (`MWH` for short) is a ready–to–use analytical but exhaustively detailed (realistic) Milky Way–type galaxy potential. It comes in two flavours: the original or pre–`SMART` version which includes the accelerations and variational equations derived by hand, and the automatic or `SMART` version where both subroutines (i.e. `acelera` and `variac`[1]) are automatically computed (as the name indicates) in a pre-processing stage by the `SMART` code. The former performs much faster than the latter due to the fact that accelerations and first variationals are also efficiently coded.

Current version 2.0 of `MWH` describes a galactic potential with the following components:

- THE NUCLEAR REGION:
  A **nuclear star cluster** (NSC) with a **supermassive black hole** (SMBH) placed in its centre is described by a Plummer potential.

- THE PEANUT–SHAPED BULGE:
  The **bulge spheroid** is described by a Hernsquist profile and the **bar** by a three–dimensional cuadrupole.

- THE SPIRAL ARMS:
  The **spiral arms** are described by a N–armed spiral pattern outside of the bar region.

- THE DISK:
  The **disk** can be described by two profiles:

  1. a Miyamoto–Nagai (MN) profile,

  2. an exponential profile.

- THE DARK MATTER HALO:
  The **dark matter halo** (DMH) can be described by two models:

---

[1]Further details in the `LP-VIcode` manual, please find it at the official webpage of the project: `http://www.fcaglp.unlp.edu.ar/LP-VIcode/`

1. a bi-triaxial extension of the Navarro–Frenk–White (NFW) DMH,

2. a modified logarithmic DMH.

The potential is written in standard `Fortran77` following the rules specified by the suite's latest version of the kernel code: the `LP-VIcode`, and each of the galaxy components are clearly identify by using separated blocks (every block is fully commented).

The result is the original or pre-`SMART` version of the `milkywayhydra.pav` file, which includes the potential, the accelerations and the first variational equations ready to use with (exclusively) the `LP-VIcode`.

Early versions of the `milkywayhydra.pav` has been successfully used in the following peer reviewed papers: [17, 18, 19, 25, 12].

The `MWH` has been conceived mainly to represent late–type galaxies and, in particular, Milky Way–type galaxies. Nevertheless, it can be used to represent early–type galaxies as well, due to its straightforward programming style. This style of programming makes it easier for the user to add, remove or modify the galactic components as desired. Actually, it is very simple to build your own galaxy: the user will eliminate the galactic components (blocks in the code) that are not needed by given a null value to some key parameters (namely, the `ADD-REM` parameters which are described in Section C.6).

2.2   *The heads of the Hydra*

If not stated otherwise, the default values for the parameters of the `MWH` model were taken from the Aq–C4/C5 simulations introduced in [20], one of their most likely Milky Way–type galaxies, and the Auriga suite [13] (check their official website for further references at https://wwwmpa.mpa-garching.mpg.de/auriga/).

Furthermore, the "Sun" is placed at $(8,0,0)$, i.e. $8\,\mathrm{kpc}$ on the X–axis (long axis).

2.2.1   The nuclear region

The nuclear region is described by a Plummer sphere:

$$\Phi_{nuclear} = -\frac{G\,\mathrm{M}_{nuclear}}{\sqrt{x^2 + y^2 + z^2 + \epsilon_{nuclear}^2}},$$

where $\mathrm{M}_{nuclear}$ is the total mass of the nuclear region which includes the NSC and the mass of the SMBH, and $\epsilon_{nuclear}$ is the scale length of the system (softening parameter), which defines the outer limit of the inner core.

The default values of the parameters in the `MWH` are the following: the mass, $\mathrm{M}_{nuclear} = 2 \times 10^8\,\mathrm{M}_\odot$ and the softening parameter, $\epsilon_{nuclear} = 0.03\,\mathrm{kpc}$, being the latter taken from [14].
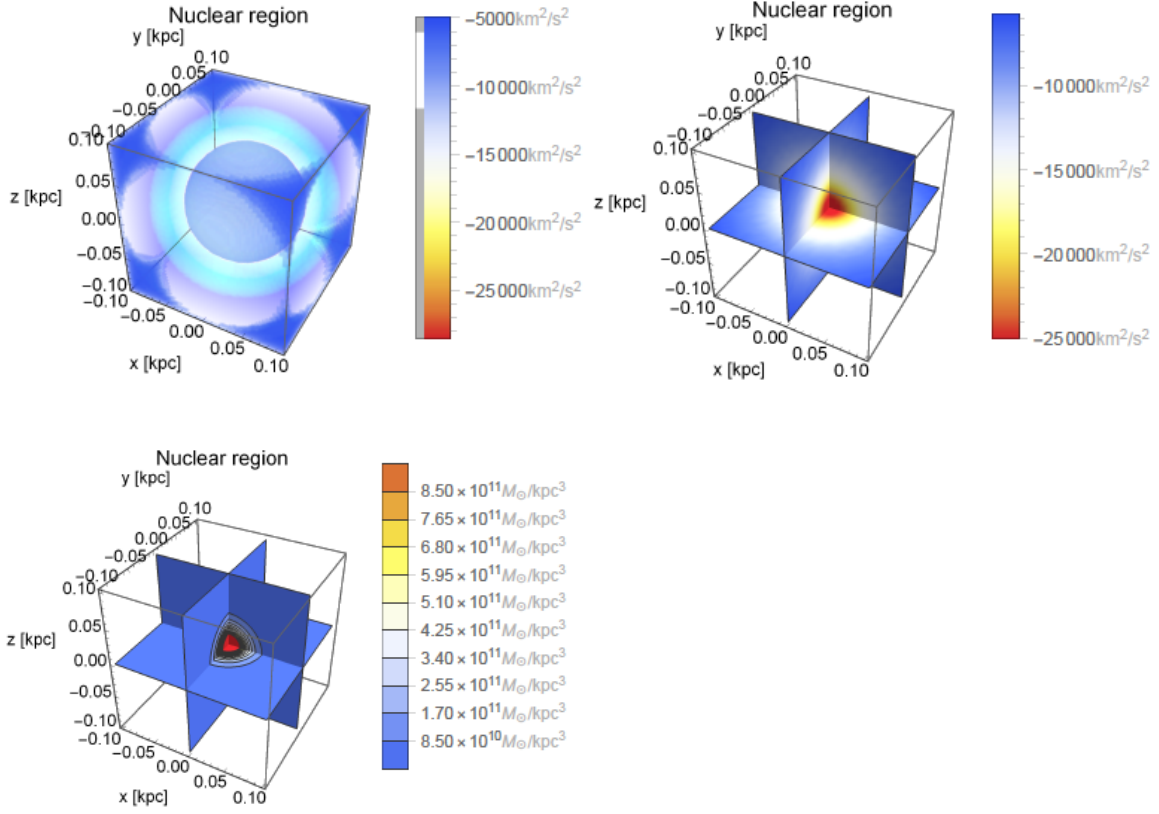
Figure 2.1: Potential–density pair for the nuclear region. Top panels: outside (left) and inside (right) potential views. Bottom panel: isodensities projected on the center planes. The region depicted is three times the scale length of the component.

In Fig. 2.1 we show the potential–density pair of our representation of the nuclear region. Top panels: the potential from an outside (left panel) and from an inside (projections on the center planes, right panel) viewpoint. Bottom panel: isodensities projected on the center planes are also depicted to give a global picture of the nuclear region component.

2.2.2 The peanut–shaped bulge

The abovementioned nuclear region dominates the most inner parts of the galaxy. On the other hand, the stellar bulge that we describe below, dominates the region between ~ 0.4 and $\sim 3\,\mathrm{kpc}$ [14].

2.2.2.1 The bulge spheroid

The bulge spheroid is described by the Hernquist profile:

$$\Phi_{bulge} = -\frac{G\,\mathrm{M}_{bulge}}{\sqrt{x^2 + y^2 + z^2} + \epsilon_{bulge}},$$
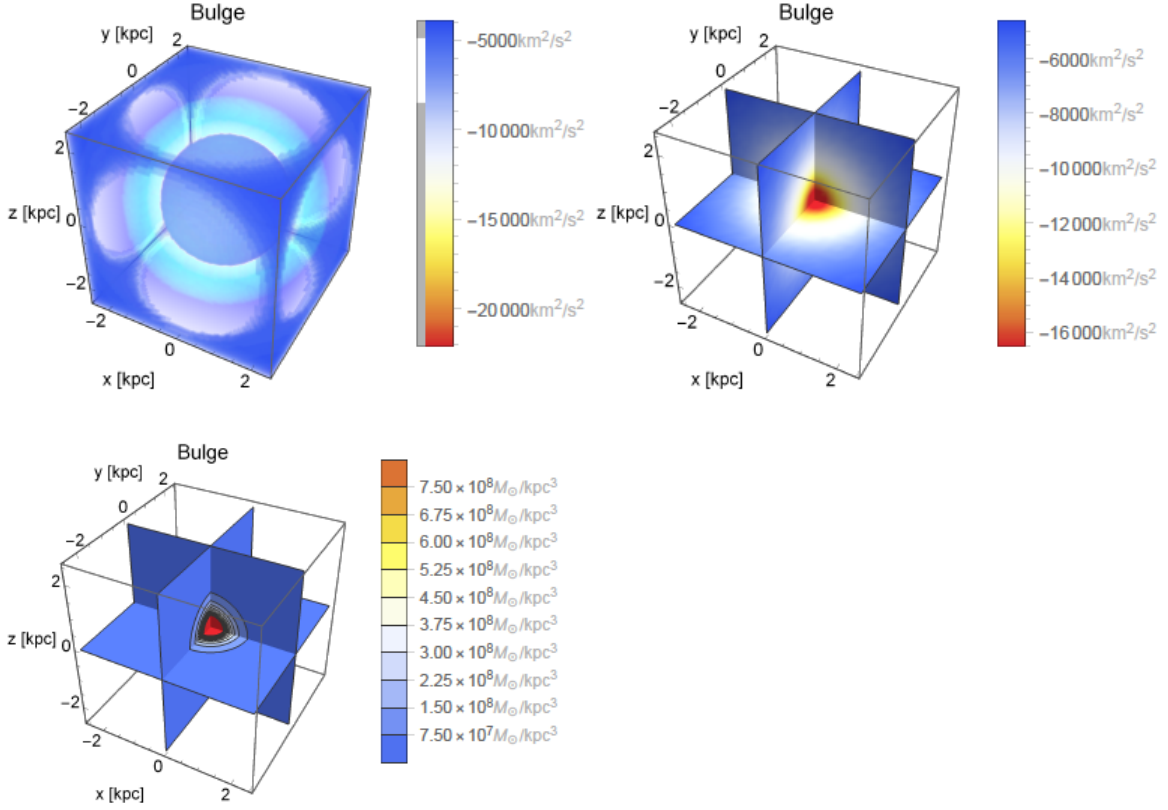
Figure 2.2: Potential–density pair for the bulge spheroid. Top panels: outside (left) and inside (right) potential views. Bottom panel: isodensities projected on the center planes. The region depicted is three times the scale length of the component.

where M_{bulge} is the mass, and ϵ_{bulge} is the scale length (or softening parameter).

The default values of the parameters in the MWH are the following: the mass, $M_{bulge} = 4.74 \times 10^9\,M_\odot$ and the softening parameter, $\epsilon_{bulge} = 0.835\,\mathrm{kpc}$.

In Fig. 2.2 we show the potential–density pair of our representation of the bulge spheroid. Top panels: the potential from an outside (left panel) and from an inside (projections on the center planes, right panel) viewpoint. Bottom panel: isodensities projected on the center planes are also depicted to give a global picture of the bulge spheroid component.

2.2.2.2   The bar

The following description of the bar [*in italics*] is taken from [22]: *The bar potential is a 3D version of the pure quadrupole model used by, e.g. Weinberg (1994) and Denhen (2000). It reads:*

$$\Phi_{bar}(R, \phi, z, t) = \alpha \frac{v_0^2}{3} \left(\frac{R_0}{R_b}\right)^3 U(r) \frac{R^2}{r^2} \cos(\gamma_b),$$

where $r^2 = R^2 + z^2$ is the spherical radius, R_b is the length of the bar, R_0 is the Galactocentric radius of the Sun, and v_0 is the circular velocity at R_0, $\gamma_b(\phi, t) \equiv 2\left(\phi - \phi_b - \Omega_b\, t\right)$, and

$$U(r) \equiv \begin{cases} -(r/R_b)^{-3} & \text{for} \quad r \geq R_b, \\[2em] (r/R_b)^3 - 2 & \text{for} \quad r < R_b. \end{cases}$$

The amplitude α is the ratio between the bar's and axisymmetric contribution to the radial force, along the bar's long axis at $(R, z) = (R_0, 0)$[2].

The default values of the parameters in the MWH are the following: $\alpha = 0.01$ as in [22], $\Omega_b = -52.2\,\mathrm{km\,s^{-1}kpc^{-1}}$ so that $\Omega_b/\Omega(R_0) = 1.89$[3] [1], $R_b = 3.5\,\mathrm{kpc}$, and ϕ_b is chosen such that at the end of the simulations: t_e[4], the bar major axis has a $-25°$ inclination w.r.t. the line connecting the Sun and the center of the Galaxy[5], i.e., $\phi_b + \Omega_b\, t_e = -25°$ [7], where t_e corresponds to the present time (i.e. the end of the simulations, as mentioned before)[6]. *The bar constructed in this way does not modify the Galaxy's total mass and circular velocity curve.* Finally we need to compute ϕ_b: $\phi_b + \Omega_b\, t_e = -25°$, which means $\phi_b - 52.2 \cdot 6.135 = \frac{67}{36}\pi$ where $[t_e] = \mathrm{u.t.}$ ($t_e = 6.135\,\mathrm{u.t.} = 6\,\mathrm{Gyr}$) and the angle units has been changed to rad ($-25° = \frac{67}{36}\pi$). Then $\phi_b = 5.65$. Furthermore, $\Omega_b = -52.2 \cdot 3.24078 \times 10^{-17} \cdot 3.15576 \times 10^{16} = -53.39$ in units of Gyr^{-1} ($1\,\mathrm{km} = 3.24078 \times 10^{-17}\,\mathrm{kpc}$ and $1\,\mathrm{Gyr} = 3.15576 \times 10^{16}\,\mathrm{s}$), then the bar pattern period is $\sim 117\,\mathrm{Myr}$ (or around $0.120\,\mathrm{u.t.}$).

In Fig. 2.3 we show the potential–density pair of our representation of the bar at the end of the simulations, $t_e = 6.135\,\mathrm{u.t.} = 6$ Gyr. Top panels: the potential from an outside (left panel) and from an inside (projections on the center planes, right panel) viewpoint. Bottom panel: isodensities projected on the center planes are also depicted to give a global picture of the bar component region. Notice the positive and negative regions in the density plot. The reason is that the bar pattern should always be used as a perturbation of a background potential.

In Fig. 2.4 we show the 1d potential along the positive X–axis ($\phi = z = 0$) for three different integration times: 0, 3 and 6 Gyr (in u.t.). No cosmological evolution is considered here for α, and the latter has the fixed value $\alpha = 0.01$ for every integration time, details in Section 2.4. Indeed, if we consider adiabatic growth, $\alpha(t) = \alpha \cdot \eta(t)$ and the potential at time $t = 0$ would be zero, due to the fact that the bar pattern would have null amplitude, i.e. $\alpha(0) = 0$. However, the other plots would remain the same because $\alpha(3.068) = \alpha(6.135) = 0.01$, i.e. α reaches its maximum at $t = 3\,\mathrm{Gyr}$ so $\alpha = 0.01$, and at the end of the simulation, $t = 6\,\mathrm{Gyr}$, we have $\alpha = 0.01$ again as if no cosmological evolution were considered in the first place (Section 2.4.1).

---

[2]See Section 2.4.1 for a fully time dependent description of this parameter.

[3]In [22], the authors use a positive velocity, but inhere we use a negative velocity to have a clockwise rotation pattern for the bar.

[4]In the simulations the final time is 6 Gyr, likewise in [22].

[5]In [22], the authors use a positive angle, but inhere we use a negative angle because following [7], the Sun's azimuth (w.r.t. the bar major semiaxis) has a value between $10°$ and $45°$, so the tilt angle of the bar w.r.t. the line connecting the Sun and the galactic center should be negative.

[6]The unit of time for t_e is u.t., see Section C.7 for further references on the unit system in the MWH.
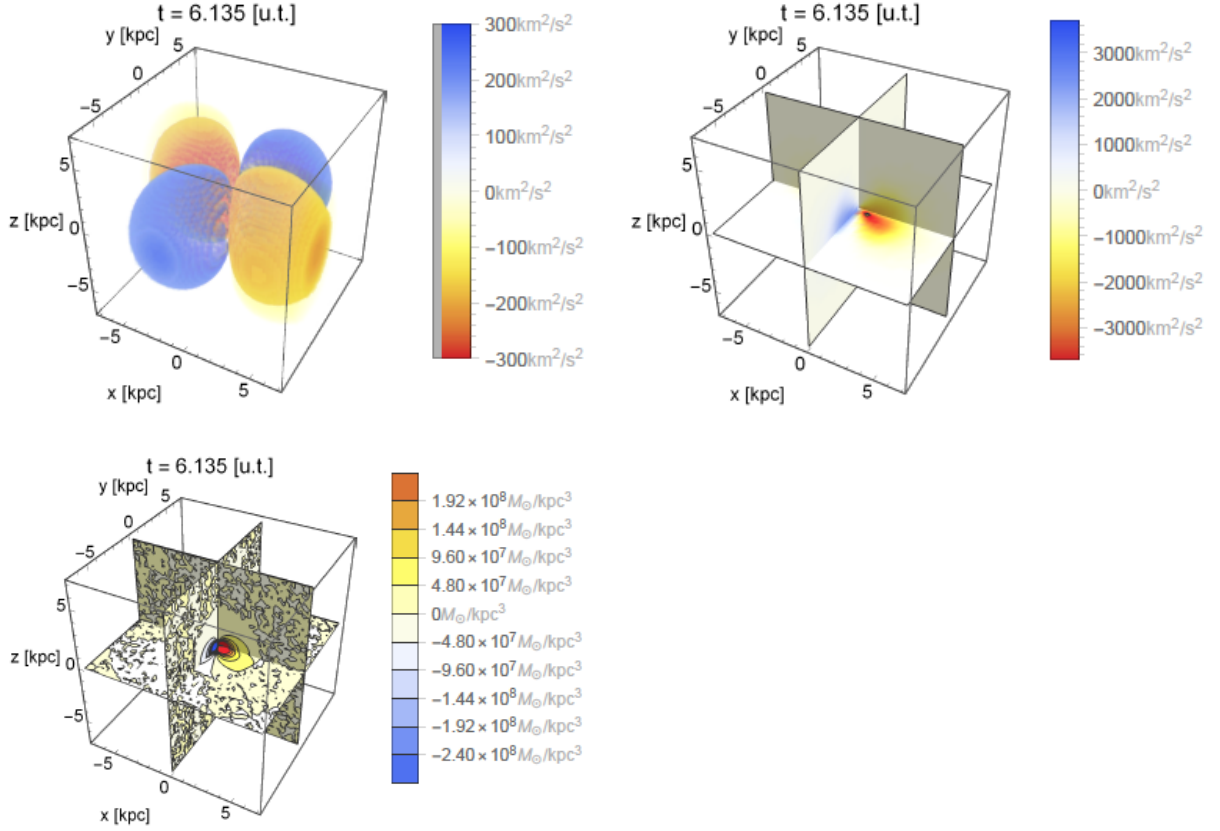
Figure 2.3: Potential–density pair for the bar. Top panels: outside (left) and inside (right) potential views. Bottom panel: isodensities projected on the center planes. The region depicted is two times the length of the bar R_b, i.e. ~ 7 kpc at each side.

Figure 2.4: 1d potential of the bar pattern along the positive X–axis ($\phi = z = 0$) for three different integration times (see text for details).

The representation of the bar is a pure cuadrupole, then it is a good approximation far away from the origin (multipolar expansion). However, there is consensus on that it is better to model the bar poorly than not modelled it at all. On behalf of this line of thinking we are keeping the same representation in the innermost part of the potential, without including any

exclusion parameter. We do otherwise in case of the spiral arms (see next section).

2.2.3 The spiral arms

The following description of the spiral arms using a N–armed potential is taken from [22] [*in italics*]: *It could be that the Galaxy's spiral pattern is composed of multiple modes with different pattern speeds (e.g. Quillen et al. 2011; Sellwood & Carlberg 2014), but observations indicate that the non–axisymmetric part of the old stellar component of the Milky Way disc is dominated by a two–armed spiral pattern outside of the bar region (namely, the Scutum– Centaurus and Perseus arms, Benjamin et al. 2005; Churchwell et al. 2009). Therefore, we consider a spiral perturbation consisting in a two–armed model, in the form originally proposed by Cox & Gómez (2002):*

$$\Phi_{spiral}(R, \phi, z, t) = -\frac{A}{R_s KD} \cdot e^{-\frac{(R-R_s)}{R_{sd}}} \cos(\gamma_s) \left[\text{sech}\left(\frac{Kz}{\beta} \right) \right]^{\beta},$$

where:

$$
\begin{cases}
K(R) = \frac{N}{R \sin(p)}, \\[2mm]
\beta(R) = K(R)h_s \left[1 + 0.4K(R)h_s \right], \\[2mm]
D(R) = \frac{1 + K(R)h_s + 0.3[K(R)h_s]^2}{1 + 0.3K(R)h_s} \\[2mm]
\gamma_s(R, \phi, t) = N \left[\phi - \phi_s - \Omega_s t - \frac{\ln(R/R_s)}{\tan(p)} \right].
\end{cases}
$$

Here, p *is the pitch angle,* A *the amplitude of the spiral potential[7], * h_s *controls the scale–height of the spiral, and* R_s *is the reference radius for the angle of the spirals.*

The default values of the parameters in the `MWH` are the following: $N = 2$ in order to have a two–armed spiral pattern (see further details on a generalization of this pattern at the end of this section), $R_s = 1\,\text{kpc}$, $R_{sd} = 3.124\,\text{kpc}$ (in agreement with the scale length of the stellar disk, see Section 2.2.4) and $\Omega_s = -18.9\,\text{km s}^{-1}\text{kpc}^{-1}$, $\phi_s + \Omega_s t_e = 26°$ and $p = 9.9°$ [2]. *Moreover, we specify two values for* A*: the first corresponds to a 30 per cent density contrast of the spiral arms w.r.t. the background disc surface density at* R_0 *('reference spirals',* A $= 341.8\,\text{km}^2\text{s}^{-2}$*), the second to a 60 per cent density contrast ('strong spirals',* A $= 683.7\,\text{km}^2\text{s}^{-2}$*). With these values of* A*, the spiral arms produce a maximum radial force of 0.5 per cent (reference spirals) and 1 per cent (strong spirals) of the force due to the axisymmetric background at* $R = R_0$*. We also use an amplitud that corresponds to a 200 per cent density contrast (super strong spirals),* A $= 2279\,\text{km}^2\text{s}^{-2}$ *in order to clearly see the spiral pattern perturbation (the latter being the default value in the* `MWH`*). Finally we need to compute* ϕ_s*:* $\phi_s + \Omega_s\,t_e = 26°$*, which means* $\phi_s - 18.9 \cdot 6.135 = 0.454$ *where* $[t_e] = \text{u.t.}$ *(*$t_e = 6.135\,\text{u.t.} = 6\,\text{Gyr}$*) and the angle units has been changed to rad (*$26° = 0.454$*). Then* $\phi_s = 3.31$*. Furthermore,* $\Omega_s = -18.9 \cdot 3.24078 \times 10^{-17} \cdot 3.15576 \times 10^{16} = -19.33$ *in units of*

---

[7]See Section 2.4.1 for a fully time dependent description of this parameter.
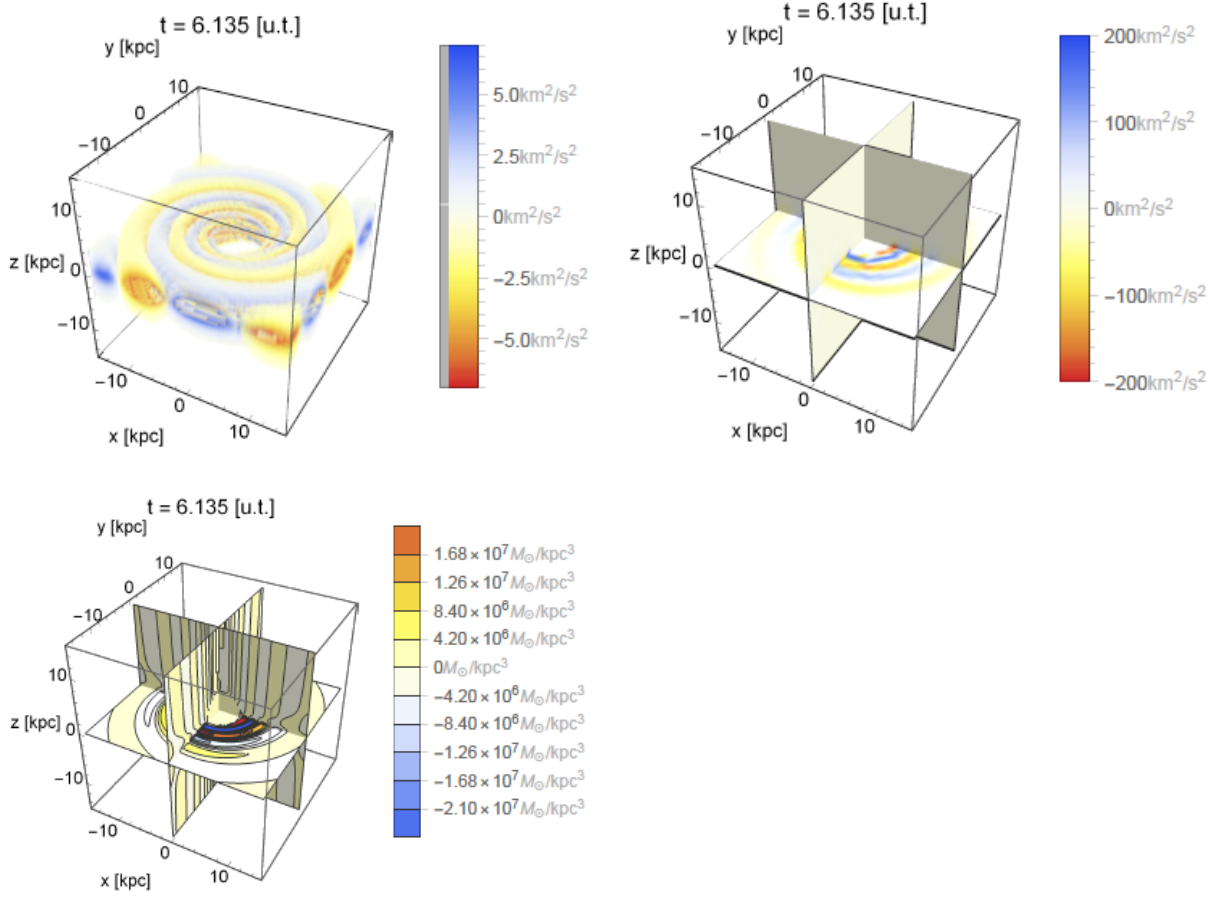
Figure 2.5: Potential–density pair for the spiral pattern outside the corrotation radius. Top panels: outside (left) and inside (right) potential views. Bottom panel: isodensities projected on the center planes. The region depicted is the usual extension of the Milky Way spiral arms (i.e. ~ 15 kpc at each side).

Gyr^{-1}, then the spiral pattern period is $\sim 330\,\mathrm{Myr}$ (or around $0.340\,\mathrm{u.t.}$).

In Fig. 2.5 we show the potential–density pair of our representation of the spiral arms ("super strong spirals", 200 per cent density contrast) at the end of the simulations, $t_e = 6.135\,\mathrm{u.t.} = 6$ Gyr. Top panels: the potential from an outside (left panel) and from an inside (projections on the center planes, right panel) viewpoint. Bottom panel: isodensities projected on the center planes are also depicted to give a global picture of the spiral arms component. The plots are truncated inside the corrotation radius (~ 4.08 kpc) because not only its representation is no longer adequate but also the spiral arms are a second–order perturbation in that region (see discussion below, and Fig. 2.7). Notice once again that there are positive and negative regions in the density plot. The reason is that the spiral pattern (like the bar pattern) should always be used as a perturbation of a background potential.

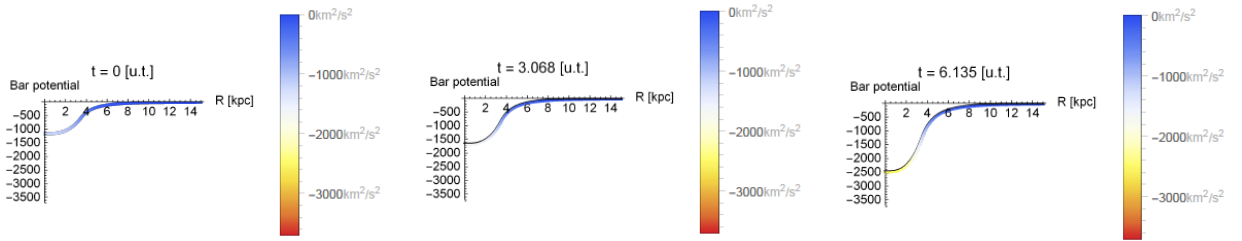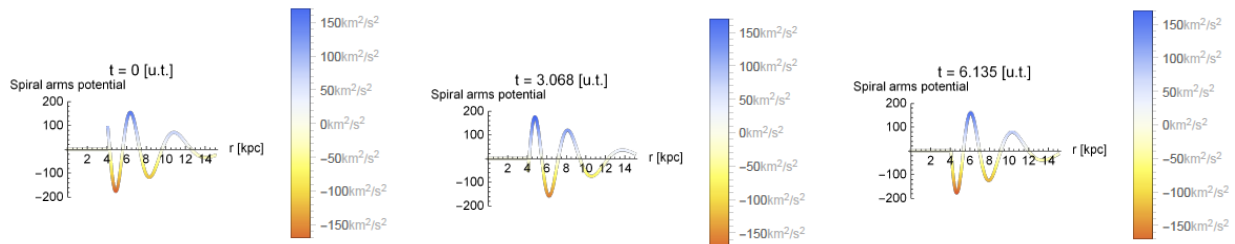Figure 2.6: 1d potential of the spiral pattern outside the corrotation zone and along the positive X–axis ($\phi = z = 0$) for three different integration times (see text for details).

In Fig. 2.6 we show the 1d potential along the positive X–axis ($\phi = z = 0$) for three different integration times: 0, 3 and 6 Gyr (in u.t.). No cosmological evolution is considered here for A, and the latter has the fixed value $A = 2279\,\mathrm{km^2 s^{-2}}$ for every integration time, details in Section 2.4. Indeed, if we consider adiabatic growth, $A(t) = A \cdot \eta(t)$ and the potential at time $t = 0$ would be zero, due to the fact that the spiral pattern would have null amplitude, i.e. $A(0) = 0\,\mathrm{km^2 s^{-2}}$. However, the other plots would remain the same because $A(3.068) = A(6.135) = 2279\,\mathrm{km^2 s^{-2}}$, i.e. A reaches its maximum at $t = 3\,\mathrm{Gyr}$ so $A = 2279\,\mathrm{km^2 s^{-2}}$, and at the end of the simulation, $t = 6\,\mathrm{Gyr}$, we have $A = 2279\,\mathrm{km^2 s^{-2}}$ again as if no cosmological evolution were considered in the first place (Section 2.4.1).

As mentioned before, the spiral arms representation is discarded inside the corrotation radius due to being poorly adequate for those inner locations, but also (and may be more important) because it is a second–order perturbation inside that region which is dominated by the bar[8]. Fig. 2.7 presents the potential of the spiral pattern ("super strong spirals", 200 per cent density contrast: left panels), bar pattern (middle panels) and the potential of both combined (right panels) in the region inside 3.5 kpc (the length of the bar). It is clear that the potential of the bar is the main perturber and then, the spiral arms can be safely neglected.

A generalized N–armed potential: the method to generalized our spiral pattern representation is the one explained in [4]. The user can add more modes by playing with the values of n and N in the series:

$$\Phi_{spiral}(R, \phi, z, t) = -\frac{A}{R_s} \cdot e^{-\frac{(R-R_s)}{R_{sd}}} \sum_n \frac{C_n}{K_n D_n} \cos(\gamma_n^s) \left[\mathrm{sech}\left(\frac{K_n z}{\beta_n}\right) \right]^{\beta_n},$$

where:

---

[8]Let us remind the reader that the bar is poorly represented by our model in the inner regions too, however the model is still used in such locations: the bar in the inner regions is still a first-order perturbation, so it is better to use such representation that not using anything at all. Situation changes here due to the fact that the spiral pattern is no longer a first-order but a second-order perturbation. See Fig. 2.7 and text below.
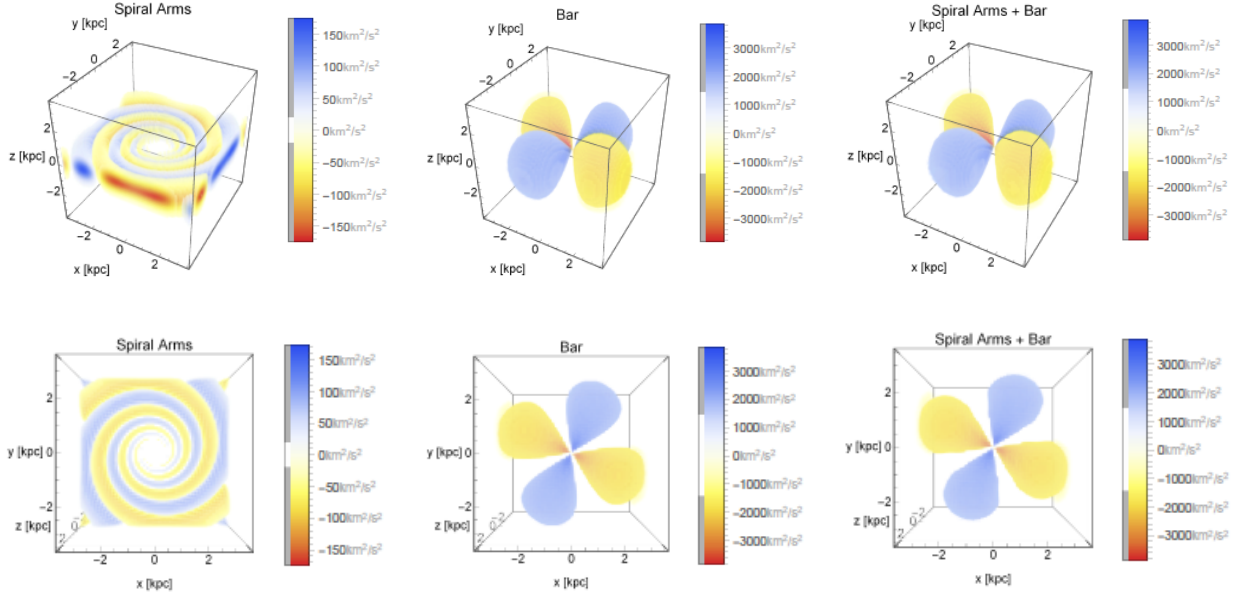
Figure 2.7: Potential of the spiral pattern (left panels), bar pattern (middle panels) and the potential of both combined (right panels) in the region inside 3.5 kpc (the length of the bar). Top and bottom panels show the potentials from different viewpoints (barely tilted to the front and from above, respectively).

$$
\begin{cases}
\mathrm{K}_n(R) = \frac{nN}{R\sin(\mathrm{p})}, \\[2mm]
\beta_n(R) = \mathrm{K}_n(R)\mathrm{h}_s\left[1 + 0.4\mathrm{K}_n(R)\mathrm{h}_s\right], \\[2mm]
\mathrm{D}_n(R) = \frac{1 + \mathrm{K}_n(R)\mathrm{h}_s + 0.3[\mathrm{K}_n(R)\mathrm{h}_s]^2}{1 + 0.3\mathrm{K}_n(R)\mathrm{h}_s} \\[2mm]
\gamma_n^s(R,\phi,t) = nN\left[\phi - \phi_s - \Omega_s t - \frac{\ln(R/\mathrm{R}_s)}{\tan(\mathrm{p})}\right].
\end{cases}
$$

and C_n are some coefficients. Notice, then, that the series is composed of terms which general expression is that of our previously described two–armed potential, with some minor changes (for instance, $2 \to N$). Then, all the first and second derivatives available in the `MWH` are the same for all those terms (albeit some constant), and the user can build a general N–armed potential with its equations of motion and first variational equations by simply (but carefully) adding those expressions.

2.2.4   The disk

The `MWH` offers two different options to represent the disk.

a) **Option (1): a Miyamoto–Nagai profile** offers analytical and fairly simple expressions for the first and second derivatives of the disk potential in order to compute the equations of motion as well as the first variational equations.

b) **Option (2): an exponential profile** for the mass distribution had to be avoided given that the resolution of the Poisson equation to obtain the potential, leads to Bessel functions and need to be integrated numerically. Instead, we used a combination of MN disks to build disk potentials with such exponential mass profiles (see [26]) and keep the analytical and rather simple form of the first and second derivatives at the same time.

2.2.4.1 Option (1): a MN profile

We first introduce the well–known MN disk potential:

$$\Phi_{disk} = -\frac{G\,M_{disk}}{\sqrt{x^2 + y^2 + \left(\epsilon_s + \sqrt{z^2 + \epsilon_h^2}\right)^2}},$$

where M_{disk} is its mass, and ϵ_s and ϵ_h are the scale length and scale height of the disk, respectively.

The default values of the parameters in the `MWH` are the following: the mass, $M_{disk} = 5.961 \times 10^{10}\,M_\odot$, $\epsilon_s = 3.124\,\text{kpc}$ and $\epsilon_h = 0.3\,\text{kpc}$, the scale length and scale height of the disk, respectively.

In Fig. 2.8 we show the potential–density pair of our representation of the MN disk.

Option (1) can be extended to be a two–component MN disk in a very easy way: the default MN disk that already appears in the `milkywayhydra.pav` file, should correspond to the thin (thick) disk profile, while another MN disk need to be added describing the thick (thin) disk profile. Then, the sum of both disks would correspond to a two–component (thin+thick) MN disk. Of course, it is necessary to add the blocks accounting for the first and second derivatives of the second MN disk in the corresponding subroutines of the `milkywayhydra.pav` file as well (just copy and paste the blocks of the first MN disk and change the labels in order to distinguish each MN disk block from the other).

2.2.4.2 Option (2): an exponential profile

Option (2) uses a combination of MN disks to build a double exponential mass profile for the disk, following the work of [26]. Therefore, the exponential disk has the density profile:

$$\rho(R, z) = \rho_0 \exp(-R/R_d) \exp(-|z|/h_z),$$

with R the radial coordinate on the plane, and where the double–exponential is described by the parameters ρ_0, R_d and h_z, which are the central density, the scale length and the scale height of the disk density profile, respectively.

In the following we are going to describe the thin and thick disks components in the framework of a two–component disk for the current option (2), which is a more delicate matter than for

Figure 2.8: Potential–density pair for the MN disk. Top panels: outside (left) and inside (right) potential views. Bottom panel: isodensities projected on the center planes. The region depicted is five times the scale length of the density profile.

option (1) (that is the reason why the two–component exponential disk is completely coded in the milkywayhydra.pav file).

2.2.4.2.1   The thin disk

The default values of the parameters representing a double–exponential density profile for the thin disk in the MWH are as follows: $M_{disk}^{thin} = 5.276 \times 10^{10}$ $M_\odot$ (88.5% of the single disk mass of the MN profile), $R_d^{thin} = 3.124$ kpc and $h_z^{thin} = 0.3$ kpc. Thus, we are applying the recipe of [26] to obtain the parameter values for the three MN disks which combination resemble the latter double–exponential profile:

First, we take the geometrical parameters of the density profile $R_d^{thin} = 3.124$ kpc and $h_z^{thin} = 0.3$ kpc and use (left panel of Fig. 5, [26]) the formula:

$$\epsilon_h^{thin}/R_d^{thin} = -0.269(h_z^{thin}/R_d^{thin})^3 + 1.080(h_z^{thin}/R_d^{thin})^2 + 1.092(h_z^{thin}/R_d^{thin}),$$

with $h_z^{thin}/R_d^{thin} = 0.09603073$ to find the scale height of the three MN disks: ϵ_h^{thin}. The result is $\epsilon_h^{thin} = 0.357969749$ kpc. Second, the ratio $\epsilon_h^{thin}/R_d^{thin} = 0.114586988$ is smaller than

1.35, so we use formula (7) with the coefficients of Table 2 from [26] (in order to have positive densities everywhere, i.e. it is not necessary to use it with a background potential) to obtain the scale parameters of the mass and scale lengths[9]:

```
M1 = 0.161020249
M2 = -5.76795197
M3 = 6.7217927


a1 = 0.560698032
a2 = 2.57529044
a3 = 2.24318123
```

Finally, the values for the three MN disks that build up the double exponential profile are:

$[\text{M1}\times \text{M}_{disk}^{thin}]$ $0.161020249 \times 5.276 \times 10^{10} \rightarrow \text{M1}_{disk}^{thin} = 0.849542834 \times 10^{10}$;

$[\text{M2}\times \text{M}_{disk}^{thin}]$ $-5.76795197 \times 5.276 \times 10^{10} \rightarrow \text{M2}_{disk}^{thin} = -30.43171459 \times 10^{10}$;

$[\text{M1}\times \text{M}_{disk}^{thin}]$ $6.7217927 \times 5.276 \times 10^{10} \rightarrow \text{M3}_{disk}^{thin} = 35.46417829 \times 10^{10}$;

$[\text{a1}\times \text{R}_d^{thin}]$ $0.560698032 \times 3.124 \rightarrow \epsilon_{s1}^{thin} = 1.751620652$;

$[\text{a2}\times \text{R}_d^{thin}]$ $2.57529044 \times 3.124 \rightarrow \epsilon_{s2}^{thin} = 8.045207335$;

$[\text{a3}\times \text{R}_d^{thin}]$ $2.24318123 \times 3.124 \rightarrow \epsilon_{s3}^{thin} = 7.007698163$.

Summary: the values of the parameters for the three MN disks that build up the double–exponential thin disk are the following: $\text{M1}_{disk}^{thin} = 0.849542834 \times 10^{10}\,\text{M}_\odot$ and $\epsilon_{s1}^{thin} = 1.751620652\,\text{kpc}$; $\text{M2}_{disk}^{thin} = -30.43171459 \times 10^{10}\,\text{M}_\odot$ and $\epsilon_{s2}^{thin} = 8.045207335\,\text{kpc}$; $\text{M3}_{disk}^{thin} = 35.46417829 \times 10^{10}\,\text{M}_\odot$ and $\epsilon_{s3}^{thin} = 7.007698163\,\text{kpc}$ and all of them with the same scale height given by $\epsilon_h^{thin} = 0.357969749\,\text{kpc}$. The fit produces 3MN models that match a radially exponential disc to < 1.0 per cent out to $4\text{R}_d^{thin} \sim 12.5\,\text{kpc}$ and $\lesssim 6.0$ per cent out to $10\text{R}_d^{thin} \sim 31.24\,\text{kpc}$ (see Figure 2 of [26], using $b/\text{R}_d = \epsilon_h^{thin}/\text{R}_d^{thin} = 0.114586988$)[10].

In Fig. 2.9 we show the potential–density pair of our representation of the thin disk.

2.2.4.2.2 The thick disk

The default values of the parameters representing a double–exponential density profile for the thick disk in the MWH are as follows: $\text{M}_{disk}^{thick} = 0.686 \times 10^{10}\,\text{M}_\odot$ (11.5% of the single disk mass of the MN profile), $\text{R}_d^{thick} = 3.124\,\text{kpc}$ and $\text{h}_z^{thick} = 1\,\text{kpc}$ (like [22]). As before, we apply the recipe of [26] to obtain the parameter values for the three MN disks that resemble the latter double–exponential profile (see Section 2.2.4.2.1 for further details on the process).

Summary: the values of the parameters for the three MN disks that build up the double–exponential thick disk are the following: $\text{M1}_{disk}^{thick} = 0.922758707 \times 10^9\,\text{M}_\odot$ and $\epsilon_{s1}^{thick} = 0.908485192\,\text{kpc}$; $\text{M2}_{disk}^{thick} = -39.22621231 \times 10^9\,\text{M}_\odot$ and $\epsilon_{s2}^{thick} = 7.026555501\,\text{kpc}$; $\text{M3}_{disk}^{thick} =$

---

[9]A user–friendly online webform is kindly provided by [26] to compute all these quantities, see http://astronomy.swin.edu.au/~cflynn/expmaker.php

[10]Accuracy matching can be improved for $> 10\text{R}_d^{thin}$ to values < 3.3 per cent if we allow the 3MN model to have negative densities in the outer parts. Being that the case, it must be used with a background potential, and the user should follow the specs of Table 1 and Figure 1 from [26] instead of Table 2 and Figure 2 as inhere.
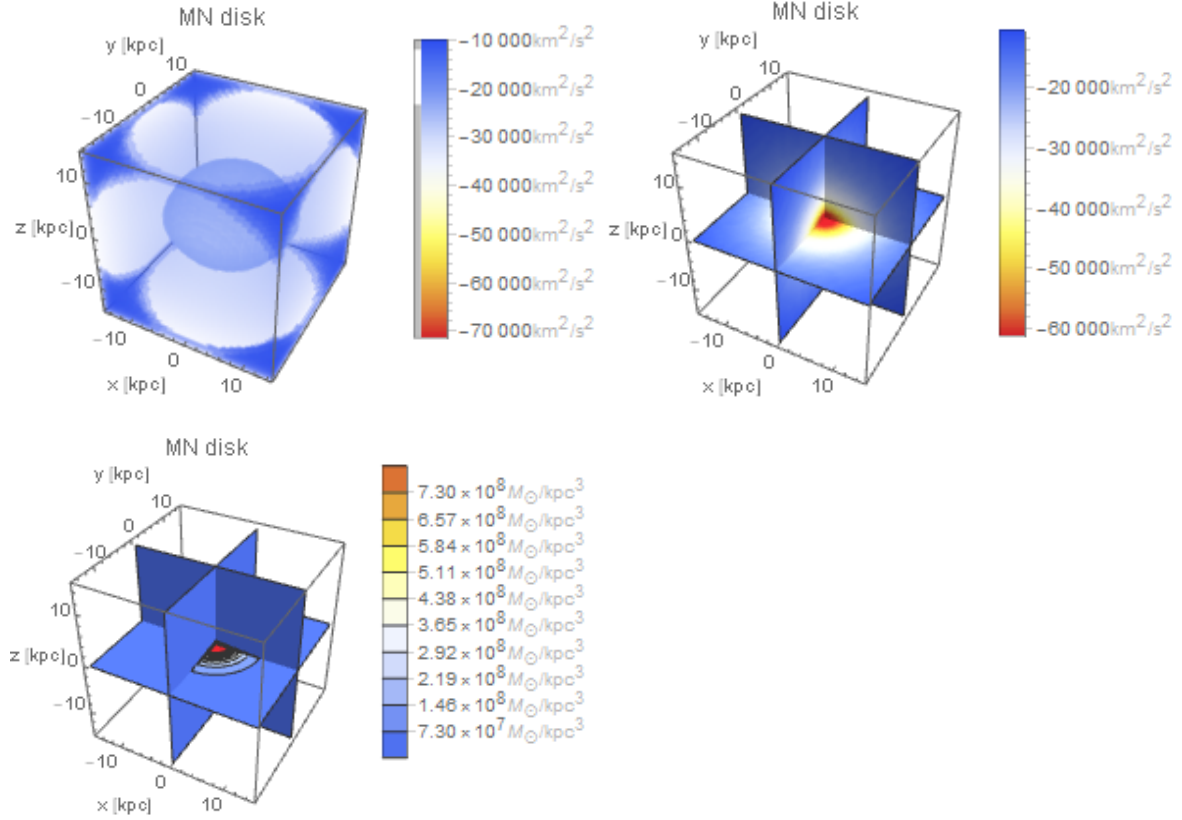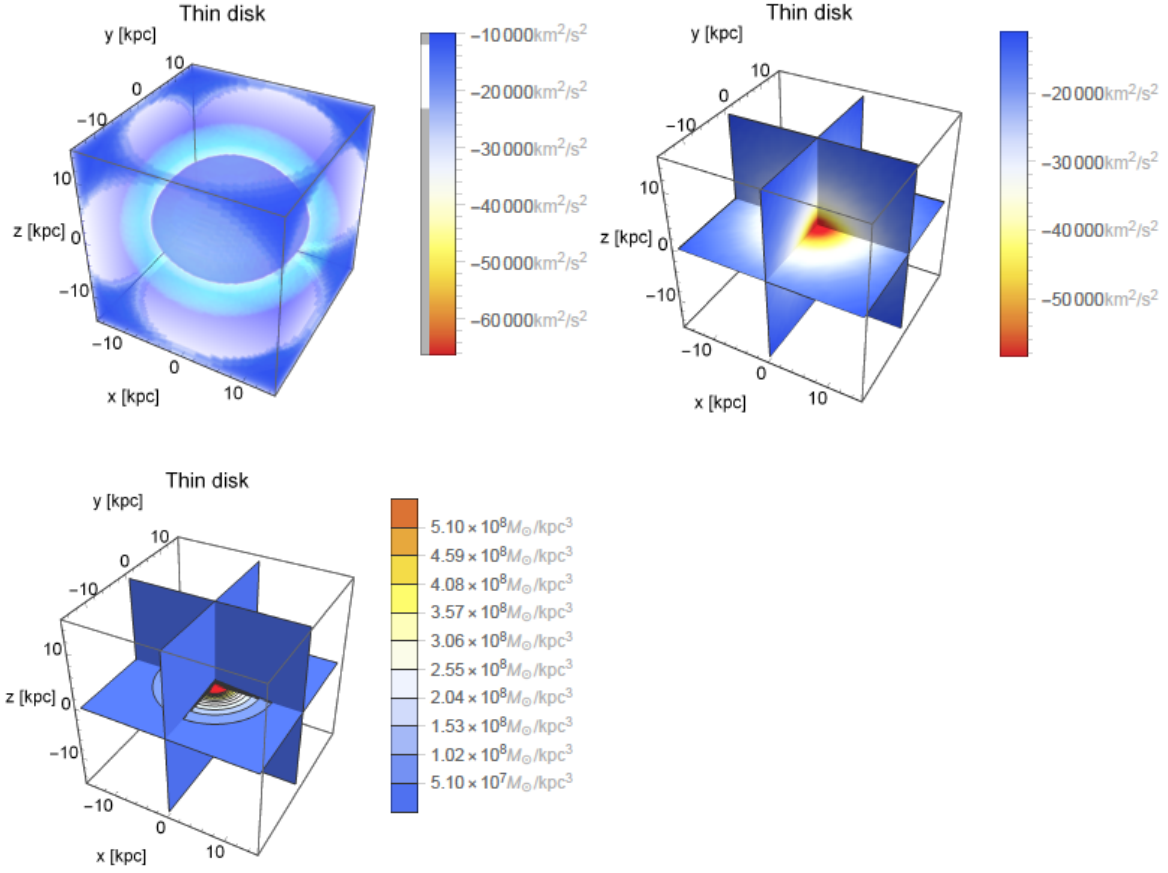
Figure 2.9: Potential–density pair for the thin disk. Top panels: outside (left) and inside (right) potential views. Bottom panel: isodensities projected on the center planes. The region depicted is five times the scale length of the density profile.

$46.18578795 \times 10^9 \, \mathrm{M_\odot}$ and $\epsilon_{s3}^{thick} = 6.213630283 \, \mathrm{kpc}$ and all of them with the same scale height given by $\epsilon_h^{thick} = 1.41014739 \, \mathrm{kpc}$. The fit produces 3MN models that match a radially exponential disc to < 1.0 per cent out to $4\mathrm{R}_d^{thin} \sim 12.5 \, \mathrm{kpc}$ and $\lesssim 7.0$ per cent out to $10\mathrm{R}_d^{thin} \sim 31.24 \, \mathrm{kpc}$ (see Figure 2 of [26], using $b/\mathrm{R}_d = \epsilon_h^{thin}/\mathrm{R}_d^{thin} = 0.45139161$)[11]

In Fig. 2.10 we show the potential–density pair of our representation of the thick disk.

Comment on the stellar halo

The stellar halo may be oblate and then, it can strengthen the chaotic effects given by the triaxiality of the dark matter halo [6]. However, its mass is $\sim 1\%$ of the stellar component of the galaxy. Then, for many studies its representation can be safely neglected and that is the main reason why the current version of the MWH does not have a stellar halo component: it

---

[11] Accuracy matching can be improved for $> 10\mathrm{R}_d^{thin}$ to values < 3.3 per cent if we allow the 3MN model to have negative densities in the outer parts. See footnote in Section 2.2.4.2.1.
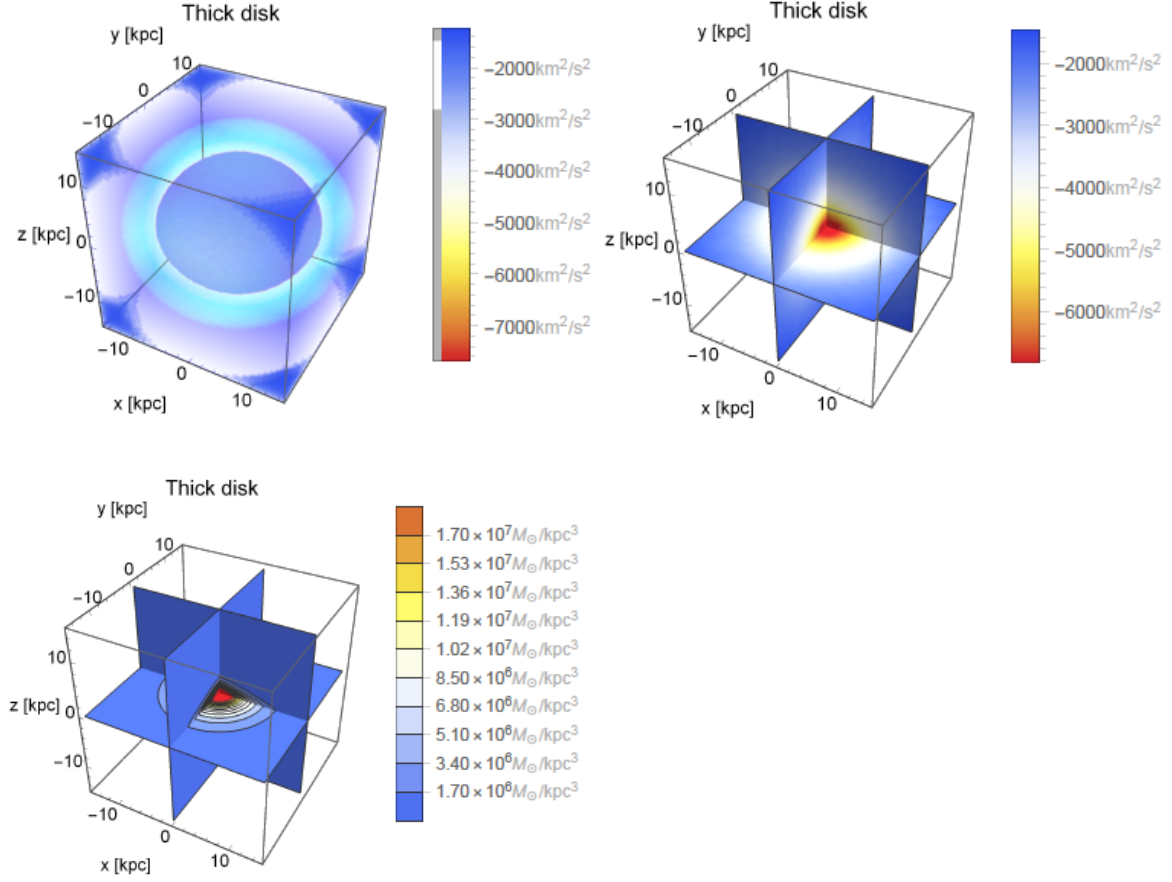
Figure 2.10: Potential–density pair for the thick disk. Top panels: outside (left) and inside (right) potential views. Bottom panel: isodensities projected on the center planes. The region depicted is five times the scale length of the density profile.

is not a priority component because it might be important just for a very particular line of research.

2.2.5 The dark matter halo

Finally, the hypothetical outermost galactic component: the DMH. The `MWH` offers two different options to represent such component.

a) **Option (1): a bi–triaxial extension of the NFW DMH** used in [28]. Vogelsberger et al. introduce a transition scale to have a triaxial profile (defined by an ellipsoidal radius) in the inner regions while leaving the outer regions round shaped as dark matter only simulations showed. In [19] we apply a second parameter to introduce triaxiality in the outer parts as well. The idea is to have an oblate profile in the inner regions due to the impact of baryonic matter, while leaving the outer regions mildly triaxial as hydrodynamic simulations show.

b) **Option (2): a modified logarithmic DMH** formerly used in [27]. The authors try to fit the observations of the Sagittarius Dwarf Galaxy [15] but at the same time guaranteeing a stable configuration for the disk. Therefore, they also use a transition scale to obtain an oblate (axisymmetric) shape in the inner parts (as hydrodynamic simulations suggest) and triaxial in the outer parts because of the effect of the Sagittarius Dwarf Galaxy orbit (and round shaped in the outermost regions).

2.2.5.1   Option (1): a bi–triaxial extension of the NFW profile

Option (1) is described by the following expression:

$$\Phi_{dmh} = -\frac{A_d}{r'} \ln\left[1 + \frac{r'}{r_s}\right],$$

where $A_d = \frac{G\,M_{200}}{\ln(1+c_{\mathrm{nfw}}) - \frac{c_{\mathrm{nfw}}}{1+c_{\mathrm{nfw}}}}$ and $r' = \frac{(r_s+r_{oe})}{r_s+r_{ie}}r_{ie}$ the modified scale radius adapted from [28]. Furthermore, $r_{ie}^2 = \frac{x^2}{a^2} + \frac{y^2}{b^2} + \frac{z^2}{c^2}$ is the inner ellipsoidal radius while $r_{oe}^2 = \frac{x^2}{a'^2} + \frac{y^2}{b'^2} + \frac{z^2}{c'^2}$ is its outer counterpart. Both ellipsoidal radii satisfy the condition that the sum of their squared semi–axes is equal to three: $a^2 + b^2 + c^2 = a'^2 + b'^2 + c'^2 = 3$. Finally, $r_s = r_{200}/c_{\mathrm{nfw}}$.

The default values of the parameters in the MWH are the following: $M_{200} = 145.64 \times 10^{10}\,M_\odot$, $r_{200} = 234.5\,\mathrm{kpc}$ and $r_s = 14.63\,\mathrm{kpc}$ (then, $c_{\mathrm{nfw}} = 16.0287081$). The values of the inner semi–axes are $a = 1.023737002$, $b = 1.010633169$, $c = 0.964667377$, then inside the first $10\,\mathrm{kpc}$ we have an oblate shape given by $b/a = 0.9872$ and $c/a = 0.9423$. In case of the outer semi–axes, the values are $a' = 1.069901231$, $b' = 0.984309133$, $c' = 0.941513084$, so between $40\,\mathrm{kpc}$ and $70\,\mathrm{kpc}$ we have a more triaxial shape: $b'/a' = 0.92$ and $c'/a' = 0.88$.

In Fig. 2.11 we show the potential–density pair of our representation of the DMH. Top panels: the potential from an outside (left panel) and from an inside (projections on the center planes, right panel) viewpoint in the inner $8\,\mathrm{kpc}$ region. Middle panels: idem top row but for the region enclosed by the first $25\,\mathrm{kpc}$, i.e. beyond the transition scale at $r_s = 14.63\,\mathrm{kpc}$. Bottom panels: isodensities projected on the center planes are also depicted in both regions (inside $8\,\mathrm{kpc}$ on the left and inside $25\,\mathrm{kpc}$ on the right) to give a global picture of the DMH component.

2.2.5.2   Option (2): a modified logarithmic profile

This form for the DMH potential describes an ellipsoid rotated by an angle ϕ about the galactic Z–axis, in which q_1 and q_2 are the axial flattenings along the equatorial axes and q_z is the axial flattening perpendicular to the galactic disk. The transition scale is introduced like [28]:

$$\Phi_{dmh} = v_{halo}^2 \ln[(r^\star)^2 + d^2],$$

with $r^\star = \frac{(r_s+r_{oe})}{r_s+r_{ie}}r_{ie}$, $r_{ie}^2 = x^2 + y^2 + \frac{z^2}{q_z^2}$, $r_{oe}^2 = Wx^2 + Vy^2 + Uxy + \frac{z^2}{q_3^2}$ and $W = \frac{a_1^2}{q_1^2} + \frac{a_2^2}{q_2^2}$, $V = \frac{a_1^2}{q_2^2} + \frac{a_2^2}{q_1^2}$, $U = 2a_1a_2\left(\frac{1}{q_1^2} - \frac{1}{q_2^2}\right)$, where $a_1 = \cos(\phi)$, $a_2 = \sin(\phi)$.
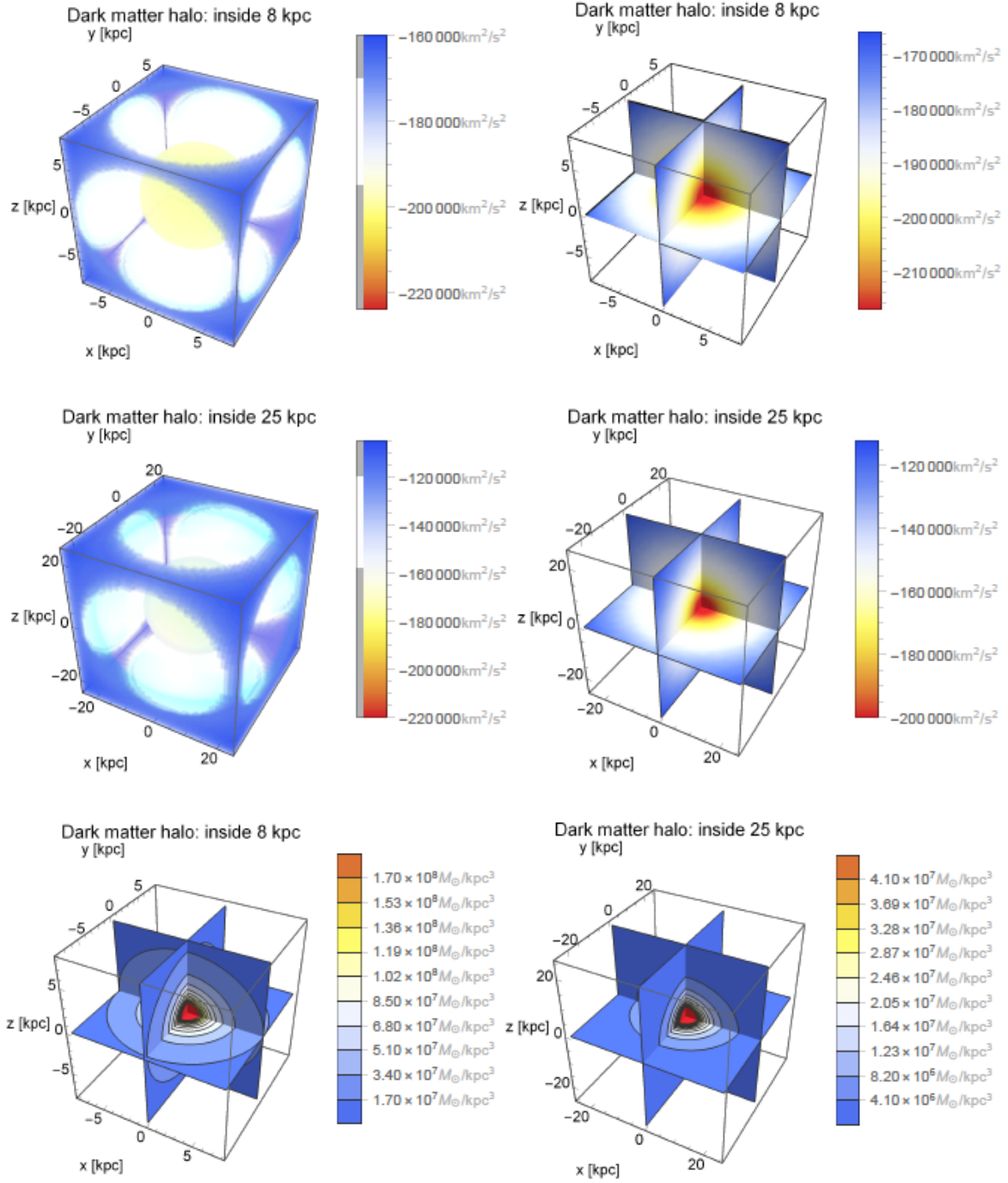
Figure 2.11: Potential–density pair for the (option 1) DMH. Top panels: outside (left) and inside (right) potential views of the innermost region. Middle panels: idem top panels but for the regions beyond the transition scale. Bottom panels: isodensities projected on the center planes for both regions.

The default values of the parameters in the `MWH` are the following: the halo mass renormalization parameter is $v_{halo} = 176.26$ km/s in order to have a $v_{\mathrm{LSR}}(R_\odot = 8\,\mathrm{kpc}) = 225.2\,\mathrm{km\,s}^{-1}$ (the effect of the LMC is not taken into account, see [27] for further details). Therefore, the v_{halo} parameter need to be re-computed for each particular model (see below). The softening parameter is $d = 12$ kpc and the transition scale, $r_s = 30$ kpc, is selected by the authors such that the region of dominance of the disk resides inside the axisymmetric part of the halo potential. However, the effective transition between the axisymmetric and triaxial regions occurs at a smaller radius, around 10 kpc. Furthermore, the tilt angle is $\phi = 277°$ (as in the `MWH` the Sun is located at $+8$ kpc on the X–axis), $q_z = 0.9$, $q_1 = 1.38$, $q_2 = 1$ and $q_3 = 1.36$ (once again, the effect of the LMC is not considered). Finally, notice that if we are in the inner region, i.e. $r_{ie} \ll r_s$ and $r_{oe} \ll r_s$, then: $r^\star \simeq r_{ie}$, an oblate profile given that $r_{ie}^2 = x^2 + y^2 + \frac{z^2}{q_z^2}$ and $q_z = 0.9$. On the other hand, if we are in the outer region, where $r_{ie} \gg r_s$ as well as $r_{oe} \gg r_s$, then $r^\star \simeq r_{oe}$, with a mildly triaxial profile (somehow prolate given that $q_1 = 1.38$, $q_2 = 1$, $q_3 = 1.36$) and rotated: $r_{oe}^2 = \mathrm{W}x^2 + \mathrm{V}y^2 + \mathrm{U}xy + \frac{z^2}{q_3^2}$.

In Fig. 2.12 we show the potential–density pair of our representation of the DMH. Top panels: the potential from an outside (left panel) and from an inside (projections on the center planes, right panel) viewpoint in the inner 12 kpc region (i.e. inside the softening parameter value). Middle panels: idem top row but for the region enclosed by the first 40 kpc, i.e. beyond the transition scale at $r_s = 30$ kpc. Bottom panels: isodensities projected on the center planes are also depicted in both regions (inside 12 kpc on the left and inside 40 kpc on the right) to give a global picture of the DMH component.

The value $v_{halo} = 176.26$ km/s given here is computed for the time independent `MWH` 2.0 model using all the default values for the rest of the galactic components. That is, we are considering the nuclear region, the spheroidal component of the bulge, the thin and thick exponential disks and, of course, option 2 of the DMH. In Fig. 2.13 we show the circular velocity of the model mentioned before. Indeed, notice that at 8 kpc we have $v_{\mathrm{LSR}} = 225.2\,\mathrm{km\,s}^{-1}$, as expected after the calibration of the v_{halo}.

2.3 *A Hydra 2.0*

The goal of this section is to show a Milky Way–type galaxy (*Hydra 2.0*) by choosing one of the many posible `MWH` configurations. In this case, we are trying to capture roughly the potential form of the Aq–C5 model, from [20], one of their most likely Milky Way galaxies. In that regard, we are considering a `MWH` consisting of: a nuclear region, a peanut–shaped bulge, two–armed spiral pattern ("super strong spirals"), two–component exponential stellar disk and the option (1) for the DMH, all of them calibrated with the default values of the parameters (see previous Section 2.2 for further details).

2.3.1 Goal: circular velocity curve

In Fig. 2.14 (left panel) we show rotation curves for model Aq–C5 (Fig. 19 in [20]). The total rotation curve is depicted in solid black. On the right panel we show the rotation curve for our *Hydra 2.0* model, which time independent part in solid blue line try to mimic the Aq–C5 (the full time dependent model is depicted in solid red line, i.e. bar and spiral arms
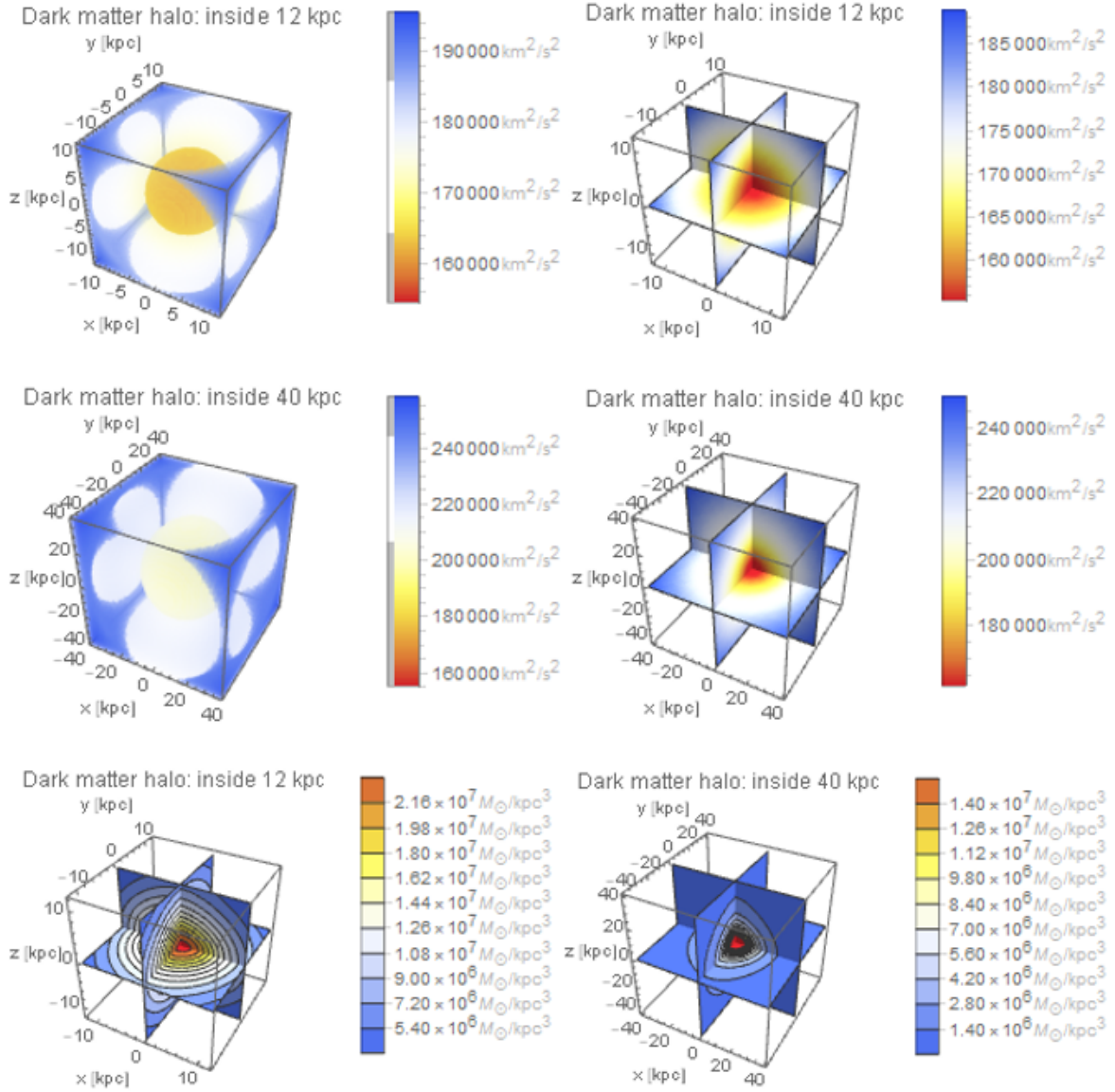
Figure 2.12: Potential–density pair for the (option 2) DMH. Top panels: outside (left) and inside (right) potential views of the innermost region. Middle panels: idem top panels but for the regions beyond the transition scale. Bottom panels: isodensities projected on the center planes for both regions.

are included). The resemblance between the rotation curves is auspicious.

Now that we have reproduced one fundamental constraint given by the circular velocity curve of the target galaxy, we can describe the full MWH *Hydra 2.0* model that is behind.
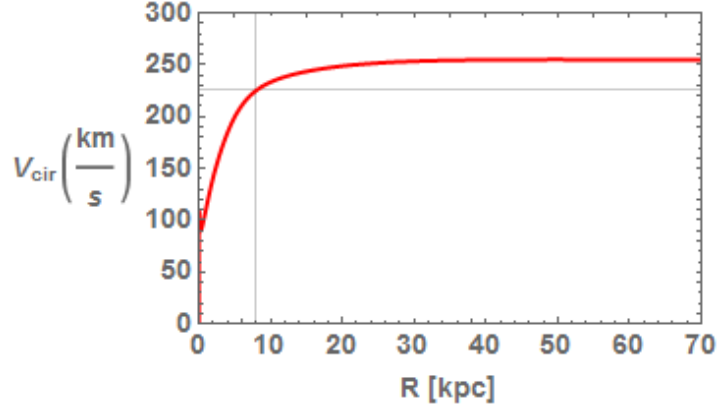
Figure 2.13: Circular velocity for (option 2) DMH. The model obeys the relation $v_{\mathrm{LSR}}(R_\odot = 8\,\mathrm{kpc}) = 225.2\,\mathrm{km\,s^{-1}}$ (indicated with grey solid lines) due to the calibration of the halo mass renormalization parameter, that results in the value of $v_{halo} = 176.26\,\mathrm{km/s}$.
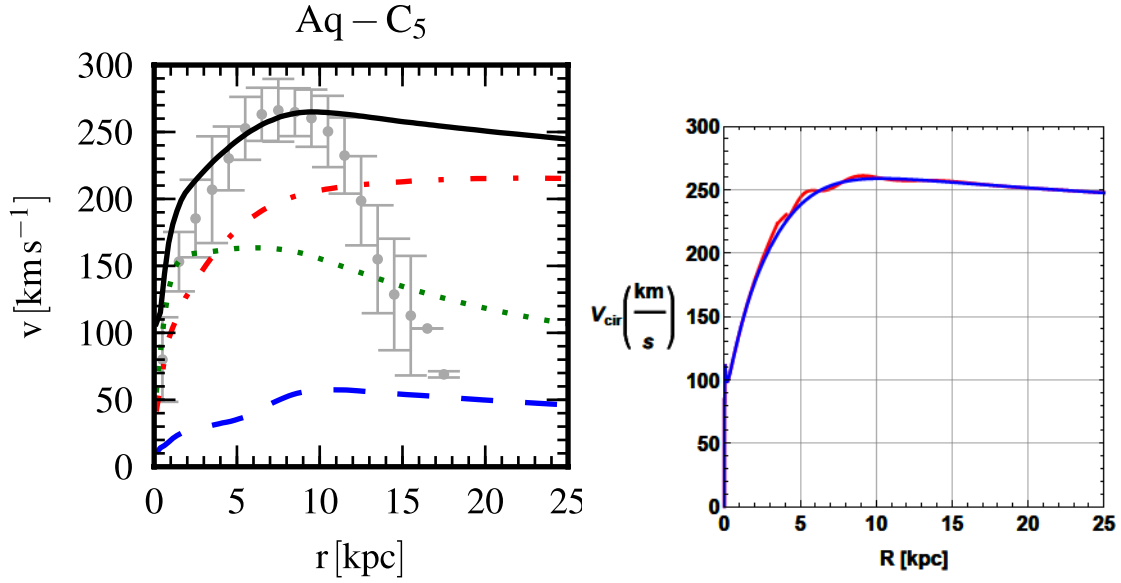
Figure 2.14: Circular velocity curves. Left panel: different line types give the contributions of various mass components to the total circular velocity: stars (dotted green lines), dark matter (dot–dashed red lines) and gas (dashed blue lines). The total rotation curves are given by solid (black) lines, while (grey) points with error bars show the rotation velocity of the star–forming gas (image taken from [20]). Right panel: total rotation curve for our model. In solid blue line the time independent model, in solid red line the full time dependent model (i.e. bar and spiral arms are included). Compare both curves on the right panel with the solid black line in the left panel.
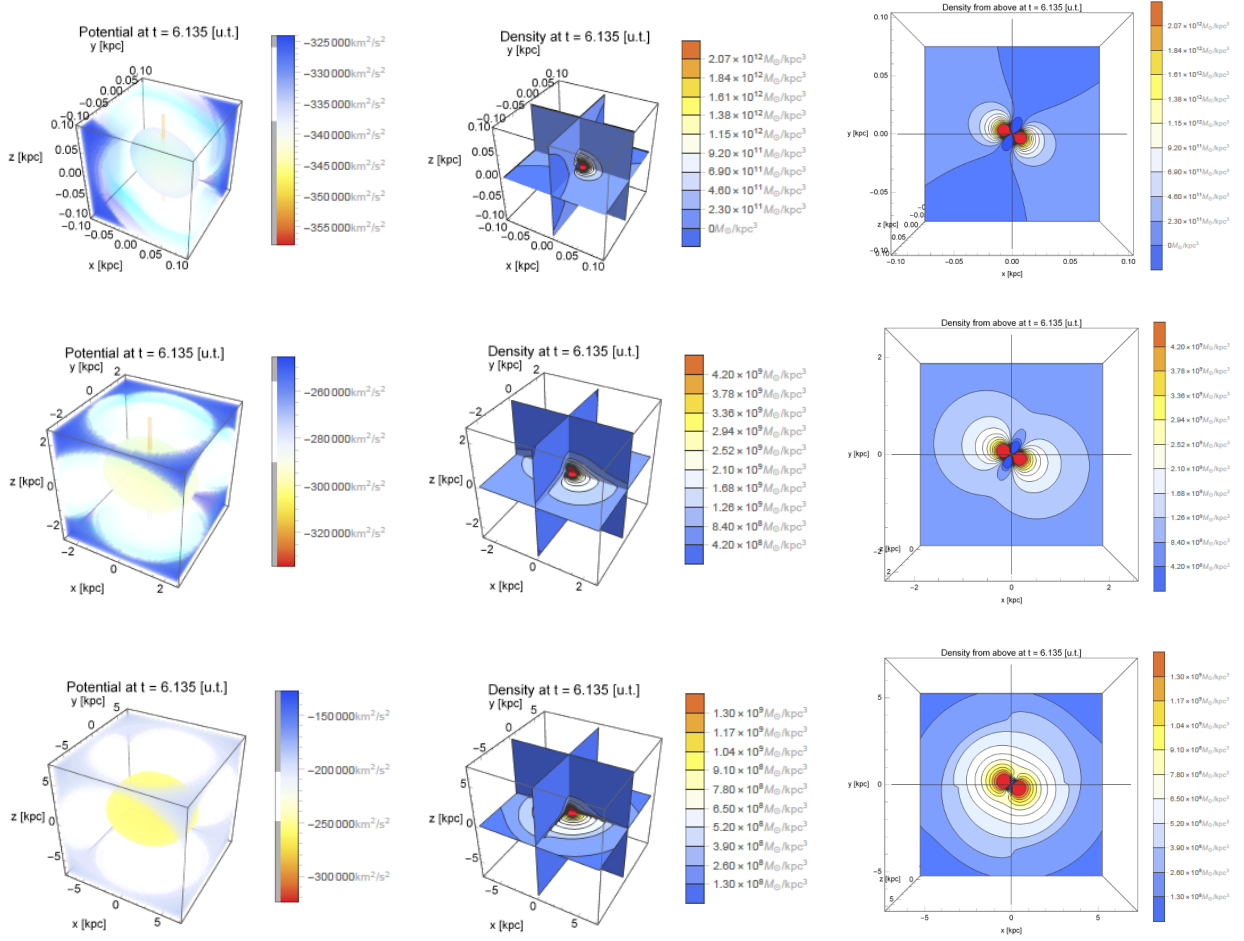
Figure 2.15: Potential–density pairs inside $\sim 7\,\text{kpc}$. Left panels: isopotentials. Middle panels: isodensities projected on the center planes. Right panels: isodensities on the plane.

2.3.2 Model: potential–density pair

Figs. 2.15 and 2.16 show potential–density pairs for our Milky Way–type *Hydra 2.0* model from the inside out. On the left column we show isopotentials from an outside viewpoint, middle column presents projections of the isodensities on the center planes, and right column, top viewpoint of the latter. The consecutive regions of dominance of the bar, then the disk and finally of the DMH, as expected, is clearly shown when going away from the center.

2.3.3 Result: a Milky Way–type galaxy

Finally, on the left panel of Fig. 2.17 we show the isodensities (face-on) on the plane for the time dependent components combined (bar and spiral arms) for our *Hydra 2.0* model at the final time of integration, 6 Gyr in u.t. (i.e. "today"). The Scutum–Centaurus and Perseus Arms as well as the position of the Sun is indicated. On the right panel, a face-on sketch of our Milky Way galaxy with the Scutum–Centaurus and Perseus Arms also indicated (the region
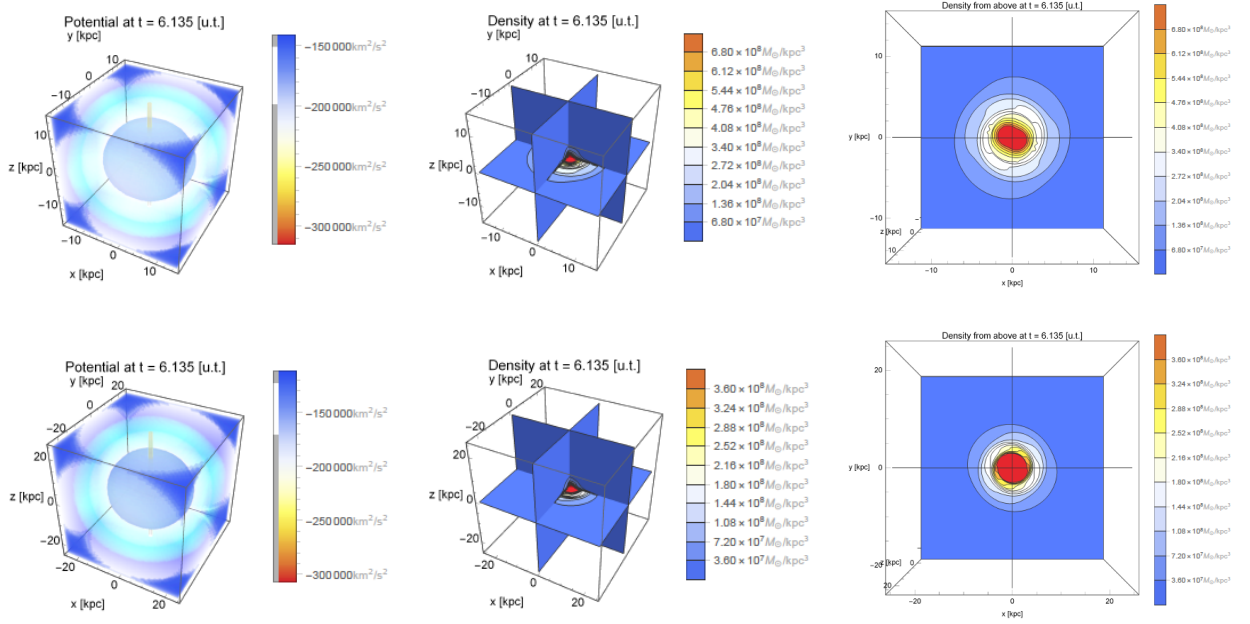
Figure 2.16: Potential–density pairs between ~ 15 and $\sim 25\,\mathrm{kpc}$. Left panels: isopotentials. Middle panels: isodensities projected on the center planes. Right panels: isodensities on the plane.

on the left panel is framed with a solid red line on the right panel). The stellar structure of the Milky Way seems to be well reproduced by our *Hydra 2.0* analytical model.

2.4   Cosmological evolution

In the current MWH 2.0, only the bar and the spiral arms amplitudes are affected by cosmological evolution. Therefore, those are the only components that can be adiabatically introduced during a simulation. However, we are working on MWH 3.0: a fully time dependent model, introducing multiple growth factors to consider cosmological evolution for the rest of the components (see ongoing work in Chapter 3).

2.4.1   Bar and spiral arms: growth factor $\eta(t)$

The bar and the spiral arms can be introduced adiabatically during the first $3\,\mathrm{Gyr}$ of a $6\,\mathrm{Gyr}$–long simulation following [22]: *The bar and the spiral arms forces are present in the simulations only for $t > 0$. These are introduced in the simulations by letting their respective amplitudes α and A grow by a factor (Dehnen 2000):*

$$\eta(t) = \left(\frac{3}{16}\xi^5 - \frac{5}{8}\xi^3 + \frac{15}{16}\xi + \frac{1}{2} \right), \ \xi \equiv 2\frac{t}{3\,\mathrm{Gyrs}} - 1,$$

until, at $t = 3\,\mathrm{Gyr}$ they reach their final amplitude which is kept constant until the end of the simulation at $t = t_e \equiv 6\,\mathrm{Gyr}$.
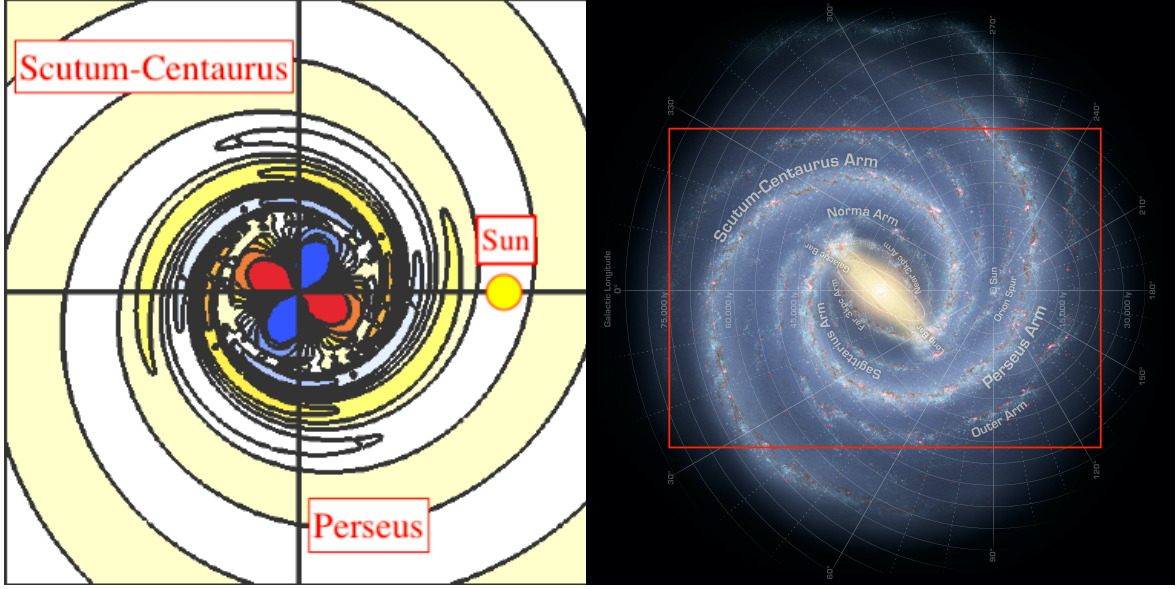
Figure 2.17: Left panel: isodensities on the plane (warm colours indicate high-density regions) for our time dependent components (bar and spiral arms) combined of our *Hydra 2.0* model at the final time of integration, the Scutum–Centaurus and Perseus Arms are indicated as well as the position of the Sun with a filled yellow circle. Right panel: a sketch of a face-on Milky Way (credits: NASA/JPL-Caltech/R. Hurt, SSC/Caltech) with the region enclosed on the left panel framed in solid red.

Then, at $t = 0$, we have $\xi = -1$ and the growth factor $\eta(0) = 0$, besides at $t = 3$, we have $\xi = 1$ and the growth factor $\eta(3) = 1$. As mentioned before, for $t \geq 3$ the amplitudes are kept constant at the value reached by $t = 3$. In the `MWH` model we are going to generalize the previous expression introducing a new quantity, "`atime`":

$$\eta(t) = \left(\frac{3}{16}\xi^5 - \frac{5}{8}\xi^3 + \frac{15}{16}\xi + \frac{1}{2} \right), \ \xi \equiv 2\frac{t}{\text{atime}} - 1,$$

where `atime` is measured in u.t. and it is the time–interval that the bar and spiral arms needs to reach their final amplitudes. For instance, in case we want to reproduce the experiments of [22], we use `atime`= 3.068 (due to the unit conversion between Gyr and u.t., see Section C.7 for details). Furthermore, in case the user sets `atime`= 0, the `LP-VIcode` interprets that there is no need of cosmological evolution and the amplitudes of the bar and the spiral arms are set at their final values from the beginning of the simulation.

In conclusion, in case the user needs to introduce adiabatically the bar and the spiral arms during the first `atime` u.t. of a simulation, the amplitudes of the bar, $\alpha(t)$ and that of the spiral arms, $A(t)$ take the following form: $\alpha(t) = \alpha \cdot \eta(t)$ and $A(t) = A \cdot \eta(t)$ where α and A are the fixed amplitudes of the bar and spiral arms, respectively (Sections 2.2.2.2 and 2.2.3), and $\eta(t)$ is the associated growth factor.

Chapter 3

Ongoing work: `MilkyWayHydra` **3.0**

We are working on two projects, the first one deals with making a fully time dependent `MWH` model. The second project is about introducing new components.

1. **Time evolution:** we are extending the growth factors used to model the bar and the spiral arms' cosmological evolution in `MWH` 2.0, to many other parameters in the `MWH` 3.0, in order to make it a fully time dependent model.

2. **New components:** we are coding a more detailed nuclear region, an ISM disk and, last but not least, a new option for the DMH.

The more detailed nuclear region presents a subcomponent inside the $\epsilon_{nuclear}$ where the dynamics is now essentially flat, which would be accomplished by the combination of a Plummer sphere with a softened point–particle potential describing the naked singularity of the SMBH at the center. The representation will try to obey the following scales: the first $200 - 300\,\mathrm{pc}$ would be dominated by the nuclear bulge where the stellar component would be a nuclear stellar disk of $1.4 \times 10^9\,\mathrm{M_\odot}$ mass with a scale height of $45\,\mathrm{pc}$. The compact NSC dominates the inner $20 - 30\,\mathrm{pc}$ region, with a mass of $2.5 - 3 \times 10^7\,\mathrm{M_\odot}$ and centered in Sgr A* (the SMBH, [23, 24, 10]). Finally, the SMBH dominates inside the first $1.25\,\mathrm{pc}$, with a mass of $4.3 - 3.3 \times 10^6\,\mathrm{M_\odot}$ ([14, 11, 8, 9]).

The ISM disk will be introduced as a double exponential density profile such as the thin and thick disks in order to have a three–component exponential disk made of a two–component stellar (thin and thick) disk and the aforementioned ISM disk. However, the main difference with the stellar disks is that the ISM disk will contemplate an exclusion region inside the corrotation limit, like the spiral arms. Also, the R_d^{ISM} will double the R_d^{thin}. Furthermore, $h_z^{ISM} = 0.08\,\mathrm{kpc}$.

Finally, the third option for the DMH component will be the Einasto profile.

Our final goal is to update the `MWH` into a fully time dependent Milky Way–type galaxy model with the most cited DMH profiles available as options for such theoretical but crucial component.

Chapter 4

Final remarks

`MilkyWayHydra` 2.0 is a ready-to-use realistic Milky Way–type galaxy potential and one of the three main elements of the `LP-VIsuite` project (Chapter 1). It has available all of the basic components of a late–type galaxy (Chapter 2)[1]: a nuclear region, a peanut–shaped bulge composed of a bulge spheroid and a bar, the spiral arms, two options for the two–component (thin and thick) stellar disk (Miyamoto–Nagai profile or exponential profile) and two options for the dark matter halo (a bi–triaxial extension of the Navarro–Frenk–White profile or a modified logarithmic profile). The `milkywayhydra.pav` (Appendix A) includes the `potinit` initialization subroutine as well as the `acelera` and `variac` subroutines where all the first and second derivatives are calculated to compute the equations of motions and first variational equations necessary to obtain the CIs (Appendix B and C). All components can be easily modified by tunning the corresponding parameters in order to build the target galaxy. Finally, the `MWH` 2.0 associated `milkywayhydra.pav` file is fully functional and validated (Appendix D), and can be used right out of the box with the latest version (v. 2.0.2) of the `LP-VIcode`. For further information about the `LP-VIcode`, please visit the webpage of the project at:

<div align="center">

http://www.fcaglp.unlp.edu.ar/LP-VIcode/

</div>

The next version of the `MilkyWayHydra` (3.0, Chapter 3) is on its way, and it will include more galactic components as well as time–dependence for all the structure parameters in order to be able to introduce in a simulation every single component in a more realistic way, likewise the bar and the spiral arms in the present 2.0 version.

---

[1]An early–type galaxy can be also modelled by removing the unnecessary galactic components and adjusting the remaining parameters.

Acknowledgements

Bibliography

[1] Antoja, T., Helmi, A., Dehnen, W., Bienaymé, O., Bland-Hawthorn, J., Famaey, B., Freeman, K., Gibson, B., Gilmore, G., Grebel, E., Kordopatis, G., Kunder, A., Minchev, I., Munari, U., Navarro, J., Parker, Q., Reid, W., Seabroke, G., Siebert, A., Steinmetz, M., Wyse, R. & Zwitter, T. 2014, A&A, 563, idA60, 17pp.

[2] Banik, N. & Bovy, J. 2019, MNRAS, 484, 2009-2020.

[3] Carpintero, D., Maffione, N. & Darriba, L. 2014, Astronomy and Computing, 5, 19-27.

[4] Cox, D. & Gómez, G. 2002, ApJS, 142, 261-267.

[5] Darriba, L., Maffione, N., Cincotta, P. & Giordano, C., 2012: 3rd La Plata International School on Astronomy and Geophysics "Chaos, Diffusion and Non-integrability in Hamiltonian Systems-Application to Astronomy". P.M. Cincotta, C.M. Giordano & C. Efthymiopoulos eds. Universidad Nacional de La Plata and Asociación Argentina de Astronomía Publishers, La Plata, Argentina, 345-366.

[6] Deason, A., Belokurov, V. & Evans, N. 2011, MNRAS, 416, 2903-2915.

[7] Denhen, W. 2000, AJ, 119, 800-812.

[8] Do, T., Ghez, A., Morris, M., Lu, J., Matthews, K., Yelda, S., Wright, S. & Larkin, J. 2011, ASPC, 439, p200.

[9] Do, T., Martinez, G., Yelda, S., Ghez, A., Bullock, J., Kaplinghat, M., Lu, J., Peter, A. & Phifer, K. 2013, ApJL, 779, L6, 7pp.

[10] Ghez, A., Salim, S., Weinberg, N., Lu, J., Do, T., Dunn, J., Matthews, K., Morris, M., Yelda, S., Becklin, E., Kremenek, T., Milosavljevic, M. & Naiman, J. 2008, ApJ, 689, 1044-1062.

[11] Gillessen, S., Eisenhauer, F., Fritz, T., Bartko, H., Dodds-Eden, K., Pfuhl, O., Ott, T. & Genzel, R. 2009, ApJL, L114-L117.

[12] Gómez, F., Torres-Flores, S., Mora-Urrejola, C., Monachesi, A., White, S., Maffione, N., Grand, R., Marinacci, F., Pakmor, R., Springel, V., Frenk, C., Amram, P., Epinat, B. & Mendes de Oliveira, C. 2021, ApJ, 908, 27-37.

[13] Grand, R., Gómez, Facundo., Marinacci, F., Pakmor, R., Springel, V., Campbell, D., Frenk, C., Jenkins, A. & White, S. 2017, MNRAS, 467, 179-207

[14] Launhardt, R., Zylka, R. & Mezger, P. 2002, A&A, 284, 112-139.

[15] Law, David. & Majewski, S. 2010, ApJ, 714, 229-254.

[16] Maffione, N., Darriba, L., Cincotta, P. & Giordano, C. 2011, CeMDA, 111, 285-307.

[17] Maffione, N., Darriba, L., Cincotta, P. & Giordano, C. 2013, MNRAS, 429, 2700-2717.

[18] Maffione, N., Gómez, F., Cincotta, P., Giordano, C., Cooper, A. & O'Shea, B. 2015, MNRAS, 453, 2830-2847.

[19] Maffione, N., Gómez, F., Cincotta, P., Giordano, C., Grand, R., Marinacci, F., Pakmor, R., Simpson, C., Springel, V. & Frenk, C. 2018, MNRAS, 478, 4052-4067.

[20] Marinacci, F., Pakmor, R. & Springel, V. 2014, MNRAS, 437, 1750-1775.

[21] Miki, Y. & Umemura, M. 2018, MNRAS, 475, 2269-2281.

[22] Monari, G., Famaey, B., Siebert, A., Grand, R., Kawata, D. & Boily, C. 2016, MNRAS, 461, 3835-3846.

[23] Schödel R., 2014, Proceedings of the IAU, 312, 274-281.

[24] Schdel, R., Feldmeier, A., Kunneriath, D., Stolovy, S., Neumayer, N., Amaro-Seoane, P. & Nishiyama, S. 2014, A&A, 566, idA47, 17pp.

[25] Simpson, C., Gargiulo, I., Gómez, F., Grand, R., Maffione, N., Cooper, A., Deason, A., Frenk, C., Helly, J., Marinacci, F. & Pakmor, R. 2019, MNRAS, 490, L32-L37.

[26] Smith, R., Flynn, C., Candlish, G., Fellhauer, M. & Gibson, B. 2015, MNRAS, 448, 2934-2940.

[27] Vera-Ciro, C. & Helmi, A. 2013, ApJL, 773, L4, 5pp.

[28] Vogelsberger, M., White, S., Helmi, A., Springel, V. 2008, MNRAS, 385, 236-254.

Appendix A

The `milkywayhydra.pav`

The computation of the equations of motion as well as the first variational equations for such a convoluted multi-component potential as the present `MWH` is a very difficult task: being a non–automatic process, we need to check and recheck at every step. Indeed, all the expressions were carefully calculated by hand and further on, every one of them were also checked with an algebraic manipulator. It is straightforward to realise that such complex procedure has multiple sources for mistakes that might be extremely difficult to identify. Just recently, however, we were able to apply the `SMART` code to our potential, the automatic differentiation pre-processing slave program of the `LP-VIsuite` which was used to compute all the equations (motion and first variationals) from the scratch once again. Then, a fairly well coincidence between the results using both procedures would imply a solid validation test for our `milkywayhydra.pav` file.

In the appendix B we present the derivation of all the equations of motion and first variational equations for the `MWH` 2.0, that are necessary to build the `milkywayhydra.pav`.

In the appendix C we describe the `milkywayhydra.pav`.

In the appendix D we present the results of comparing the two flavours of the `milkywayhydra.pav` on a variety of experiments: the original, a.k.a. pre–`SMART` version and the automatic, a.k.a. `SMART` version.

Appendix B

Construction

In the present appendix we are going to present all the expressions involved in the calculation of the equations of motion and first variational equations included in the `milkywayhydra.pav`. Every single expression presented here was calculated by hand and checked with an algebraic manipulator.

B.1   First and second derivatives

B.1.1   The nuclear region

Being the potential:

$$\Phi_{nuclear} = -\frac{GM_{nuclear}}{\sqrt{x^2 + y^2 + z^2 + \epsilon_{nuclear}^2}}, \tag{B.1}$$

and introducing the quantities:

$$
\begin{cases}
R_{nuclear} & = & \sqrt{x^2 + y^2 + z^2 + \epsilon_{nuclear}^2}, \\[2ex]
\frac{\partial R_{nuclear}}{\partial x_i} & = & \frac{x_i}{R_{nuclear}},
\end{cases}
$$

we can rewrite the potential associated with the nuclear region (Eq. B.1), and the corresponding derivatives like:

$$
\begin{cases}
\Phi_{nuclear} & = & -\frac{GM_{nuclear}}{R_{nuclear}}, \\[2ex]
\frac{\partial \Phi_{nuclear}}{\partial x_i} & = & -\frac{\Phi_{nuclear}}{R_{nuclear}} \frac{\partial R_{nuclear}}{\partial x_i}, \\[2ex]
\frac{\partial}{\partial x_i}\left(\frac{\partial \Phi_{nuclear}}{\partial x_j}\right) & = & \frac{\Phi_{nuclear}}{R_{nuclear}^2}\left[3\left(\frac{\partial R_{nuclear}}{\partial x_i}\right)\left(\frac{\partial R_{nuclear}}{\partial x_j}\right) - \delta_{ij}\right],
\end{cases}
$$

with $x_1 = x$, $x_2 = y$ and $x_3 = z$.

B.1.2 The peanut–shaped bulge

B.1.2.1 The bulge spheroid

Being the potential:

$$\Phi_{bulge} = -\frac{GM_{bulge}}{\sqrt{x^2 + y^2 + z^2} + \epsilon_{bulge}}, \tag{B.2}$$

and introducing the quantities:

$$
\begin{cases}
\mathrm{R}_{bulge} &= \sqrt{x^2 + y^2 + z^2} + \epsilon_{bulge}, \\[2mm]
\frac{\partial \mathrm{R}_{bulge}}{\partial x_i} &= \frac{x_i}{\mathrm{R}_{bulge} - \epsilon_{bulge}},
\end{cases}
$$

we can rewrite the potential associated with the bulge (Eq. B.2), and the corresponding derivatives like:

$$
\begin{cases}
\Phi_{bulge} &= -\frac{GM_{bulge}}{\mathrm{R}_{bulge}}, \\[3mm]
\frac{\partial \Phi_{bulge}}{\partial x_i} &= -\frac{\Phi_{bulge}}{\mathrm{R}_{bulge}} \frac{\partial \mathrm{R}_{bulge}}{\partial x_i}, \\[3mm]
\frac{\partial}{\partial x_i}\left(\frac{\partial \Phi_{bulge}}{\partial x_j}\right) &= \frac{\Phi_{bulge}}{\mathrm{R}_{bulge}^2}\left(\frac{\partial \mathrm{R}_{bulge}}{\partial x_i}\right)\left(\frac{\partial \mathrm{R}_{bulge}}{\partial x_j}\right)\left(3 + \frac{\epsilon_{bulge}}{\mathrm{R}_{bulge} - \epsilon_{bulge}}\right) - \delta_{ij}\frac{\Phi_{bulge}}{\mathrm{R}_{bulge}(\mathrm{R}_{bulge} - \epsilon_{bulge})},
\end{cases}
$$

with $x_1 = x$, $x_2 = y$ and $x_3 = z$.

B.1.2.2 The bar

Being the potential:

$$\Phi_{bar}(R, \phi, z, t) = \alpha \frac{v_0^2}{3}\left(\frac{\mathrm{R}_0}{\mathrm{R}_b}\right)^3 U(r)\frac{R^2}{r^2}\cos(\gamma_b), \tag{B.3}$$

first we identify the hereinafter "first level variables", and calculate their first and second derivatives:

$$\text{First level variables} \rightarrow \begin{cases} R(x_1, x_2) \, (\geq 0) \quad = \quad \sqrt{x_1^2 + x_2^2}; \\[2em] \phi(x_1, x_2) \, (\in [-\pi, \pi]) \quad = \quad \begin{cases} \arctan\left(\frac{x_2}{x_1}\right) & x_1 > 0, \\[1em] \arctan\left(\frac{x_2}{x_1}\right) + \pi & x_1 < 0 \text{ and } x_2 \geq 0, \\[1em] \arctan\left(\frac{x_2}{x_1}\right) - \pi & x_1 < 0 \text{ and } x_2 < 0, \\[1em] \frac{\pi}{2} & x_1 = 0 \text{ and } x_2 > 0, \\[1em] -\frac{\pi}{2} & x_1 = 0 \text{ and } x_2 < 0, \\[1em] \text{not defined} & x_1 = x_2 = 0; \end{cases} \\[6em] x_3 \quad = \quad x_3. \end{cases}$$

First derivatives $\rightarrow$
$$
\begin{cases}
\dfrac{\partial R}{\partial x_i} &= \dfrac{x_i}{R} \ \text{ with } i = 1, 2, \\[2em]
\dfrac{\partial \phi}{\partial x_1} &=
\begin{cases}
\dfrac{-x_2/x_1^2}{(x_2/x_1)^2 + 1} & x_1 \neq 0, \\[1.5em]
0 & x_1 = 0 \ \text{ and } \ x_2 \neq 0, \\[1.5em]
\text{not defined} & x_1 = x_2 = 0,
\end{cases} \\[5em]
\dfrac{\partial \phi}{\partial x_2} &=
\begin{cases}
\dfrac{1/x_1}{(x_2/x_1)^2 + 1} & x_1 \neq 0, \\[1.5em]
0 & x_1 = 0 \ \text{ and } \ x_2 \neq 0, \\[1.5em]
\text{not defined} & x_1 = x_2 = 0.
\end{cases}
\end{cases}
$$

$$
\text{Second derivatives} \rightarrow
\begin{cases}
\dfrac{\partial^2 R}{\partial x_i \partial x_j} &= \dfrac{1}{R}\left[\delta_{ij} - \left(\dfrac{\partial R}{\partial x_i}\dfrac{\partial R}{\partial x_j}\right)\right] \quad \text{with } i,j = 1,2; \\[2em]
\dfrac{\partial^2 \phi}{\partial x_1^2} &=
\begin{cases}
\dfrac{2x_1}{x_2}\left(\dfrac{\partial \phi}{\partial x_1}\right)^2 & x_1 \neq 0, \\[1.5em]
0 & x_1 = 0 \text{ and } x_2 \neq 0, \\[1.5em]
\text{not defined} & x_1 = x_2 = 0,
\end{cases} \\[5em]
\dfrac{\partial^2 \phi}{\partial x_2^2} &=
\begin{cases}
-\dfrac{2x_2}{x_1}\left(\dfrac{\partial \phi}{\partial x_2}\right)^2 & x_1 \neq 0, \\[1.5em]
0 & x_1 = 0 \text{ and } x_2 \neq 0, \\[1.5em]
\text{not defined} & x_1 = x_2 = 0,
\end{cases} \\[5em]
\dfrac{\partial^2 \phi}{\partial x_1 \partial x_2} &=
\begin{cases}
-\dfrac{1}{x_1}\left(\dfrac{\partial \phi}{\partial x_2}\right)\left[1 + 2x_2\dfrac{\partial \phi}{\partial x_1}\right] & x_1 \neq 0, \\[1.5em]
0 & x_1 = 0 \text{ and } x_2 \neq 0, \\[1.5em]
\text{not defined} & x_1 = x_2 = 0.
\end{cases}
\end{cases}
$$

Second, we build our first–level group of composite quantities and compute their first and second derivatives:

$$
\text{Composite constants} \rightarrow
\begin{cases}
\text{CA} &= \dfrac{v_0^2}{3} \cdot \text{R}_0^3.
\end{cases}
$$

$$\text{Composite variables} \rightarrow \begin{cases} r(R, x_3)\,(\geq 0) & = \sqrt{R^2 + x_3^2}; \\[2em] \gamma_b(\phi; t)) & = 2\,(\phi - \phi_b - \Omega_b \cdot t)\,; \\[2em] U(r) & = \begin{cases} -(r/\mathrm{R}_b)^{-3} \ \text{ for } \ r \geq \mathrm{R}_b, \\[1em] (r/\mathrm{R}_b)^3 - 2 \ \text{ for } \ r < \mathrm{R}_b. \end{cases} \end{cases}$$

$$\text{First derivatives} \rightarrow \begin{cases} \dfrac{\partial r}{\partial R} & = \dfrac{R}{r}\,, \\[1.5em] \dfrac{\partial r}{\partial x_i} & = \dfrac{\partial r}{\partial R}\dfrac{\partial R}{\partial x_i} \ \text{ with } i = 1, 2, \\[1.5em] \dfrac{\partial r}{\partial x_3} & = \dfrac{x_3}{r}\,; \\[2.5em] \dfrac{\partial \gamma_b}{\partial \phi} & = 2, \\[1.5em] \dfrac{\partial \gamma_b}{\partial x_i} & = \dfrac{\partial \gamma_b}{\partial \phi}\dfrac{\partial \phi}{\partial x_i} \ \text{ with } i = 1, 2, \\[1.5em] \dfrac{\partial \gamma_b}{\partial x_3} & = 0; \\[2.5em] \dfrac{d\,U(r)}{d\,r} & = \begin{cases} -\dfrac{3}{r}U(r) \ \text{ for } \ r \geq \mathrm{R}_b, \\[1.5em] \dfrac{3}{r}\,(U(r) + 2) \ \text{ for } \ r < \mathrm{R}_b, \end{cases} \\[3em] \dfrac{\partial U(r)}{\partial x_i} & = \dfrac{d\,U(r)}{d\,r}\dfrac{\partial r}{\partial x_i} \ \text{ with } i = 1, 2, 3. \end{cases}$$

Second derivatives →

$$
\frac{\partial^2 r}{\partial R^2} = \frac{1}{r}\left[1 - \left(\frac{\partial r}{\partial R}\right)^2\right],
$$

$$
\frac{\partial^2 r}{\partial x_i \partial x_j} = \frac{\partial^2 r}{\partial R^2}\frac{\partial R}{\partial x_i}\frac{\partial R}{\partial x_j} + \frac{\partial r}{\partial R}\frac{\partial^2 R}{\partial x_i \partial x_j}\ \text{ with } i,j = 1,2,
$$

$$
\frac{\partial^2 r}{\partial x_3^2} = \frac{1}{r}\left[1 - \left(\frac{\partial r}{\partial x_3}\right)^2\right],
$$

$$
\frac{\partial^2 r}{\partial x_3 \partial R} = -\frac{1}{r}\frac{\partial r}{\partial R}\frac{\partial r}{\partial x_3},
$$

$$
\frac{\partial^2 r}{\partial x_3 \partial x_i} = \frac{\partial^2 r}{\partial x_3 \partial R}\frac{\partial R}{\partial x_i}\ \text{ with } i = 1,2;
$$

$$
\frac{\partial^2 \gamma_b}{\partial x_i \partial x_j} = \frac{\partial \gamma_b}{\partial \phi}\frac{\partial^2 \phi}{\partial x_i \partial x_j}\ \text{ with } i,j = 1,2;
$$

$$
\frac{d^2\,U(r)}{d\,r^2} =
\begin{cases}
+\frac{3}{r^2}U(r) - \frac{3}{r}\frac{d\,U(r)}{d\,r}\ \text{ for } r \geq R_b, \\[2em]
-\frac{3}{r^2}\left(U(r) + 2\right) + \frac{3}{r}\frac{d\,U(r)}{d\,r}\ \text{ for } r < R_b,
\end{cases}
$$

$$
\frac{\partial^2 U(r)}{\partial x_i \partial x_j} = \frac{d^2\,U(r)}{d\,r^2}\frac{\partial r}{\partial x_i}\frac{\partial r}{\partial x_j} + \frac{d\,U(r)}{d\,r}\frac{\partial^2 r}{\partial x_i \partial x_j}\ \text{ with } i,j = 1,2,
$$

$$
\frac{\partial^2 U(r)}{\partial x_3^2} = \frac{1}{r}\frac{d\,U(r)}{d\,r}\left[1 - \left(\frac{\partial r}{\partial x_3}\right)^2\right] + \frac{d^2\,U(r)}{d\,r^2}\left(\frac{\partial r}{\partial x_3}\right)^2,
$$

$$
\frac{\partial^2 U(r)}{\partial x_3 \partial x_i} = \frac{d^2\,U(r)}{d\,r^2}\frac{\partial r}{\partial x_3}\frac{\partial r}{\partial x_i} + \frac{d\,U(r)}{d\,r}\frac{\partial^2 r}{\partial x_3 \partial x_i}\ \text{ with } i = 1,2.
$$

Third, we build our second–level group of composite quantities and, again, compute their first and second derivatives:

Composite variables →
$$
\begin{cases}
\mathrm{OCA}_1(R,r) = \left(\frac{R}{r}\right)^2; \\[1.5em]
\mathrm{OCA}_2(\gamma_b) = \cos(\gamma_b),
\end{cases}
$$

where OCA_1 is a function of R (first level variable) as well as $r(R, x_3)$ (composite variable) and not simply a function of the first level variable pair (R, x_3). This is our election to

preserve recursiveness for programming purposes[1].

First derivatives $\rightarrow$
$$
\begin{cases}
\dfrac{\partial \mathrm{OCA}_1}{\partial r} &= -\dfrac{2}{r}\left(\dfrac{\partial r}{\partial R}\right)^2, \\[3mm]
\dfrac{\partial \mathrm{OCA}_1}{\partial R} &= \dfrac{2}{r}\dfrac{\partial r}{\partial R}, \\[3mm]
\dfrac{\partial \mathrm{OCA}_1}{\partial x_i} &= \left(\dfrac{\partial \mathrm{OCA}_1}{\partial R} + \dfrac{\partial \mathrm{OCA}_1}{\partial r}\dfrac{\partial r}{\partial R}\right)\dfrac{\partial R}{\partial x_i} \text{ with } i = 1,2, \\[3mm]
\dfrac{\partial \mathrm{OCA}_1}{\partial x_3} &= \dfrac{\partial \mathrm{OCA}_1}{\partial r}\dfrac{\partial r}{\partial x_3}; \\[8mm]
\dfrac{d\,\mathrm{OCA}_2}{d\,\gamma_b} &= -\sin(\gamma_b), \\[3mm]
\dfrac{\partial \mathrm{OCA}_2}{\partial x_i} &= \dfrac{d\,\mathrm{OCA}_2}{d\,\gamma_b}\dfrac{\partial \gamma_b}{\partial x_i} \text{ with } i = 1,2, \\[3mm]
\dfrac{\partial \mathrm{OCA}_2}{\partial x_3} &= 0.
\end{cases}
$$

---

[1]In order to preserve the recursive chain when it is possible, second–level group of composite quantities should depend on first–level group of composite quantities and first level quantities, and first–level group of composite quantities should depend only on first level quantities.

Second derivatives →

$$
\begin{cases}
\dfrac{\partial^2 \text{OCA}_1}{\partial r^2} &= \dfrac{2}{r}\left(\dfrac{\text{OCA}_1}{r} - \dfrac{\partial \text{OCA}_1}{\partial r}\right), \\[4mm]
\dfrac{\partial^2 \text{OCA}_1}{\partial R^2} &= \dfrac{2}{r^2}, \\[4mm]
\dfrac{\partial^2 \text{OCA}_1}{\partial r \partial R} &= -\dfrac{4}{r^2}\dfrac{\partial r}{\partial R}, \\[4mm]
\dfrac{\partial^2 \text{OCA}_1}{\partial x_i \partial x_j} &= \dfrac{\partial^2 \text{OCA}_1}{\partial R^2}\dfrac{\partial R}{\partial x_i}\dfrac{\partial R}{\partial x_j} + \dfrac{\partial^2 \text{OCA}_1}{\partial r^2}\dfrac{\partial r}{\partial x_i}\dfrac{\partial r}{\partial x_j} + \\[4mm]
&\quad + \dfrac{\partial^2 \text{OCA}_1}{\partial r \partial R}\left(\dfrac{\partial R}{\partial x_i}\dfrac{\partial r}{\partial x_j} + \dfrac{\partial r}{\partial x_i}\dfrac{\partial R}{\partial x_j}\right) + \dfrac{\partial \text{OCA}_1}{\partial R}\dfrac{\partial^2 R}{\partial x_i \partial x_j} + \\[4mm]
&\quad + \dfrac{\partial \text{OCA}_1}{\partial r}\dfrac{\partial^2 r}{\partial x_i \partial x_j} \quad \text{with } i,j = 1,2, \\[4mm]
\dfrac{\partial^2 \text{OCA}_1}{\partial x_3^2} &= \dfrac{\partial^2 \text{OCA}_1}{\partial r^2}\left(\dfrac{\partial r}{\partial x_3}\right)^2 + \dfrac{\partial \text{OCA}_1}{\partial r}\dfrac{\partial^2 r}{\partial x_3^2}, \\[4mm]
\dfrac{\partial^2 \text{OCA}_1}{\partial x_3 \partial x_i} &= \dfrac{\partial^2 \text{OCA}_1}{\partial r^2}\dfrac{\partial r}{\partial x_3}\dfrac{\partial r}{\partial x_i} + \dfrac{\partial^2 \text{OCA}_1}{\partial r \partial R}\dfrac{\partial r}{\partial x_3}\dfrac{\partial R}{\partial x_i} + \dfrac{\partial \text{OCA}_1}{\partial r}\dfrac{\partial^2 r}{\partial x_3 \partial x_i} \quad \text{with } i = 1,2; \\[8mm]
\dfrac{d^2 \text{OCA}_2}{d^2 \gamma_b} &= -\text{OCA}_2, \\[4mm]
\dfrac{\partial^2 \text{OCA}_2}{\partial x_i \partial x_j} &= \dfrac{d^2 \text{OCA}_2}{d^2 \gamma_b}\dfrac{\partial \gamma_b}{\partial x_i}\dfrac{\partial \gamma_b}{\partial x_j} + \dfrac{d \text{OCA}_2}{d \gamma_b}\dfrac{\partial^2 \gamma_b}{\partial x_i \partial x_j} \quad \text{with } i,j = 1,2.
\end{cases}
$$

We can rewrite the potential associated with the bar (Eq. B.3), and the corresponding derivatives like:

$$
\text{Potential} \rightarrow
\begin{cases}
\Phi_{bar} &= \alpha \cdot \dfrac{\text{CA}}{\text{R}_b^3} \cdot U \cdot \text{OCA}_1 \text{OCA}_2.
\end{cases}
$$

First derivatives $\rightarrow$

$$
\begin{cases}
\dfrac{\partial \Phi_{bar}}{\partial U} &= \alpha \cdot \dfrac{\text{CA}}{\text{R}_b^3} \cdot \text{OCA}_1 \text{OCA}_2; \\[3em]
\dfrac{\partial \Phi_{bar}}{\partial \text{OCA}_1} &= \alpha \cdot \dfrac{\text{CA}}{\text{R}_b^3} \cdot U \cdot \text{OCA}_2, \\[2em]
\dfrac{\partial \Phi_{bar}}{\partial \text{OCA}_2} &= \alpha \cdot \dfrac{\text{CA}}{\text{R}_b^3} \cdot U \cdot \text{OCA}_1; \\[3em]
\dfrac{\partial \Phi_{bar}}{\partial x_i} &= \dfrac{\partial \Phi_{bar}}{\partial U}\dfrac{\partial U}{\partial x_i} + \dfrac{\partial \Phi_{bar}}{\partial \text{OCA}_1}\dfrac{\partial \text{OCA}_1}{\partial x_i} + \dfrac{\partial \Phi_{bar}}{\partial \text{OCA}_2}\dfrac{\partial \text{OCA}_2}{\partial x_i} \ \text{ with } i = 1, 2, \\[2em]
\dfrac{\partial \Phi_{bar}}{\partial x_3} &= \dfrac{\partial \Phi_{bar}}{\partial U}\dfrac{\partial U}{\partial x_3} + \dfrac{\partial \Phi_{bar}}{\partial \text{OCA}_1}\dfrac{\partial \text{OCA}_1}{\partial x_3}.
\end{cases}
$$

$$
\text{Second derivatives} \rightarrow
\begin{cases}
\dfrac{\partial^2 \Phi_{bar}}{\partial U \partial \mathrm{OCA_1}} &= \alpha \cdot \dfrac{\mathrm{CA}}{\mathrm{R}_b^3} \cdot \mathrm{OCA_2}, \\[2em]
\dfrac{\partial^2 \Phi_{bar}}{\partial U \partial \mathrm{OCA_2}} &= \alpha \cdot \dfrac{\mathrm{CA}}{\mathrm{R}_b^3} \cdot \mathrm{OCA_1}; \\[3em]
\dfrac{\partial^2 \Phi_{bar}}{\partial \mathrm{OCA_1} \partial \mathrm{OCA_2}} &= \alpha \cdot \dfrac{\mathrm{CA}}{\mathrm{R}_b^3} \cdot U; \\[3em]
\dfrac{\partial^2 \Phi_{bar}}{\partial x_i \partial x_j} &= \dfrac{\partial^2 \Phi_{bar}}{\partial U \partial \mathrm{OCA_1}} \left(\dfrac{\partial U}{\partial x_i} \dfrac{\partial \mathrm{OCA_1}}{\partial x_j} + \dfrac{\partial U}{\partial x_j} \dfrac{\partial \mathrm{OCA_1}}{\partial x_i} \right) + \\[1.5em]
& \quad + \dfrac{\partial^2 \Phi_{bar}}{\partial U \partial \mathrm{OCA_2}} \left(\dfrac{\partial U}{\partial x_i} \dfrac{\partial \mathrm{OCA_2}}{\partial x_j} + \dfrac{\partial U}{\partial x_j} \dfrac{\partial \mathrm{OCA_2}}{\partial x_i} \right) + \\[1.5em]
& \quad + \dfrac{\partial^2 \Phi_{bar}}{\partial \mathrm{OCA_1} \partial \mathrm{OCA_2}} \left(\dfrac{\partial \mathrm{OCA_1}}{\partial x_i} \dfrac{\partial \mathrm{OCA_2}}{\partial x_j} + \dfrac{\partial \mathrm{OCA_1}}{\partial x_j} \dfrac{\partial \mathrm{OCA_2}}{\partial x_i} \right) + \\[1.5em]
& \quad + \dfrac{\partial \Phi_{bar}}{\partial U} \dfrac{\partial^2 U}{\partial x_i \partial x_j} + \dfrac{\partial \Phi_{bar}}{\partial \mathrm{OCA_1}} \dfrac{\partial^2 \mathrm{OCA_1}}{\partial x_i \partial x_j} + \dfrac{\partial \Phi_{bar}}{\partial \mathrm{OCA_2}} \dfrac{\partial^2 \mathrm{OCA_2}}{\partial x_i \partial x_j} \ \text{with } i,j = 1,2, \\[1.5em]
\dfrac{\partial^2 \Phi_{bar}}{\partial x_3^2} &= \dfrac{\partial^2 \Phi_{bar}}{\partial U \partial \mathrm{OCA_1}} \left(2 \dfrac{\partial U}{\partial x_3} \dfrac{\partial \mathrm{OCA_1}}{\partial x_3} \right) + \dfrac{\partial \Phi_{bar}}{\partial U} \dfrac{\partial^2 U}{\partial x_3^2} + \dfrac{\partial \Phi_{bar}}{\partial \mathrm{OCA_1}} \dfrac{\partial^2 \mathrm{OCA_1}}{\partial x_3^2}, \\[1.5em]
\dfrac{\partial^2 \Phi_{bar}}{\partial x_3 \partial x_i} &= \dfrac{\partial^2 \Phi_{bar}}{\partial U \partial \mathrm{OCA_1}} \left(\dfrac{\partial U}{\partial x_3} \dfrac{\partial \mathrm{OCA_1}}{\partial x_i} + \dfrac{\partial U}{\partial x_i} \dfrac{\partial \mathrm{OCA_1}}{\partial x_3} \right) + \\[1.5em]
& \quad + \dfrac{\partial^2 \Phi_{bar}}{\partial U \partial \mathrm{OCA_2}} \dfrac{\partial U}{\partial x_3} \dfrac{\partial \mathrm{OCA_2}}{\partial x_i} + \dfrac{\partial^2 \Phi_{bar}}{\partial \mathrm{OCA_1} \partial \mathrm{OCA_2}} \dfrac{\partial \mathrm{OCA_1}}{\partial x_3} \dfrac{\partial \mathrm{OCA_2}}{\partial x_i} + \\[1.5em]
& \quad + \dfrac{\partial \Phi_{bar}}{\partial U} \dfrac{\partial^2 U}{\partial x_3 \partial x_i} + \dfrac{\partial \Phi_{bar}}{\partial \mathrm{OCA_1}} \dfrac{\partial^2 \mathrm{OCA_1}}{\partial x_3 \partial x_i} \ \text{with } i = 1,2,
\end{cases}
$$

with $x_1 = x$, $x_2 = y$ y $x_3 = z$.

B.1.3 The spiral arms

Being the potential:

$$
\Phi_{spiral}(R, \phi, z, t) = -\frac{\mathrm{A}}{\mathrm{R}_s \mathrm{KD}} e^{-\frac{(R - \mathrm{R}_s)}{\mathrm{R}_{sd}}} \cos(\gamma_s) \left[\mathrm{sech} \left(\frac{\mathrm{K}z}{\beta} \right) \right]^{\beta}, \tag{B.4}
$$

where the first level variables are the same as in the bar potential (Section B.1.2.2) because both are written in cylindrical coordinates (and they need to be transformed to cartesian coordinates as the rest of the potential components). Then, we start with our first–level group of composite quantities. We use the functional form of the expressions in the generalized N–armed potential (Section 2.2.3) ir order to cover the general case. For instance, a two–armed

spiral pattern as the one used in the default `milkywayhydra.pav` is achieved by setting the values to $n = 1$ and $N = 2$.

$$
\text{Composite variables} \rightarrow
\begin{cases}
\mathrm{K_n}(R) \rightarrow \mathrm{K}(R) & = & \frac{nN}{R\sin(p)}, \\[2em]
\gamma_n^s(R, \phi, t) \rightarrow \gamma_s(R, \phi; t) & = & nN\left[\phi - \phi_s - \Omega_s t - \frac{\ln(R/\mathrm{R}_s)}{\tan(\mathrm{p})}\right].
\end{cases}
$$

$$
\text{First derivatives} \rightarrow
\begin{cases}
\frac{d\,\mathrm{K}}{d\,R} & = & -\frac{\mathrm{K}}{R}, \\[1.5em]
\frac{\partial \mathrm{K}}{\partial x_i} & = & \frac{d\,\mathrm{K}}{d\,R}\frac{\partial R}{\partial x_i} \ \text{ with } i = 1,2; \\[3em]
\frac{\partial \gamma_s}{\partial R} & = & \frac{-nN}{\tan(\mathrm{p})\cdot R}, \\[1.5em]
\frac{\partial \gamma_s}{\partial \phi} & = & nN, \\[1.5em]
\frac{\partial \gamma_s}{\partial x_i} & = & \frac{\partial \gamma_s}{\partial R}\frac{\partial R}{\partial x_i} + \frac{\partial \gamma_s}{\partial \phi}\frac{\partial \phi}{\partial x_i} \ \text{ with } i = 1,2.
\end{cases}
$$

$$
\text{Second derivatives} \rightarrow
\begin{cases}
\frac{d^2\,\mathrm{K}}{d\,R^2} & = & -2\frac{d\,\mathrm{K}}{d\,R}\frac{1}{R}, \\[1.5em]
\frac{\partial^2 \mathrm{K}}{\partial x_i \partial x_j} & = & \frac{d^2\,\mathrm{K}}{d\,R^2}\left(\frac{\partial R}{\partial x_i}\frac{\partial R}{\partial x_j}\right) + \frac{d\,\mathrm{K}}{d\,R}\frac{\partial^2 R}{\partial x_i \partial x_j} \ \text{ with } i,j = 1,2; \\[3em]
\frac{\partial^2 \gamma_s}{\partial R^2} & = & -\frac{\partial \gamma_s}{\partial R}\frac{1}{R} \\[1.5em]
\frac{\partial^2 \gamma_s}{\partial x_i \partial x_j} & = & \frac{\partial \gamma_s}{\partial R}\frac{\partial^2 R}{\partial x_i \partial x_j} + \frac{\partial^2 \gamma_s}{\partial R^2}\left(\frac{\partial R}{\partial x_i}\frac{\partial R}{\partial x_j}\right) + \frac{\partial \gamma_s}{\partial \phi}\frac{\partial^2 \phi}{\partial x_i \partial x_j} \ \text{ with } i,j = 1,2.
\end{cases}
$$

Notice that we try to write the second derivatives as functions of the first derivatives whenever possible.

From Eq. B.4 we see that variables β and D depend only on the composite variable K, thus both former variables are in a second–level group in the recursive chain. Therefore:

$$\text{Composite variables} \rightarrow \begin{cases} \beta(\text{K}) &= \text{K} \cdot \text{h}_s \left[1 + 0.4\text{K} \cdot \text{h}_s \right], \\[2em] \text{D}(\text{K}) &= \frac{1 + \text{K} \cdot \text{h}_s + 0.3[\text{K} \cdot \text{h}_s]^2}{1 + 0.3\text{K} \cdot \text{h}_s}. \end{cases}$$

$$\text{First derivatives} \rightarrow \begin{cases} \frac{d\beta}{d\text{K}} &= \text{h}_s + 0.8\text{K} \cdot \text{h}_s^2, \\[1.5em] \frac{\partial\beta}{\partial x_i} &= \frac{d\beta}{d\text{K}} \frac{\partial\text{K}}{\partial x_i} \text{ with } i = 1, 2; \\[3em] \frac{d\text{D}}{d\text{K}} &= \frac{\left(\text{h}_s + 0.6\text{K} \cdot \text{h}_s^2 \right)(1 + 0.3\text{K} \cdot \text{h}_s) - \left[1 + \text{K} \cdot \text{h}_s + 0.3(\text{K} \cdot \text{h}_s)^2 \right](0.3\text{h}_s)}{(1 + 0.3\text{K} \cdot \text{h}_s)^2}, \\[1.5em] \frac{\partial\text{D}}{\partial x_i} &= \frac{d\text{D}}{d\text{K}} \frac{\partial\text{K}}{\partial x_i} \text{ with } i = 1, 2. \end{cases}$$

$$\text{Second derivatives} \rightarrow \begin{cases} \frac{d^2\beta}{d\text{K}^2} &= 0.8 \cdot \text{h}_s^2, \\[1.5em] \frac{\partial^2\beta}{\partial x_i \partial x_j} &= \frac{d^2\beta}{d\text{K}^2} \left(\frac{\partial\text{K}}{\partial x_i} \frac{\partial\text{K}}{\partial x_j} \right) + \frac{d\beta}{d\text{K}} \frac{\partial^2\text{K}}{\partial x_i \partial x_j} \text{ with } i, j = 1, 2; \\[3em] \frac{d^2\text{D}}{d\text{K}^2} &= \frac{0.6 \cdot \text{h}_s^2}{(1 + 0.3\text{K} \cdot \text{h}_s)} - \frac{0.6 \cdot \text{h}_s^2 + 0.18\text{K} \cdot \text{h}_s^3}{(1 + 0.3\text{K} \cdot \text{h}_s)^2} + \frac{0.18 \cdot \text{h}_s^2}{(1 + 0.3\text{K} \cdot \text{h}_s)^3}, \\[1.5em] \frac{\partial^2\text{D}}{\partial x_i \partial x_j} &= \frac{d^2\text{D}}{d\text{K}^2} \left(\frac{\partial\text{K}}{\partial x_i} \frac{\partial\text{K}}{\partial x_j} \right) + \frac{d\text{D}}{d\text{K}} \frac{\partial^2\text{K}}{\partial x_i \partial x_j} \text{ with } i, j = 1, 2. \end{cases}$$

Finally, we introduce a third–level group of composite quantities:

$$\text{Composite variables} \rightarrow \begin{cases} \text{OCAB}_1(\text{K}, \text{D}) & = & \frac{1}{\text{R}_s \cdot \text{D} \cdot \text{K}}; \\[2em] \text{OCAB}_2(\gamma_s) & = & \cos(\gamma_s); \\[2em] \text{OCAB}_3(\text{K}, \beta, x_3) & = & \begin{cases} \text{sech}^{\beta}\left(\frac{\text{K} \cdot x_3}{\beta}\right) & \text{if } \left|\frac{\text{K} \cdot x_3}{\beta}\right| < 20, \\[1.5em] 2^{\beta} e^{-\beta \left|\frac{\text{K} \cdot x_3}{\beta}\right|} & \text{if } \left|\frac{\text{K} \cdot x_3}{\beta}\right| \geq 20, \end{cases} \\[3em] \text{OCAB}_4(R) & = & e^{-\frac{(R - \text{R}_s)}{\text{R}_{\text{sd}}}}. \end{cases}$$

Also notice that we deal differently with the expression $\text{OCAB}_3(\text{K}, \beta, x_3)$ due to its dependence on function $\text{sech}^{\beta}\left(\frac{\text{K} \cdot x_3}{\beta}\right)$. The `FORTRAN` function in such case is the `COSH` and for many situations we found a divergent behaviour. Consequently, the algorithm turns to be unstable. In order to fix this, we consider the following line of thinking: $\ln\left[\text{sech}^{\beta}\left(\frac{\text{K} \cdot x_3}{\beta}\right)\right] = \ln\left[\cosh^{-\beta}\left(\frac{\text{K} \cdot x_3}{\beta}\right)\right] = -\beta \ln\left[\cosh\left(\frac{\text{K} \cdot x_3}{\beta}\right)\right]$. Since when $\left|\frac{\text{K} \cdot x_3}{\beta}\right| = 20$, the hyperbolic function takes the value: $\frac{1}{2}\left(e^{20} + e^{-20}\right) \sim \frac{1}{2}\left(4 \times 10^8 + 2 \times 10^{-9}\right)$ where the negative exponential does not affect any significative number given by the positive exponential part and thus, when the argument of the hyperbolic function has an absolute value ≥ 20, the latter can be simplified to a single exponential function without loosing any numerical precision in the computation. In that case, $-\beta \ln\left[\cosh\left(\frac{\text{K} \cdot x_3}{\beta}\right)\right] \rightarrow -\beta \ln\left[\frac{1}{2}e^{\left|\frac{\text{K} \cdot x_3}{\beta}\right|}\right] = -\beta\left(\left|\frac{\text{K} \cdot x_3}{\beta}\right| - \ln(2)\right)$. Then, all $\text{sech}(\cdot)$ are treated in that way, independently of its exponent.

First derivatives →

$$
\frac{d\,\mathrm{OCAB}_1}{d\,\mathrm{K}} = -\mathrm{OCAB}_1\left(\frac{1}{\mathrm{D}}\frac{d\,\mathrm{D}}{d\,\mathrm{K}} + \frac{1}{\mathrm{K}}\right),
$$

$$
\frac{\partial\mathrm{OCAB}_1}{\partial x_i} = \frac{d\,\mathrm{OCAB}_1}{d\,\mathrm{K}}\frac{\partial\mathrm{K}}{\partial x_i} \ \text{with } i = 1,2;
$$

$$
\frac{d\,\mathrm{OCAB}_2}{d\,\gamma_s} = -\sin(\gamma_s),
$$

$$
\frac{\partial\mathrm{OCAB}_2}{\partial x_i} = \frac{d\,\mathrm{OCAB}_2}{d\,\gamma_s}\frac{\partial\gamma_s}{\partial x_i} \ \text{with } i = 1,2;
$$

$$
\frac{\partial\mathrm{OCAB}_3}{\partial\mathrm{K}} = \begin{cases} \mathrm{OCAB}_3 \cdot \left\{\frac{d\,\beta}{d\,\mathrm{K}}\ln\left[\mathrm{sech}\left(\frac{\mathrm{K}\cdot x_3}{\beta}\right)\right] - \right. \\[2mm] \left. -\beta\cdot\tanh\left(\frac{\mathrm{K}\cdot x_3}{\beta}\right)\left[\frac{x_3}{\beta} - \frac{\mathrm{K}\cdot x_3}{\beta^2}\frac{d\,\beta}{d\,\mathrm{K}}\right]\right\} \ \text{if } \left|\frac{\mathrm{K}\cdot x_3}{\beta}\right| < 20, \\[4mm] \mathrm{OCAB}_3 \cdot \left\{\frac{d\,\beta}{d\,\mathrm{K}}\left[\ln(2) - \left|\frac{\mathrm{K}\cdot x_3}{\beta}\right|\right] - \right. \\[2mm] \left. -\beta\cdot\tanh\left(\frac{\mathrm{K}\cdot x_3}{\beta}\right)\left[\frac{x_3}{\beta} - \frac{\mathrm{K}\cdot x_3}{\beta^2}\frac{d\,\beta}{d\,\mathrm{K}}\right]\right\} \ \text{if } \left|\frac{\mathrm{K}\cdot x_3}{\beta}\right| \geq 20, \end{cases}
$$

$$
\frac{\partial\mathrm{OCAB}_3}{\partial x_i} = \frac{\partial\mathrm{OCAB}_3}{\partial\mathrm{K}}\frac{\partial\mathrm{K}}{\partial x_i} \ \text{with } i = 1,2,
$$

$$
\frac{\partial\mathrm{OCAB}_3}{\partial x_3} = -\mathrm{OCAB}_3 \cdot \mathrm{K}\tanh\left(\frac{\mathrm{K}\cdot x_3}{\beta}\right);
$$

$$
\frac{d\,\mathrm{OCAB}_4}{d\,R} = -\frac{\mathrm{OCAB}_4}{\mathrm{R}_{\mathrm{sd}}},
$$

$$
\frac{\partial\mathrm{OCAB}_4}{\partial x_i} = \frac{d\,\mathrm{OCAB}_4}{d\,R}\frac{\partial R}{\partial x_i} \ \text{with } i = 1,2.
$$

The reader may notice that in the first derivatives of third–level group composite variables, it seems to be that $\frac{\partial\mathrm{OCAB}_1}{\partial\mathrm{D}}$ and $\frac{\partial\mathrm{OCAB}_3}{\partial\beta}$ are missing in order to have a complete recursive structure. However, D as well as β (second–level group) are functions of K and the latter also appears explicitly in the expressions (and not only through D or β). Then, we choose to use $\frac{d\,\mathrm{OCAB}_1}{d\,\mathrm{K}}$ and $\frac{\partial\mathrm{OCAB}_3}{\partial\mathrm{K}}$ alone.

$$\frac{d^2\,\mathrm{OCAB_1}}{d\,\mathrm{K}^2} = -\left(\tfrac{1}{\mathrm{D}}\tfrac{d\,\mathrm{D}}{d\,\mathrm{K}} + \tfrac{1}{\mathrm{K}}\right)\left(\tfrac{d\,\mathrm{OCAB_1}}{d\,\mathrm{K}}\right) +$$

$$+\mathrm{OCAB_1}\left[\tfrac{1}{\mathrm{D}^2}\left(\tfrac{d\,\mathrm{D}}{d\,\mathrm{K}}\right)^2 - \tfrac{1}{\mathrm{D}}\tfrac{d^2\,\mathrm{D}}{d\,\mathrm{K}^2} + \tfrac{1}{\mathrm{K}^2}\right],$$

$$\frac{\partial^2\mathrm{OCAB_1}}{\partial x_i\partial x_j} = \frac{d^2\,\mathrm{OCAB_1}}{d\,\mathrm{K}^2}\left(\frac{\partial\mathrm{K}}{\partial x_i}\frac{\partial\mathrm{K}}{\partial x_j}\right) + \frac{d\,\mathrm{OCAB_1}}{d\,\mathrm{K}}\frac{\partial^2\mathrm{K}}{\partial x_i\partial x_j}\ \text{ with } i,j = 1,2;$$

$$\frac{d^2\,\mathrm{OCAB_2}}{d\,\gamma_s^2} = -\cos(\gamma_s),$$

$$\frac{\partial^2\mathrm{OCAB_2}}{\partial x_i\partial x_j} = \frac{d^2\,\mathrm{OCAB_2}}{d\,\gamma_s^2}\left(\frac{\partial\gamma_s}{\partial x_i}\frac{\partial\gamma_s}{\partial x_j}\right) + \frac{d\,\mathrm{OCAB_2}}{d\,\gamma_s}\frac{\partial^2\gamma_s}{\partial x_i\partial x_j}\ \text{ with } i,j = 1,2;$$

Second derivatives →

$$\frac{\partial^2\mathrm{OCAB_3}}{\partial\mathrm{K}^2} = \begin{cases} \left\{\frac{d\,\beta}{d\,\mathrm{K}}\ln\left[\mathrm{sech}\left(\frac{\mathrm{K}\cdot x_3}{\beta}\right)\right] - \beta\cdot\tanh\left(\frac{\mathrm{K}\cdot x_3}{\beta}\right)\left[\frac{x_3}{\beta} - \frac{\mathrm{K}\cdot x_3}{\beta^2}\frac{d\,\beta}{d\,\mathrm{K}}\right]\right\}\cdot \\[2mm] \cdot\left(\frac{\partial\mathrm{OCAB_3}}{\partial\mathrm{K}}\right) + \mathrm{OCAB_3}\left\{\frac{\partial^2\beta}{\partial\mathrm{K}^2}\left[\ln\left(\mathrm{sech}\left(\frac{\mathrm{K}\cdot x_3}{\beta}\right)\right)\right] + \right. \\[2mm] \left. +\tanh\left(\frac{\mathrm{K}\cdot x_3}{\beta}\right)\frac{\mathrm{K}\cdot x_3}{\beta}\right] + \left(\frac{\partial\beta}{\partial\mathrm{K}}\right)^2\left[-\mathrm{sech}^2\left(\frac{\mathrm{K}\cdot x_3}{\beta}\right)\frac{\mathrm{K}^2\cdot x_3^2}{\beta^3}\right] + \\[2mm] +\frac{\partial\beta}{\partial\mathrm{K}}\left[2\mathrm{sech}^2\left(\frac{\mathrm{K}\cdot x_3}{\beta}\right)\frac{\mathrm{K}\cdot x_3^2}{\beta^2}\right] - \mathrm{sech}^2\left(\frac{\mathrm{K}\cdot x_3}{\beta}\right)\frac{x_3^2}{\beta}\right\}\ \text{if }\left|\frac{\mathrm{K}\cdot x_3}{\beta}\right| < 20, \\[4mm] \left\{\frac{d\,\beta}{d\,\mathrm{K}}\left[\ln(2) - \left|\frac{\mathrm{K}\cdot x_3}{\beta}\right|\right] - \beta\cdot\tanh\left(\frac{\mathrm{K}\cdot x_3}{\beta}\right)\left[\frac{x_3}{\beta} - \frac{\mathrm{K}\cdot x_3}{\beta^2}\frac{d\,\beta}{d\,\mathrm{K}}\right]\right\}\cdot \\[2mm] \cdot\left(\frac{\partial\mathrm{OCAB_3}}{\partial\mathrm{K}}\right) + \mathrm{OCAB_3}\left\{\frac{\partial^2\beta}{\partial\mathrm{K}^2}\left[\ln(2) - \left|\frac{\mathrm{K}\cdot x_3}{\beta}\right| + \right.\right. \\[2mm] \left. +\tanh\left(\frac{\mathrm{K}\cdot x_3}{\beta}\right)\frac{\mathrm{K}\cdot x_3}{\beta}\right] + \left(\frac{\partial\beta}{\partial\mathrm{K}}\right)^2\left[-4e^{-2\left|\frac{\mathrm{K}\cdot x_3}{\beta}\right|}\frac{\mathrm{K}^2\cdot x_3^2}{\beta^3}\right] + \\[2mm] +\frac{\partial\beta}{\partial\mathrm{K}}\left[8e^{-2\left|\frac{\mathrm{K}\cdot x_3}{\beta}\right|}\frac{\mathrm{K}\cdot x_3^2}{\beta^2}\right] - 4e^{-2\left|\frac{\mathrm{K}\cdot x_3}{\beta}\right|}\frac{x_3^2}{\beta}\right\}\ \text{if }\left|\frac{\mathrm{K}\cdot x_3}{\beta}\right| \geq 20, \end{cases}$$

$$\frac{\partial^2\mathrm{OCAB_3}}{\partial x_3\partial\mathrm{K}} = \begin{cases} \left\{\frac{d\,\beta}{d\,\mathrm{K}}\ln\left[\mathrm{sech}\left(\frac{\mathrm{K}\cdot x_3}{\beta}\right)\right] - \beta\cdot\tanh\left(\frac{\mathrm{K}\cdot x_3}{\beta}\right)\left[\frac{x_3}{\beta} - \frac{\mathrm{K}\cdot x_3}{\beta^2}\frac{d\,\beta}{d\,\mathrm{K}}\right]\right\}\cdot \\[2mm] \cdot\left(\frac{\partial\mathrm{OCAB_3}}{\partial x_3}\right) + \mathrm{OCAB_3}\left[\mathrm{sech}^2\left(\frac{\mathrm{K}\cdot x_3}{\beta}\right)\left(\frac{\mathrm{K}^2\cdot x_3}{\beta^2}\frac{\partial\beta}{\partial\mathrm{K}} - \frac{\mathrm{K}\cdot x_3}{\beta}\right) - \right. \\[2mm] \left. -\tanh\left(\frac{\mathrm{K}\cdot x_3}{\beta}\right)\right]\ \text{if }\left|\frac{\mathrm{K}\cdot x_3}{\beta}\right| < 20, \\[4mm] \left\{\frac{d\,\beta}{d\,\mathrm{K}}\left[\ln(2) - \left|\frac{\mathrm{K}\cdot x_3}{\beta}\right|\right] - \beta\cdot\tanh\left(\frac{\mathrm{K}\cdot x_3}{\beta}\right)\left[\frac{x_3}{\beta} - \frac{\mathrm{K}\cdot x_3}{\beta^2}\frac{d\,\beta}{d\,\mathrm{K}}\right]\right\}\cdot \\[2mm] \cdot\left(\frac{\partial\mathrm{OCAB_3}}{\partial x_3}\right) + \mathrm{OCAB_3}\left[4e^{-2\left|\frac{\mathrm{K}\cdot x_3}{\beta}\right|}\left(\frac{\mathrm{K}^2\cdot x_3}{\beta^2}\frac{\partial\beta}{\partial\mathrm{K}} - \frac{\mathrm{K}\cdot x_3}{\beta}\right) - \right. \\[2mm] \left. -\tanh\left(\frac{\mathrm{K}\cdot x_3}{\beta}\right)\right]\ \text{if }\left|\frac{\mathrm{K}\cdot x_3}{\beta}\right| \geq 20, \end{cases}$$

Second derivatives (cont.) $\rightarrow$

$$
\begin{cases}
\dfrac{\partial^2 \mathrm{OCAB_3}}{\partial x_i \partial x_j} &= \dfrac{\partial^2 \mathrm{OCAB_3}}{\partial \mathrm{K}^2}\left(\dfrac{\partial \mathrm{K}}{\partial x_i}\dfrac{\partial \mathrm{K}}{\partial x_j}\right) + \dfrac{\partial \mathrm{OCAB_3}}{\partial \mathrm{K}}\dfrac{\partial^2 \mathrm{K}}{\partial x_i \partial x_j} \ \text{ with } i,j=1,2; \\[2ex]
\dfrac{\partial^2 \mathrm{OCAB_3}}{\partial x_3 \partial x_i} &= \dfrac{\partial^2 \mathrm{OCAB_3}}{\partial x_3 \partial \mathrm{K}}\dfrac{\partial \mathrm{K}}{\partial x_i} \ \text{ with } i=1,2; \\[2ex]
\dfrac{\partial^2 \mathrm{OCAB_3}}{\partial x_3^2} &= \begin{cases} -\mathrm{K}\tanh\left(\dfrac{\mathrm{K}\cdot x_3}{\beta}\right)\left(\dfrac{\partial \mathrm{OCAB_3}}{\partial x_3}\right)+ \\[2ex] +\mathrm{OCAB_3}\cdot\dfrac{\mathrm{K}}{\beta}\mathrm{sech}^2\left(\dfrac{\mathrm{K}\cdot x_3}{\beta}\right) \text{ if } \left|\dfrac{\mathrm{K}\cdot x_3}{\beta}\right|<20, \\[2ex] -\mathrm{K}\tanh\left(\dfrac{\mathrm{K}\cdot x_3}{\beta}\right)\left(\dfrac{\partial \mathrm{OCAB_3}}{\partial x_3}\right)+ \\[2ex] +\mathrm{OCAB_3}\cdot\dfrac{\mathrm{K}}{\beta}\left(4e^{-2\left|\frac{\mathrm{K}\cdot x_3}{\beta}\right|}\right) \text{ if } \left|\dfrac{\mathrm{K}\cdot x_3}{\beta}\right|\geq 20; \end{cases} \\[10ex]
\dfrac{d^2\,\mathrm{OCAB_4}}{d\,R^2} &= \dfrac{\mathrm{OCAB_4}}{\mathrm{R}_{\mathrm{sd}}^2}, \\[2ex]
\dfrac{\partial^2 \mathrm{OCAB_4}}{\partial x_i \partial x_j} &= \dfrac{d^2\,\mathrm{OCAB_4}}{d\,R^2}\dfrac{\partial R}{\partial x_i}\dfrac{\partial R}{\partial x_j} - \dfrac{1}{\mathrm{R}_{\mathrm{sd}}}\mathrm{OCAB_4}\dfrac{\partial^2 R}{\partial x_i \partial x_j} \ \text{ with } i,j=1,2.
\end{cases}
$$

Furthermore, the following expressions: $\frac{\partial^2 \mathrm{OCAB_3}}{\partial \mathrm{K}^2}$, $\frac{\partial^2 \mathrm{OCAB_3}}{\partial x_3 \partial \mathrm{K}}$ and $\frac{\partial^2 \mathrm{OCAB_3}}{\partial x_3^2}$ are written in a less recursive fashion in order to avoid non–essential singularities due to the $\mathrm{OCAB_3}$ term. Then, we can rewrite the potential associated with the spiral arms (Eq. B.4), and the corresponding derivatives like:

Potential $\rightarrow$

$$
\begin{cases}
\Phi_{spiral} &= -\mathrm{A}\cdot\mathrm{OCAB_1}\mathrm{OCAB_2}\mathrm{OCAB_3}\mathrm{OCAB_4}.
\end{cases}
$$

$$\text{First derivatives} \rightarrow \begin{cases} \dfrac{\partial \Phi_{spiral}}{\partial \text{OCAB}_1} &= -\text{A} \cdot \text{OCAB}_2\text{OCAB}_3\text{OCAB}_4, \\[2.5em] \dfrac{\partial \Phi_{spiral}}{\partial \text{OCAB}_2} &= -\text{A} \cdot \text{OCAB}_1\text{OCAB}_3\text{OCAB}_4, \\[2.5em] \dfrac{\partial \Phi_{spiral}}{\partial \text{OCAB}_3} &= -\text{A} \cdot \text{OCAB}_1\text{OCAB}_2\text{OCAB}_4, \\[2.5em] \dfrac{\partial \Phi_{spiral}}{\partial \text{OCAB}_4} &= -\text{A} \cdot \text{OCAB}_1\text{OCAB}_2\text{OCAB}_3; \\[4em] \dfrac{\partial \Phi_{spiral}}{\partial x_i} &= \dfrac{\partial \Phi_{spiral}}{\partial \text{OCAB}_1}\dfrac{\partial \text{OCAB}_1}{\partial x_i} + \dfrac{\partial \Phi_{spiral}}{\partial \text{OCAB}_2}\dfrac{\partial \text{OCAB}_2}{\partial x_i} + \dfrac{\partial \Phi_{spiral}}{\partial \text{OCAB}_3}\dfrac{\partial \text{OCAB}_3}{\partial x_i} + \\[2.5em] &\quad + \dfrac{\partial \Phi_{spiral}}{\partial \text{OCAB}_4}\dfrac{\partial \text{OCAB}_4}{\partial x_i} \ \text{ with } i = 1, 2, \\[2.5em] \dfrac{\partial \Phi_{spiral}}{\partial x_3} &= \dfrac{\partial \Phi_{spiral}}{\partial \text{OCAB}_3}\dfrac{\partial \text{OCAB}_3}{\partial x_3}. \end{cases}$$

Second derivatives →

$$\frac{\partial^2 \Phi_{spiral}}{\partial \text{OCAB}_1 \partial \text{OCAB}_2} = -\text{A} \cdot \text{OCAB}_3 \text{OCAB}_4,$$

$$\frac{\partial^2 \Phi_{spiral}}{\partial \text{OCAB}_1 \partial \text{OCAB}_3} = -\text{A} \cdot \text{OCAB}_2 \text{OCAB}_4,$$

$$\frac{\partial^2 \Phi_{spiral}}{\partial \text{OCAB}_1 \partial \text{OCAB}_4} = -\text{A} \cdot \text{OCAB}_2 \text{OCAB}_3,$$

$$\frac{\partial^2 \Phi_{spiral}}{\partial \text{OCAB}_2 \partial \text{OCAB}_3} = -\text{A} \cdot \text{OCAB}_1 \text{OCAB}_4,$$

$$\frac{\partial^2 \Phi_{spiral}}{\partial \text{OCAB}_2 \partial \text{OCAB}_4} = -\text{A} \cdot \text{OCAB}_1 \text{OCAB}_3,$$

$$\frac{\partial^2 \Phi_{spiral}}{\partial \text{OCAB}_3 \partial \text{OCAB}_4} = -\text{A} \cdot \text{OCAB}_1 \text{OCAB}_2;$$

$$\frac{\partial^2 \Phi_{spiral}}{\partial x_i \partial x_j} = \frac{\partial^2 \Phi_{spiral}}{\partial \text{OCAB}_1 \partial \text{OCAB}_2} \left(\frac{\partial \text{OCAB}_1}{\partial x_i} \frac{\partial \text{OCAB}_2}{\partial x_j} + \frac{\partial \text{OCAB}_1}{\partial x_j} \frac{\partial \text{OCAB}_2}{\partial x_i} \right) +$$

$$+ \frac{\partial^2 \Phi_{spiral}}{\partial \text{OCAB}_1 \partial \text{OCAB}_3} \left(\frac{\partial \text{OCAB}_1}{\partial x_i} \frac{\partial \text{OCAB}_3}{\partial x_j} + \frac{\partial \text{OCAB}_1}{\partial x_j} \frac{\partial \text{OCAB}_3}{\partial x_i} \right) +$$

$$+ \frac{\partial^2 \Phi_{spiral}}{\partial \text{OCAB}_1 \partial \text{OCAB}_4} \left(\frac{\partial \text{OCAB}_1}{\partial x_i} \frac{\partial \text{OCAB}_4}{\partial x_j} + \frac{\partial \text{OCAB}_1}{\partial x_j} \frac{\partial \text{OCAB}_4}{\partial x_i} \right) +$$

$$+ \frac{\partial^2 \Phi_{spiral}}{\partial \text{OCAB}_2 \partial \text{OCAB}_3} \left(\frac{\partial \text{OCAB}_2}{\partial x_i} \frac{\partial \text{OCAB}_3}{\partial x_j} + \frac{\partial \text{OCAB}_2}{\partial x_j} \frac{\partial \text{OCAB}_3}{\partial x_i} \right) +$$

$$+ \frac{\partial^2 \Phi_{spiral}}{\partial \text{OCAB}_2 \partial \text{OCAB}_4} \left(\frac{\partial \text{OCAB}_2}{\partial x_i} \frac{\partial \text{OCAB}_4}{\partial x_j} + \frac{\partial \text{OCAB}_2}{\partial x_j} \frac{\partial \text{OCAB}_4}{\partial x_i} \right) +$$

$$+ \frac{\partial^2 \Phi_{spiral}}{\partial \text{OCAB}_3 \partial \text{OCAB}_4} \left(\frac{\partial \text{OCAB}_3}{\partial x_i} \frac{\partial \text{OCAB}_4}{\partial x_j} + \frac{\partial \text{OCAB}_3}{\partial x_j} \frac{\partial \text{OCAB}_4}{\partial x_i} \right) +$$

$$+ \frac{\partial \Phi_{spiral}}{\partial \text{OCAB}_1} \frac{\partial^2 \text{OCAB}_1}{\partial x_i \partial x_j} + \frac{\partial \Phi_{spiral}}{\partial \text{OCAB}_2} \frac{\partial^2 \text{OCAB}_2}{\partial x_i \partial x_j} +$$

$$+ \frac{\partial \Phi_{spiral}}{\partial \text{OCAB}_3} \frac{\partial^2 \text{OCAB}_3}{\partial x_i \partial x_j} + \frac{\partial \Phi_{spiral}}{\partial \text{OCAB}_4} \frac{\partial^2 \text{OCAB}_4}{\partial x_i \partial x_j} \text{ with } i, j = 1, 2,$$

$$\frac{\partial^2 \Phi_{spiral}}{\partial x_3 \partial x_i} = \frac{\partial^2 \Phi_{spiral}}{\partial \text{OCAB}_1 \partial \text{OCAB}_3} \frac{\partial \text{OCAB}_3}{\partial x_3} \frac{\partial \text{OCAB}_1}{\partial x_i} + \frac{\partial^2 \Phi_{spiral}}{\partial \text{OCAB}_2 \partial \text{OCAB}_3} \frac{\partial \text{OCAB}_3}{\partial x_3} \frac{\partial \text{OCAB}_2}{\partial x_i} +$$

$$+ \frac{\partial^2 \Phi_{spiral}}{\partial \text{OCAB}_3 \partial \text{OCAB}_4} \frac{\partial \text{OCAB}_3}{\partial x_3} \frac{\partial \text{OCAB}_4}{\partial x_i} + \frac{\partial \Phi_{spiral}}{\partial \text{OCAB}_3} \frac{\partial^2 \text{OCAB}_3}{\partial x_3 \partial x_i} \text{ with } i = 1, 2,$$

$$\frac{\partial^2 \Phi_{spiral}}{\partial x_3^2} = \frac{\partial \Phi_{spiral}}{\partial \text{OCAB}_3} \frac{\partial^2 \text{OCAB}_3}{\partial x_3^2},$$

with $x_1 = x$, $x_2 = y$ and $x_3 = z$.

B.1.4   The disk

Being the potential of one MN profile:

$$\Phi_{disk} = -\frac{GM_{disk}}{\sqrt{x^2 + y^2 + \left(\epsilon_s + \sqrt{z^2 + \epsilon_h^2}\right)^2}}, \tag{B.5}$$

and introducing the quantities:

$$\begin{cases} \mathrm{R}_{disk:1} & = \quad \epsilon_s + \sqrt{z^2 + \epsilon_h^2}, \\[2ex] \mathrm{R}_{disk:2} & = \quad \sqrt{x^2 + y^2 + \mathrm{R}_{disk:1}^2}, \\[2ex] \frac{\partial \mathrm{R}_{disk:2}}{\partial x_i} & = \quad \frac{x_i}{\mathrm{R}_{disk:2}}, \\[2ex] \frac{\partial \mathrm{R}_{disk:2}}{\partial x_3} & = \quad \frac{x_3 \mathrm{R}_{disk:1}}{\mathrm{R}_{disk:2}(\mathrm{R}_{disk:1} - \epsilon_s)}, \end{cases}$$

we can rewrite the potential associated with the disk (Eq. B.5), and the corresponding derivatives like:

$$\begin{cases} \Phi_{disk} & = \quad -\frac{GM_{disk}}{\mathrm{R}_{disk:2}}, \\[2ex] \frac{\partial \Phi_{disk}}{\partial x_i} & = \quad -\frac{\Phi_{disk}}{\mathrm{R}_{disk:2}} \frac{\partial \mathrm{R}_{disk:2}}{\partial x_i}, \\[2ex] \frac{\partial}{\partial x_i}\left(\frac{\partial \Phi_{disk}}{\partial x_j}\right) & = \quad \left\{-\frac{3}{\mathrm{R}_{disk:2}} \frac{\partial \mathrm{R}_{disk:2}}{\partial x_i} + \left[\frac{x_i}{\mathrm{R}_{disk:1} - \epsilon_s}\left(\frac{1}{\mathrm{R}_{disk:1}} - \frac{1}{\mathrm{R}_{disk:1} - \epsilon_s}\right)\delta_{3i} + \frac{1}{x_i}\right]\delta_{ij}\right\} \frac{\partial \Phi_{disk}}{\partial x_j}, \end{cases}$$

with $x_1 = x$, $x_2 = y$ y $x_3 = z$.

However, the second derivatives have a non–essential singularity (indicated in red). Therefore, next we expand and rewrite such expressions to show in this simple case[2] how we deal with these kind of singularities:

---

[2] The reader may remember the non–essential singularities mentioned in the spiral arms potential (Section B.1.3), but their treatment is much longer to describe so we decided to show the general treatment applied to this sort of singularities only in this case.

$$
\left\{
\begin{aligned}
\frac{\partial}{\partial x_i}\left(\frac{\partial \Phi_{disk}}{\partial x_j}\right) &= -\frac{3}{\mathrm{R}_{disk:2}}\frac{\partial \mathrm{R}_{disk:2}}{\partial x_i}\frac{\partial \Phi_{disk}}{\partial x_j} && \text{si } i \neq j \\[2ex]
\frac{\partial^2 \Phi_{disk}}{\partial x_i^2} &= \left(-\frac{3}{\mathrm{R}_{disk:2}}\frac{\partial \mathrm{R}_{disk:2}}{\partial x_i}\right)\frac{\partial \Phi_{disk}}{\partial x_i} - \frac{\Phi_{disk}}{\mathrm{R}_{disk:2}^2} && \text{si } i = j \neq 3 \\[2ex]
\frac{\partial^2 \Phi_{disk}}{\partial x_3^2} &= \left\{-\frac{3}{\mathrm{R}_{disk:2}}\frac{\partial \mathrm{R}_{disk:2}}{\partial x_3} + \left[\frac{x_3}{\mathrm{R}_{disk:1-\epsilon_s}}\left(\frac{1}{\mathrm{R}_{disk:1}} - \frac{1}{\mathrm{R}_{disk:1-\epsilon_s}}\right)\right]\right\}\frac{\partial \Phi_{disk}}{\partial x_3} - \frac{\Phi_{disk}}{\mathrm{R}_{disk:2}^2}\frac{\mathrm{R}_{disk:1}}{\mathrm{R}_{disk:1-\epsilon_s}}
\end{aligned}
\right.
$$

We presented here the first and second derivatives of one MN profile, but in order to build an exponential profile, we consider the sum of three MN profiles (see Section 2.2.4.2 for further details). However, due to the linearity of first and second derivatives as the user is perfectly aware of, the derivatives of three MN disks is just the sum of the derivatives of each MN disk, and there is no need to compute more derivatives, just copy and paste as many times as MN disks the model has.

B.1.5   The dark matter halo

B.1.5.1   Option (1): a bi–triaxial extension of the NFW DMH

Being the potential:

$$
\Phi_{dmh1} = -\frac{GM_{200}}{\left[\ln(1 + c_{\mathrm{nfw}}) - \frac{c_{\mathrm{nfw}}}{1+c_{\mathrm{nfw}}}\right]r'}\ln\left[1 + \frac{r'}{r_s}\right], \tag{B.6}
$$

and introducing the quantities:

$$
\begin{cases}
A_d &= \dfrac{GM_{200}}{\ln(1+c_{\mathrm{nfw}})-\frac{c_{\mathrm{nfw}}}{1+c_{\mathrm{nfw}}}}, \\[2ex]
B &= r_s + r_{oe}, \\[2ex]
r_{ie} &= \sqrt{\frac{x^2}{a^2}+\frac{y^2}{b^2}+\frac{z^2}{c^2}}, \\[2ex]
r_{oe} &= \sqrt{\frac{x^2}{a'^2}+\frac{y^2}{b'^2}+\frac{z^2}{c'^2}}, \\[2ex]
C &= r_{ie} + r_s, \\[2ex]
r' &= \frac{B r_{ie}}{C}, \\[2ex]
D &= \left(\frac{B-r'}{C}\right), \\[2ex]
\frac{\partial r_{oe}}{\partial x_i} &= \frac{x_i}{d_i'^2 r_{oe}}, \\[2ex]
\frac{\partial r_{ie}}{\partial x_i} &= \frac{x_i}{d_i^2 r_{ie}}, \\[2ex]
\frac{\partial r'}{\partial x_i} &= \frac{r_{ie}}{C}\frac{\partial r_{oe}}{\partial x_i} + D\frac{\partial r_{ie}}{\partial x_i}, \\[2ex]
E_i &= \frac{\partial r_{ie}}{\partial x_i}\frac{1}{C}\left(1-\frac{r_{ie}}{C}\right), \\[2ex]
F_i &= \frac{1}{C}\left(\frac{\partial r_{oe}}{\partial x_i} - \frac{\partial r'}{\partial x_i} - \frac{\partial r_{ie}}{\partial x_i}D\right), \\[2ex]
\frac{\partial^2 r_{oe}}{\partial x_i^2} &= \frac{1}{r_{oe}}\left[\frac{1}{d_i'^2}-\left(\frac{\partial r_{oe}}{\partial x_i}\right)^2\right], \\[2ex]
\frac{\partial^2 r_{oe}}{\partial x_i \partial x_j} &= -\frac{1}{r_{oe}}\frac{\partial r_{oe}}{\partial x_i}\frac{\partial r_{oe}}{\partial x_j}, \\[2ex]
\frac{\partial^2 r_{ie}}{\partial x_i^2} &= \frac{1}{r_{ie}}\left[\frac{1}{d_i^2}-\left(\frac{\partial r_{ie}}{\partial x_i}\right)^2\right], \\[2ex]
\frac{\partial^2 r_{ie}}{\partial x_i \partial x_j} &= -\frac{1}{r_{ie}}\frac{\partial r_{ie}}{\partial x_i}\frac{\partial r_{ie}}{\partial x_j}, \\[2ex]
\frac{\partial^2 r'}{\partial x_i \partial x_j} &= \frac{\partial^2 r_{oe}}{\partial x_i \partial x_j}\frac{r_{ie}}{C} + \frac{\partial r_{oe}}{\partial x_i}E_j + \frac{\partial^2 r_E}{\partial x_i \partial x_j}D + \frac{\partial r_{ie}}{\partial x_i}F_j,
\end{cases}
$$

we can rewrite the potential associated with the DMH1 (Eq. B.6), and the corresponding derivatives like:

$$
\left\{
\begin{aligned}
\Phi_{dmh1} &= -\frac{A_d}{r'} \ln\left[1 + \frac{r'}{r_s}\right], \\[2mm]
\frac{\partial \Phi_{dmh1}}{\partial r'} &= -\left(\frac{\Phi_{dmh1}}{r'} + \frac{A_d}{r'(r_s+r')}\right), \\[2mm]
\frac{\partial \Phi_{dmh1}}{\partial x_i} &= \frac{\partial \Phi_{dmh1}}{\partial r'}\frac{\partial r'}{\partial x_i}, \\[2mm]
\frac{\partial^2 \Phi_{dmh1}}{\partial r'^2} &= \frac{\Phi_{dmh1}}{r'^2} - \frac{1}{r'}\frac{\partial \Phi_{dmh1}}{\partial r'} + \frac{A_d(r_s+2r')}{r'^2(r_s+r')^2}, \\[2mm]
\frac{\partial^2 \Phi_{dmh1}}{\partial x_i \partial r'} &= \frac{\partial^2 \Phi_{dmh1}}{\partial r'^2}\frac{\partial r'}{\partial x_i}, \\[2mm]
\frac{\partial^2 \Phi_{dmh1}}{\partial x_i \partial x_j} &= \frac{\partial^2 \Phi_{dmh1}}{\partial x_i \partial r'}\frac{\partial r'}{\partial x_j} + \frac{\partial \Phi_{dmh1}}{\partial r'}\frac{\partial^2 r'}{\partial x_i \partial x_j},
\end{aligned}
\right.
$$

with $x_1 = x$, $x_2 = y$ and $x_3 = z$ and $d_1 = a$, $d_2 = b$, $d_3 = c$, $d'_1 = a'$, $d'_2 = b'$ and $d'_3 = c'$.

B.1.5.2 Option (2): a modified logarithmic DMH

Being the potential:

$$
\Phi_{dmh2} = v_{halo}^2 \ln[(r^\star)^2 + d^2),
$$

and introducing the quantities:

$$
\left\{
\begin{aligned}
r_{ie} &= \sqrt{x^2 + y^2 + \frac{z^2}{q_z^2}}, \\[2ex]
r_{oe} &= \sqrt{\mathrm{W}x^2 + \mathrm{V}y^2 + \mathrm{U}xy + \frac{z^2}{q_3^2}}, \\[2ex]
\mathrm{T} &= \frac{r_{ie}}{r_a + r_{ie}}, \\[2ex]
r^{\star} &= (r_a + r_{oe})\mathrm{T}, \\[2ex]
\mathrm{Q} &= r^{\star}\frac{r_a}{r_{ie}(r_a + r_{ie})}, \\[2ex]
\frac{\partial r_{ie}}{\partial x_i} &= \frac{x_i}{q_{x_i}^2 r_{ie}}, \\[2ex]
\frac{\partial r_{oe}}{\partial x_i} &= \left[\left(\frac{2\mathrm{W}x + \mathrm{U}y}{2}\right)\delta_{1i} + \left(\frac{2\mathrm{V}y + \mathrm{U}x}{2}\right)\delta_{2i} + \frac{z}{q_3^2}\delta_{3i}\right]\frac{1}{r_{oe}}, \\[2ex]
\frac{\partial r^{\star}}{\partial x_i} &= \mathrm{T}\frac{\partial r_{oe}}{\partial x_i} + \mathrm{Q}\frac{\partial r_{ie}}{\partial x_i}, \\[2ex]
\frac{\partial \mathrm{T}}{\partial x_i} &= \mathrm{T}\frac{r_a}{(r_a + r_{ie})r_{ie}}\frac{\partial r_{ie}}{\partial x_i}, \\[2ex]
\frac{\partial \mathrm{Q}}{\partial x_i} &= \mathrm{T}\frac{r_a}{(r_a + r_{ie})r_{ie}}\frac{\partial r_{oe}}{\partial x_i} - \mathrm{Q}\frac{2}{r_a + r_{ie}}\frac{\partial r_{ie}}{\partial x_i}, \\[2ex]
\frac{\partial^2 r_{ie}}{\partial x_i \partial x_j} &= \left(\frac{\delta_{ij}}{q_{x_i}^2} - \frac{\partial r_{ie}}{\partial x_i}\frac{\partial r_{ie}}{\partial x_j}\right)\frac{1}{r_{ie}}, \\[2ex]
\frac{\partial^2 r_{oe}}{\partial x_i \partial x_j} &= \left[\left(\mathrm{W}\delta_{1i} + \mathrm{V}\delta_{2i} + \frac{\delta_{3i}}{q_3^2}\right)\delta_{ij} + \frac{\mathrm{U}}{2}(\delta_{i1}\delta_{2j} + \delta_{i2}\delta_{1j}) - \frac{\partial r_{oe}}{\partial x_i}\frac{\partial r_{oe}}{\partial x_j}\right]\frac{1}{r_{oe}}, \\[2ex]
\frac{\partial^2 r^{\star}}{\partial x_i \partial x_j} &= \mathrm{T}\frac{\partial^2 r_{oe}}{\partial x_i \partial x_j} + \frac{\partial r_{oe}}{\partial x_j}\frac{\partial \mathrm{T}}{\partial x_i} + \mathrm{Q}\frac{\partial^2 r_{ie}}{\partial x_i \partial x_j} + \frac{\partial r_{ie}}{\partial x_j}\frac{\partial \mathrm{Q}}{\partial x_i},
\end{aligned}
\right.
$$

we can rewrite the corresponding derivatives like:

$$
\begin{cases}
\dfrac{\partial \Phi_{dmh2}}{\partial r^\star} &=\quad \dfrac{2v_{halo}^2}{(r^\star)^2+d^2}r^\star, \\[2.5em]
\dfrac{\partial \Phi_{dmh2}}{\partial x_i} &=\quad \dfrac{\partial \Phi_{dmh2}}{\partial r^\star}\dfrac{\partial r^\star}{\partial x_i}, \\[2.5em]
\dfrac{\partial^2 \Phi_{dmh2}}{\partial r^{\star 2}} &=\quad \dfrac{2v_{halo}^2[d^2-(r^\star)^2]}{[(r^\star)^2+d^2]^2}, \\[2.5em]
\dfrac{\partial^2 \Phi_{dmh2}}{\partial x_i \partial r^\star} &=\quad \dfrac{\partial^2 \Phi_{dmh2}}{\partial r^{\star 2}}\dfrac{\partial r^\star}{\partial x_i}, \\[2.5em]
\dfrac{\partial^2 \Phi_{dmh2}}{\partial x_i \partial x_j} &=\quad \dfrac{\partial^2 \Phi_{dmh2}}{\partial x_i \partial r^\star}\dfrac{\partial r^\star}{\partial x_j}+\dfrac{\partial \Phi_{dmh2}}{\partial r^\star}\dfrac{\partial^2 r^\star}{\partial x_i \partial x_j},
\end{cases}
$$

with $x_1 = x$, $x_2 = y$ and $x_3 = z$ and $q_x = 1$, $q_y = 1$ and q_z.

Now that we have calculated all the first and second derivatives of every galactic component, in next section we proceed with the construction of the equations of motion and first variational equations in order to compute the CIs.

B.2   Equations of motion

Finally, we have the full `MWH` 2.0 potential:

$$
\Phi_{\mathrm{MWH2.0}} = \Phi_{nuclear} + \Phi_{bulge} + \Phi_{bar} + \Phi_{spiral} + \Phi_{disk} + \Phi_{dmh}
$$

where $\Phi_{disk} = \Phi_{disk}^{MN}$[3] or $\Phi_{disk} = \Phi_{disk}^{thin} + \Phi_{disk}^{thick}$[4] and Φ_{dmh} can be either Φ_{dmh1} or Φ_{dmh2}, and given also that the equations of motion take the following general form:

$$
\frac{d\vec{\rho}}{dt} = \vec{f}(\vec{\rho};t) \text{ with}:
\begin{cases}
\vec{\rho}(0) &=\quad \vec{\rho}_0, \\[1.5em]
\vec{\rho} &=\quad (x_1, x_2, x_3, p_{x_1}, p_{x_2}, p_{x_3}), \\[1.5em]
\vec{f} &=\quad \left(p_{x_1}, p_{x_2}, p_{x_3}, -\dfrac{\partial \Phi}{\partial x_1}, -\dfrac{\partial \Phi}{\partial x_2}, -\dfrac{\partial \Phi}{\partial x_3}\right),
\end{cases}
$$

where $\vec{p}_x = \dot{\vec{x}}$, we can compute the equations of motion for our particular problem, yielding:

---

[3]Only one MN disk is considered to resemble a MN profile.

[4]Each of them is the sum of 3 MN disks to resemble an exponential profile: $\Phi_{disk}^{thin/thick} = \Phi_{\mathrm{MN:1}}^{thin/thick} + \Phi_{\mathrm{MN:2}}^{thin/thick} + \Phi_{\mathrm{MN:3}}^{thin/thick}$.

$$\dot{\vec{x}} = \vec{p}_x \rightarrow \begin{cases} \dot{x}_1 = p_{x_1}, \\[2ex] \dot{x}_2 = p_{x_2}, \\[2ex] \dot{x}_3 = p_{x_3}, \end{cases}$$

$$\ddot{\vec{x}} = -\vec{\nabla}\Phi_{\mathrm{MWH2.0}}$$

with $\vec{\nabla}\Phi_{\mathrm{MWH2.0}}$ the corresponding gradient of the full potential `MWH 2.0`. The latter vector identity can be further expanded into:

$$\ddot{\vec{x}} = -\vec{\nabla}\Phi_{\mathrm{MWH2.0}} \rightarrow \begin{cases} \ddot{x}_1 = -\frac{\partial \Phi_{\mathrm{MWH2.0}}}{\partial x_1}, \\[2ex] \ddot{x}_2 = -\frac{\partial \Phi_{\mathrm{MWH2.0}}}{\partial x_2}, \\[2ex] \ddot{x}_3 = -\frac{\partial \Phi_{\mathrm{MWH2.0}}}{\partial x_3}, \end{cases}$$

where the elements of the gradient are:

$$\vec{\nabla}\Phi_{\mathrm{MWH2.0}} \rightarrow \begin{cases} \frac{\partial \Phi_{\mathrm{MWH2.0}}}{\partial x_1} = \frac{\partial \Phi_{nuclear}}{\partial x_1} + \frac{\partial \Phi_{bulge}}{\partial x_1} + \frac{\partial \Phi_{bar}}{\partial x_1} + \frac{\partial \Phi_{spiral}}{\partial x_1} + \frac{\partial \Phi_{disk}}{\partial x_1} + \frac{\partial \Phi_{dmh}}{\partial x_1}, \\[2ex] \frac{\partial \Phi_{\mathrm{MWH2.0}}}{\partial x_2} = \frac{\partial \Phi_{nuclear}}{\partial x_2} + \frac{\partial \Phi_{bulge}}{\partial x_2} + \frac{\partial \Phi_{bar}}{\partial x_2} + \frac{\partial \Phi_{spiral}}{\partial x_2} + \frac{\partial^2 \Phi_{disk}}{\partial x_2} + \frac{\partial \Phi_{dmh}}{\partial x_2}, \\[2ex] \frac{\partial \Phi_{\mathrm{MWH2.0}}}{\partial x_3} = \frac{\partial \Phi_{nuclear}}{\partial x_3} + \frac{\partial \Phi_{bulge}}{\partial x_3} + \frac{\partial \Phi_{bar}}{\partial x_3} + \frac{\partial \Phi_{spiral}}{\partial x_3} + \frac{\partial \Phi_{disk}}{\partial x_3} + \frac{\partial \Phi_{dmh}}{\partial x_3}, \end{cases}$$

with $x_1 = x$, $x_2 = y$ and $x_3 = z$, then $\vec{x} = (x, y, z)$ and $\vec{p}_x = (p_x, p_y, p_z)$ and where the first derivatives are the ones calculated in Section B.1

B.3   Linearized variational equations

Finally, given the linearized variational equations in its general form[5]:

---

[5]Let us remind the reader that the lineraized variational equations need to be solved simultaneously with the equations of motion.

$$
\left[\frac{d\vec{\xi}}{dt}\right]^T = \left[\frac{\partial \vec{f}\,(\vec{\rho};t)}{\partial \vec{\rho}}\right]\left[\vec{\xi}\right]^T \text{ with :}
\begin{cases}
\vec{\xi}(0) &= \dfrac{\vec{f}(\vec{\rho}_0;0)}{\|\vec{f}(\vec{\rho}_0;0)\|}, \\[2mm]
\vec{\xi} &= \left(\delta_{x_1},\delta_{x_2},\delta_{x_3},\delta_{p_{x_1}},\delta_{p_{x_2}},\delta_{p_{x_3}}\right), \\[2mm]
\vec{\rho} &= (x_1,x_2,x_3,p_{x_1},p_{x_2},p_{x_3})\,, \\[2mm]
\vec{f} &= \left(p_{x_1},p_{x_2},p_{x_3},-\dfrac{\partial\Phi}{\partial x_1},-\dfrac{\partial\Phi}{\partial x_2},-\dfrac{\partial\Phi}{\partial x_3}\right),
\end{cases}
$$

we can rewrite them for our particular problem, obtaining:

$$
\dot{\vec{\delta}}_x = \vec{\delta}_{p_x} \rightarrow
\begin{cases}
\dot{\delta}_{x_1} &= \delta_{p_{x_1}}, \\[2mm]
\dot{\delta}_{x_2} &= \delta_{p_{x_2}}, \\[2mm]
\dot{\delta}_{x_3} &= \delta_{p_{x_3}}.
\end{cases}
$$

$$
\left[\dot{\vec{\delta}}_{p_x}\right]^T = -\mathbf{H}\left(\Phi_{\text{MWH2.0}}\right)\left[\vec{\delta}_x\right]^T,
$$

with $\mathbf{H}\left(\Phi_{\text{MWH2.0}}\right)$ the corresponding hessian matrix of the full potential `MWH 2.0`. The latter vector identity can be further expanded into:

$$
\left[\dot{\vec{\delta}}_{p_x}\right]^T = -\mathbf{H}\left(\Phi_{\text{MWH2.0}}\right)\left[\vec{\delta}_x\right]^T \rightarrow
\begin{cases}
\dot{\delta}_{p_{x_1}} &= -\left[\dfrac{\partial^2\Phi_{\text{MWH2.0}}}{\partial x_1^2}\delta_{x_1} + \dfrac{\partial^2\Phi_{MW}}{\partial x_1\partial x_2}\delta_{x_2} + \dfrac{\partial^2\Phi_{\text{MWH2.0}}}{\partial x_1\partial x_3}\delta_{x_3}\right], \\[3mm]
\dot{\delta}_{p_{x_2}} &= -\left[\dfrac{\partial^2\Phi_{\text{MWH2.0}}}{\partial x_2\partial x_1}\delta_{x_1} + \dfrac{\partial^2\Phi_{\text{MWH2.0}}}{\partial x_2^2}\delta_{x_2} + \dfrac{\partial^2\Phi_{\text{MWH2.0}}}{\partial x_2\partial x_3}\delta_{x_3}\right], \\[3mm]
\dot{\delta}_{p_{x_3}} &= -\left[\dfrac{\partial^2\Phi_{\text{MWH2.0}}}{\partial x_3\partial x_1}\delta_{x_1} + \dfrac{\partial^2\Phi_{\text{MWH2.0}}}{\partial x_3\partial x_2}\delta_{x_2} + \dfrac{\partial^2\Phi_{\text{MWH2.0}}}{\partial x_3^2}\delta_{x_3}\right],
\end{cases}
$$

where the elements of the hessian matrix are:

$$\mathbf{H}\left(\Phi_{\mathrm{MWH2.0}}\right) \rightarrow \begin{cases} \dfrac{\partial^2 \Phi_{\mathrm{MWH2.0}}}{\partial x_1^2} &= \dfrac{\partial^2 \Phi_{nuclear}}{\partial x_1^2} + \dfrac{\partial^2 \Phi_{bulge}}{\partial x_1^2} + \dfrac{\partial^2 \Phi_{bar}}{\partial x_1^2} + \dfrac{\partial^2 \Phi_{spiral}}{\partial x_1^2} + \dfrac{\partial^2 \Phi_{disk}}{\partial x_1^2} + \dfrac{\partial^2 \Phi_{dmh}}{\partial x_1^2}, \\[2.5ex] \dfrac{\partial^2 \Phi_{\mathrm{MWH2.0}}}{\partial x_2^2} &= \dfrac{\partial^2 \Phi_{nuclear}}{\partial x_2^2} + \dfrac{\partial^2 \Phi_{bulge}}{\partial x_2^2} + \dfrac{\partial^2 \Phi_{bar}}{\partial x_2^2} + \dfrac{\partial^2 \Phi_{spiral}}{\partial x_2^2} + \dfrac{\partial^2 \Phi_{disk}}{\partial x_2^2} + \dfrac{\partial^2 \Phi_{dmh}}{\partial x_2^2}, \\[2.5ex] \dfrac{\partial^2 \Phi_{\mathrm{MWH2.0}}}{\partial x_3^2} &= \dfrac{\partial^2 \Phi_{nuclear}}{\partial x_3^2} + \dfrac{\partial^2 \Phi_{bulge}}{\partial x_3^2} + \dfrac{\partial^2 \Phi_{bar}}{\partial x_3^2} + \dfrac{\partial^2 \Phi_{spiral}}{\partial x_3^2} + \dfrac{\partial^2 \Phi_{disk}}{\partial x_3^2} + \dfrac{\partial^2 \Phi_{dmh}}{\partial x_3^2}, \\[2.5ex] \dfrac{\partial^2 \Phi_{\mathrm{MWH2.0}}}{\partial x_1 \partial x_2} &= \dfrac{\partial^2 \Phi_{nuclear}}{\partial x_1 \partial x_2} + \dfrac{\partial^2 \Phi_{bulge}}{\partial x_1 \partial x_2} + \dfrac{\partial^2 \Phi_{bar}}{\partial x_1 \partial x_2} + \dfrac{\partial^2 \Phi_{spiral}}{\partial x_1 \partial x_2} + \dfrac{\partial^2 \Phi_{disk}}{\partial x_1 \partial x_2} + \dfrac{\partial^2 \Phi_{dmh}}{\partial x_1 \partial x_2}, \\[2.5ex] \dfrac{\partial^2 \Phi_{\mathrm{MWH2.0}}}{\partial x_1 \partial x_3} &= \dfrac{\partial^2 \Phi_{nuclear}}{\partial x_1 \partial x_3} + \dfrac{\partial^2 \Phi_{bulge}}{\partial x_1 \partial x_3} + \dfrac{\partial^2 \Phi_{bar}}{\partial x_1 \partial x_3} + \dfrac{\partial^2 \Phi_{spiral}}{\partial x_1 \partial x_3} + \dfrac{\partial^2 \Phi_{disk}}{\partial x_1 \partial x_3} + \dfrac{\partial^2 \Phi_{dmh}}{\partial x_1 \partial x_3}, \\[2.5ex] \dfrac{\partial^2 \Phi_{\mathrm{MWH2.0}}}{\partial x_2 \partial x_3} &= \dfrac{\partial^2 \Phi_{nuclear}}{\partial x_2 \partial x_3} + \dfrac{\partial^2 \Phi_{bulge}}{\partial x_2 \partial x_3} + \dfrac{\partial^2 \Phi_{bar}}{\partial x_2 \partial x_3} + \dfrac{\partial^2 \Phi_{spiral}}{\partial x_2 \partial x_3} + \dfrac{\partial^2 \Phi_{disk}}{\partial x_2 \partial x_3} + \dfrac{\partial^2 \Phi_{dmh}}{\partial x_2 \partial x_3}, \end{cases}$$

with $x_1 = x$, $x_2 = y$ and $x_3 = z$, then $\vec{x} = (x, y, z)$ and $\vec{p}_x = (p_x, p_y, p_z)$ and where the second derivatives are the ones calculated in Section B.1.

Appendix C

Description

C.1   The preamble

In the preamble of the `milkywayhydra.pav` file, the user will find a brief summary of the model basics, starting with its current version (and indicating the reference document: this manual) and the description of the galactic components used. Then, there is a short paragraph dedicated to explain the mechanism employed for adding/removing the aforementioned components (`ADD-REM` parameters, Section C.6), and follows a short comment on the treatment of possible undefined limits in the computation of the equations of motion and the first variational equations. The preamble is finally closed with an enumeration of the basic working units (see Section C.7 for further details).

Before continuing with the introduction of the subroutines, we give the working definition of variable class in the recursive structure of the `milkywayhydra.pav` file:

- "Starting variable" are all those variables defined in the `pot` function.

- "Basic variable" are all those variables defined in the previous step, i.e.: (1) all variables introduced in the `pot` function are basic variables in the `acelera` subroutine, and (2) all variables introduced in the `acelera` subroutine are basic variables in the `variac` subroutine.

- "Auxiliary variable" are all those variables that are not basic variables, i.e. new variables that need to be introduced in each subroutine to build the rest of the expressions.

C.2   The `potinit` subroutine

The first subroutine is the `potinit` (for "potential initialization") subroutine, which comprises the next part of the `milkywayhydra.pav` file, and it is used to initialize the dimension and the parameters of the potential, as indicated in the `LP-VIcode` manual.

The subroutine starts with a fully commented section defining all the parameters of the `MWH` 2.0 model. Then, the declaration of the variables takes place, giving the dimension and the type for each parameter before introducing the galactic components (which are separated in

blocks). As an example of the latter, we show here the block corresponding to the peanut–shaped bulge:

```
*********************************************************************
* PEANUT-SHAPED BULGE
*********************************************************************

* Bulge spheroid
* ADD-REM Parameter
* [SOURCE: Marinacci et al. 2014 (MNRAS, 437, 1750)]
* [COMMENT: M_bulge = 4.74x10^9 M_sun]
      gmbulge=2.03875458d4
*       gmbulge=0.d0

      epsbulge=0.835d0

* Bar
* ADD-REM Parameter
* [SOURCE: Monari et al. 2016 (MNRAS, 461, 3835)]
      alpha=0.01d0
*       alpha=0.d0

      barcoef=8.331938927d6
      rbar=3.5d0
      phibar=5.65d0
* [COMMENT: bomegabar = -52.2 km s-1 kpc-1]
      bomegabar=-52.2d0
```

Every block clearly identifies its `ADD-REM` parameter at the top (always below the comment "ADD-REM Parameter"), and offers two options for its value (the reader should remember that the option that will not be used in the model needs to be commented). First, we have the default value, for instance:

`gmbulge=2.03875458d4`

in case of the bulge spheroid, and second, we have the null value, i.e.:

`gmbulge=0.d0`

which would be used to remove the bulge spheroid component (if it is the option selected and thus, the one that is not commented[1]).

Then, we have the source of the analytic description of the component for reference:

`* [SOURCE: Marinacci et al. 2014 (MNRAS, 437, 1750)]`

---

[1]Notice that in case the user does not comment any of the values, the parameter takes the null value (which is the last value) and the component is not used for the computation.

as well as the actual values of the physical quantities associated with the parameters involved
in the component that may not be straightforward to be recognized, for example:

```
* [COMMENT: M_bulge = 4.74x10^9 M_sun]
```

as the mass of the bulge spheroid involved in the `gmbulge` parameter.

C.3   The `pot` function

After the initialization of the parameters, the function `pot` (for "potential") is introduced[2].
The following is the function's header:

```
************************************************************************
      FUNCTION pot(t,x,n)
      INTEGER n
      DOUBLE PRECISION pot,t,x(n)
* t    = time
* x(n) = coordinates of the phase space
* n    = dimension of the phase space
************************************************************************
```

Then, we proceed with the definition of the starting variables. See below the case for the
peanut–shaped bulge (to continue with the same component as the one used before):

```
************************************************************************

* PEANUT-SHAPED BULGE
* BULGE SPHEROID
* rbulge = radius plus epsilon

      rbulge = SQRT(x(1)**2+x(2)**2+x(3)**2)+epsbulge

* BAR
* rsph     = spherical radius
* gammabar = includes the angular variation
* ubar     = includes the radial variation
* bocaone  = auxiliary function of rcyl and rsph
* bocatwo  = auxiliary function of gammabar

      rsph = SQRT(rcyl**2+x(3)**2)

      gammabar = 2.d0*(phicyl-phibar-bomegabar*t)

* In order to avoid singularities in the bar potential:
```

---

[2]This function is the only one needed by the pre-processing slave program SMART to automatically compute
the accelerations and first variational equations for the SMART flavour of the `milkywayhydra.pav` used in
Section D.

```
        IF(rsph.GE.rbar)THEN
         ubar = -1.d0*(rsph/rbar)**(-3)
        ELSE
         ubar = (rsph/rbar)**3-2.d0
        ENDIF


        bocaone = (rcyl/rsph)**2
        bocatwo = COS(gammabar)
```

```
***********************************************************************
```

The definition of the potential corresponding to each block follows. The case for the peanut–shaped bulge is presented next:

```
***********************************************************************
```

```
* PEANUT-SHAPED BULGE
* BULGE SPHEROID

* ADD-REM SECTION: potential
* If gmbulge = 0, the corresponding potential must be 0.
        IF(ABS(gmbulge).GT.0.d0)THEN
         potbulge = -1.d0*gmbulge/rbulge
        ELSE
         potbulge = 0.d0
        ENDIF

* BAR

* ADD-REM SECTION: potential
* If alphatime = 0, the corresponding potential must be 0.
        IF(ABS(alphatime).GT.0.d0)THEN
         potbar = alphatime*(barcoef/rbar**3)*ubar*bocaone*bocatwo
        ELSE
         potbar = 0.d0
        ENDIF
```

```
***********************************************************************
```

where it should be clear that the `IF` statement in the "`ADD-REM SECTION: potential`" is there to add or remove the components of the potential (accordingly to the value of the `ADD-REM` parameter that have been chosen).

At the end of the `potinit` subroutine, the full `MWH 2.0` potential is finally introduced in the `pot` function:

```
* Potential (MWH2.0)
```

```
 pot = potsmbh+potbulge
&       +potbar
&       +potarms
&       +potdiskmn
&       +potdisk(1)+potdisk(2)+potdisk(3)
&       +potdiskthk(1)+potdiskthk(2)+potdiskthk(3)
&       +potdmh(1)+potdmh(2)

    END
```

C.4   The `acelera` subroutine

The `acelera` (for "accelerations") subroutine is programmed with the same recursive structure seen in last section for function `pot`. First, we have the header indicating the starting point of the subroutine:

```
**************************************************************************
      SUBROUTINE acelera(t,x,n,acc)
      INTEGER n
      DOUBLE PRECISION t,x(n),acc(n/2)
* t    = time
* x(n) = coordinates of the phase space
* n    = dimension of the phase space
* acc  = accelerations (acc(1) = d[vx]/dt, etc)
**************************************************************************
```

Next, we proceed with the declaration of variables before continuing with the introduction of the basic variables. Now, as the reader will notice from the next example corresponding to the peanut–shaped bulge, the basic variables in the `acelera` subroutine are all the variables already introduced in function `pot`, as it was previously mentioned in Section C.1:

```
**************************************************************************

* PEANUT-SHAPED BULGE
* BULGE SPHEROID

      rbulge = SQRT(x(1)**2+x(2)**2+x(3)**2)+epsbulge

* ADD-REM SECTION: potential
* If gmbulge = 0, the corresponding potential must be 0.
      IF(ABS(gmbulge).GT.0.d0)THEN
       potbulge = -1.d0*gmbulge/rbulge
      ELSE
       potbulge = 0.d0
      ENDIF
```

```
* BAR

      rsph = SQRT(rcyl**2+x(3)**2)
      gammabar = 2.d0*(phicyl-phibar-bomegabar*t)
* In order to avoid singularities in the bar potential:
      IF(rsph.GE.rbar)THEN
       ubar = -1.d0*(rsph/rbar)**(-3)
      ELSE
       ubar = (rsph/rbar)**3-2.d0
      ENDIF
      bocaone = (rcyl/rsph)**2
      bocatwo = COS(gammabar)


* ADD-REM SECTION: potential
* If alphatime = 0, the corresponding potential must be 0.
      IF(ABS(alphatime).GT.0.d0)THEN
       potbar = alphatime*(barcoef/rbar**3)*ubar*bocaone*bocatwo
      ELSE
       potbar = 0.d0
      ENDIF


**************************************************************************
```

Therefore, the potential corresponding to each component turns to be another "basic variable" in this new subroutine. Then, we need to introduced the auxiliary variables (those that do not appear previously in the pot function), see the associated peanut–shaped bulge section:

```
**************************************************************************

* PEANUT-SHAPED BULGE
* BULGE SPHEROID

      arg(4) = rbulge-epsbulge

      DO i=1,nv

* Checking Arithmetic Exceptions (5) (rbulge must be > 0)
* iff x(i)=0 for every i, limit does not exist, program stops.
       IF(arg(4).GT.0.d0)THEN
        drbulgedx(i) = x(i)/(arg(4))
       ELSE
        WRITE(*,*) "Look for 5.AE-acelera in pav file"
        CONTINUE
       ENDIF

      ENDDO
```

```
* BAR

      drsphdrcyl = rcyl/rsph

      DO i=1,nv-1
       drsphdx(i) = drsphdrcyl*drcyldx(i)
      ENDDO
      drsphdx(3) = x(3)/rsph

      dgammabardphicyl = 2.d0

      DO i=1,nv-1
       dgammabardx(i) = dgammabardphicyl*dphicyldx(i)
      ENDDO
      dgammabardx(3) = 0.d0

      IF(rsph.GE.rbar)THEN
       dubardrsph = -(3.d0/rsph)*ubar
      ELSE
       dubardrsph = (3.d0/rsph)*(ubar+2.d0)
      ENDIF

      DO i=1,nv
       dubardx(i) = dubardrsph*drsphdx(i)
      ENDDO

      docaonedrsph = -1.d0*(2.d0/rsph)*drsphdrcyl**2
      docaonedrcyl = (2.d0/rsph)*drsphdrcyl

      DO i=1,nv-1
        docaonedx(i) = (docaonedrcyl+docaonedrsph*drsphdrcyl)*
     &                    drcyldx(i)
      ENDDO
      docaonedx(3) = docaonedrsph*drsphdx(3)

      docatwodgammabar = -1.d0*SIN(gammabar)

      DO i=1,nv-1
       docatwodx(i) = docatwodgammabar*dgammabardx(i)
      ENDDO


**************************************************************************
```

where the variables involved in the computation of the first derivatives of the potential are presented, which includes the first derivatives of the basic variables. Next, we compute the first derivatives of each component of the potential. As it is done with the potential, the ADD-REM SECTION: first derivatives is used in the following to eliminate all the first

derivatives of those components that are not being considered. Once again, the peanut–
shaped bulge is shown here for reference and comparison purposes:

```
*************************************************************************


* PEANUT-SHAPED BULGE
* BULGE SPHEROID

      DO i=1,nv
* ADD-REM SECTION: first derivatives
* If gmbulge = 0, the corresponding derivatives must be 0.
      IF(ABS(gmbulge).GT.0.d0)THEN
       dpotbulgedx(i) = -1.d0*(potbulge/rbulge)*(drbulgedx(i))
      ELSE
       dpotbulgedx(i) = 0.d0
      ENDIF
      ENDDO


* BAR

      dpotbardubar = alphatime*(barcoef/rbar**3)*bocaone*bocatwo
      dpotbardocaone = alphatime*(barcoef/rbar**3)*ubar*bocatwo
      dpotbardocatwo = alphatime*(barcoef/rbar**3)*ubar*bocaone

      DO i=1,nv-1
* ADD-REM SECTION: first derivatives
* If alphatime = 0, the corresponding derivatives must be 0.
      IF(ABS(alphatime).GT.0.d0)THEN
       dpotbardx(i) = dpotbardubar*dubardx(i)+
     &               dpotbardocaone*docaonedx(i)+
     &               dpotbardocatwo*docatwodx(i)
      ELSE
       dpotbardx(i) = 0.d0
      ENDIF
      ENDDO
* ADD-REM SECTION: first derivatives
* If alphatime = 0, the corresponding derivatives must be 0.
      IF(ABS(alphatime).GT.0.d0)THEN
       dpotbardx(3) = dpotbardubar*dubardx(3)+
     &               dpotbardocaone*docaonedx(3)
      ELSE
       dpotbardx(3) = 0.d0
      ENDIF


*************************************************************************
```

Finally, we present the last section of the `acelera` subroutine where we compute the equations
of motion using the first derivatives of the potentials that have been defined previously:

```
* Accelerations (MWH2.0)

      DO i=1,nv
       dpotdx(i) = dpotsmbhdx(i)+dpotbulgedx(i)
     &             +dpotbardx(i)
     &             +dpotarmsdx(i)
     &             +dpotdiskmndx(i)
     &             +dpotdiskdx(1,i)+dpotdiskdx(2,i)
     &             +dpotdiskdx(3,i)+dpotdiskthkdx(1,i)
     &             +dpotdiskthkdx(2,i)+dpotdiskthkdx(3,i)
     &             +dpotdmhdx(1,i)+dpotdmhdx(2,i)
      ENDDO

      DO i=1,n/2
       acc(i) = -1.d0*(dpotdx(i))
      ENDDO

      END
```

The whole structure of the subroutine tries to follow a recursive programming style with each component perfectly identified within a single chain of blocks. This style is also followed in the last of the subroutines that build up the `milkywayhydra.pav` file, the `variac` subroutine.

C.5   The `variac` subroutine

The `variac` (for "first variationals") subroutine starts with the header:

```
**************************************************************************
      SUBROUTINE variac(t,x,dx,n,dax)
      INTEGER n
      DOUBLE PRECISION t,x(n),dx(n),dax(n/2)
* n   = dimension of the phase space
* x   = coordinates of the phase space
* dx  = differentials (deltas) of the coordinates of the phase space
* dax = derivatives (dax(1) = d[dvx]/dt, etc)
**************************************************************************
```

and continue with the declaration of variables before continuing with the introduction of the basic variables. Now there is a new shift due to our definition of "basic variable" (Section C.1): the basic variables in the `variac` subroutine are all the variables already introduced in `acelera`. See the case of the peanut–shaped bulge:

```
**************************************************************************

* PEANUT-SHAPED BULGE
* BULGE SPHEROID
```

```
      rbulge = SQRT(x(1)**2+x(2)**2+x(3)**2)+epsbulge


* ADD-REM SECTION: potential
* If gmbulge = 0, the corresponding potential must be 0.
      IF(ABS(gmbulge).GT.0.d0)THEN
       potbulge = -1.d0*gmbulge/rbulge
      ELSE
       potbulge = 0.d0
      ENDIF


      arg(4) = rbulge-epsbulge


      DO i=1,nv
* Checking Arithmetic Exceptions (5) (rbulge must be > 0)
* iff x(i)=0 for every i, limit does not exist, program stops.
       IF(arg(4).GT.0.d0)THEN
        drbulgedx(i) = x(i)/(arg(4))
       ELSE
        WRITE(*,*) "Look for 5.AE-variac in pav file"
        CONTINUE
       ENDIF
      ENDDO


      DO i=1,nv
* ADD-REM SECTION: first derivatives
* If gmbulge = 0, the corresponding derivatives must be 0.
      IF(ABS(gmbulge).GT.0.d0)THEN
       dpotbulgedx(i) = -1.d0*(potbulge/rbulge)*(drbulgedx(i))
      ELSE
       dpotbulgedx(i) = 0.d0
      ENDIF
      ENDDO


* BAR

      rsph = SQRT(rcyl**2+x(3)**2)
      gammabar = 2.d0*(phicyl-phibar-bomegabar*t)
* In order to avoid singularities in the bar potential:
      IF(rsph.GE.rbar)THEN
       ubar = -1.d0*(rsph/rbar)**(-3)
      ELSE
       ubar = (rsph/rbar)**3-2.d0
      ENDIF
      bocaone = (rcyl/rsph)**2
      bocatwo = COS(gammabar)


* ADD-REM SECTION: potential
```

```
* If alphatime = 0, the corresponding potential must be 0.
      IF(ABS(alphatime).GT.0.d0)THEN
       potbar = alphatime*(barcoef/rbar**3)*ubar*bocaone*bocatwo
      ELSE
       potbar = 0.d0
      ENDIF

      drsphdrcyl = rcyl/rsph

      DO i=1,nv-1
        drsphdx(i) = drsphdrcyl*drcyldx(i)
      ENDDO
      drsphdx(3) = x(3)/rsph

      dgammabardphicyl = 2.d0

      DO i=1,nv-1
       dgammabardx(i) = dgammabardphicyl*dphicyldx(i)
      ENDDO
      dgammabardx(3) = 0.d0

      IF(rsph.GE.rbar)THEN
       dubardrsph = -(3.d0/rsph)*ubar
      ELSE
       dubardrsph = (3.d0/rsph)*(ubar+2.d0)
      ENDIF

      DO i=1,nv
       dubardx(i) = dubardrsph*drsphdx(i)
      ENDDO

      docaonedrsph = -1.d0*(2.d0/rsph)*drsphdrcyl**2
      docaonedrcyl = (2.d0/rsph)*drsphdrcyl
      DO i=1,nv-1
       docaonedx(i) = (docaonedrcyl+docaonedrsph*drsphdrcyl)*
     &                  drcyldx(i)
      ENDDO
      docaonedx(3) = docaonedrsph*drsphdx(3)
      docatwodgammabar = -1.d0*SIN(gammabar)

      DO i=1,nv-1
       docatwodx(i) = docatwodgammabar*dgammabardx(i)
      ENDDO

      dpotbardubar = alphatime*(barcoef/rbar**3)*bocaone*bocatwo
      dpotbardocaone = alphatime*(barcoef/rbar**3)*ubar*bocatwo
      dpotbardocatwo = alphatime*(barcoef/rbar**3)*ubar*bocaone
```

```
      DO i=1,nv-1
* ADD-REM SECTION: first derivatives
* If alphatime = 0, the corresponding derivatives must be 0.
      IF(ABS(alphatime).GT.0.d0)THEN
       dpotbardx(i) = dpotbardubar*dubardx(i)+
     &               dpotbardocaone*docaonedx(i)+
     &               dpotbardocatwo*docatwodx(i)
      ELSE
       dpotbardx(i) = 0.d0
      ENDIF
      ENDDO
* ADD-REM SECTION: first derivatives
* If alphatime = 0, the corresponding derivatives must be 0.
      IF(ABS(alphatime).GT.0.d0)THEN
       dpotbardx(3) = dpotbardubar*dubardx(3)+
     &               dpotbardocaone*docaonedx(3)
      ELSE
       dpotbardx(3) = 0.d0
      ENDIF


************************************************************************
```

Therefore, not only the potential (as in the the `acelera` subroutine) but also the first deriva-
tives corresponding to each component turns to be another "basic variable" in this new
subroutine. Then, we need to introduced the auxiliary variables (those that do not appear
previously in the `acelera` subroutine), see the associated peanut–shaped bulge section[3]:

```
************************************************************************

* PEANUT-SHAPED BULGE
* BAR

      d2rsphd2rcyl = (1.d0/rsph)*(1.d0-drsphdrcyl**2)
      d2rsphdzdrcyl = (-1.d0/rsph)*(drsphdrcyl*drsphdx(3))

      DO j=1,nv-1
       DO k=1,nv-1
        d2rsphdxdy(j,k) = d2rsphd2rcyl*drcyldx(j)*drcyldx(k)+
     &                  drsphdrcyl*d2rcyldxdy(j,k)
       ENDDO
      ENDDO

      DO j=1,nv-1
       d2rsphdxdy(3,j) = d2rsphdzdrcyl*drcyldx(j)
       d2rsphdxdy(j,3) = d2rsphdxdy(3,j)
```

---

[3]Notice that the bulge spheroid does not have any auxiliary variables.

```
  ENDDO

  d2rsphdxdy(3,3) = (1.d0/rsph)*(1.d0-drsphdx(3)**2)

  DO j=1,nv-1
   DO k=1,nv-1
     d2gammabardxdy(j,k) = dgammabardphicyl*d2phicyldxdy(j,k)
   ENDDO
  ENDDO

  IF(rsph.GE.rbar)THEN
  d2ubard2rsph = +1.d0*(3.d0/rsph**2)*ubar
&                -(3.d0/rsph)*dubardrsph
  ELSE
  d2ubard2rsph = (-3.d0/rsph**2)*(ubar+2.d0)
&                +(3.d0/rsph)*dubardrsph
  ENDIF

  DO j=1,nv-1
   DO k=1,nv-1
     d2ubardxdy(j,k) = d2ubard2rsph*drsphdx(j)*drsphdx(k)
&                +dubardrsph*d2rsphdxdy(j,k)
   ENDDO
  ENDDO

  DO j=1,nv-1
   d2ubardxdy(3,j) = d2ubard2rsph*drsphdx(3)*drsphdx(j)
&                +dubardrsph*d2rsphdxdy(3,j)
   d2ubardxdy(j,3) = d2ubardxdy(3,j)
  ENDDO

  d2ubardxdy(3,3) = (1.d0/rsph)*(dubardrsph)*(1.d0-drsphdx(3)**2)
&                +d2ubard2rsph*drsphdx(3)**2

  d2ocaoned2rsph = (2.d0/rsph)*(bocaone/rsph-docaonedrsph)
  d2ocaoned2rcyl = 2.d0/rsph**2
  d2ocaonedrsphdrcyl = (-4.d0/rsph**2)*drsphdrcyl

  DO j=1,nv-1
   DO k=1,nv-1
     d2ocaonedxdy(j,k) = d2ocaoned2rcyl*drcyldx(j)*drcyldx(k)
&                +d2ocaoned2rsph*drsphdx(j)*drsphdx(k)
&                +d2ocaonedrsphdrcyl*(drcyldx(j)*drsphdx(k)
&                +drsphdx(j)*drcyldx(k))
&                +docaonedrcyl*d2rcyldxdy(j,k)
&                +docaonedrsph*d2rsphdxdy(j,k)
   ENDDO
```

```
      ENDDO

      DO j=1,nv-1
       d2ocaonedxdy(3,j) = d2ocaoned2rsph*drsphdx(3)*drsphdx(j)
     &                     +d2ocaonedrsphdrcyl*drsphdx(3)*drcyldx(j)
     &                     +docaonedrsph*d2rsphdxdy(3,j)
       d2ocaonedxdy(j,3) = d2ocaonedxdy(3,j)
      ENDDO

      d2ocaonedxdy(3,3) = d2ocaoned2rsph*drsphdx(3)**2
     &                    +docaonedrsph*d2rsphdxdy(3,3)**2

      d2ocatwod2gammabar = -1.d0*bocatwo

      DO j=1,nv-1
       DO k=1,nv-1
        d2ocatwodxdy(j,k) = d2ocatwod2gammabar*dgammabardx(j)*
     &                     dgammabardx(k)+docatwodgammabar*
     &                     d2gammabardxdy(j,k)
       ENDDO
      ENDDO


**************************************************************************
```

where the variables involved in the computation of the second derivatives of the potential are presented, which includes second derivatives of the basic variables. Next, we compute the second derivatives of each component of the potential. Of course, as it is with the potential and the first derivatives, the `ADD-REM SECTION: second derivatives` is used in the following to eliminate all the second derivatives of those components that are not being considered. The case of the peanut–shaped bulge follows:

```
**************************************************************************

* PEANUT-SHAPED BULGE
* BULGE SPHEROID

* ADD-REM SECTION: second derivatives
* If gmbulge = 0, the corresponding derivatives must be 0.
      IF(ABS(gmbulge).GT.0.d0)THEN

      DO j=1,nv
       DO k=1,nv
        IF(j.eq.k)THEN
         d2potbulgedxdy(j,k) = (potbulge/rbulge**2)
     &                         *(drbulgedx(j)**2)*(3.d0+(epsbulge/
     &                         (arg(4))))-(potbulge
     &                         /(rbulge*(arg(4))))
```

```
      ELSE
       d2potbulgedxdy(j,k) = (potbulge/rbulge**2)
     &                        *(drbulgedx(j)*drbulgedx(k))
     &                        *(3.d0+(epsbulge/(arg(4))))
        ENDIF
      ENDDO
     ENDDO

     ELSE
      DO j=1,nv
       DO k=1,nv
        d2potbulgedxdy(j,k) = 0.d0
       ENDDO
      ENDDO
      ENDIF

* BAR

      d2potbardubardocaone = alphatime*(barcoef/rbar**3)*bocatwo
      d2potbardubardocatwo = alphatime*(barcoef/rbar**3)*bocaone
      d2potbardocaonedocatwo = alphatime*(barcoef/rbar**3)*ubar

* ADD-REM SECTION: second derivatives
* If alphatime = 0, the corresponding derivatives must be 0.
      IF(ABS(alphatime).GT.0.d0)THEN

      DO j=1,nv-1
       DO k=1,nv-1
        d2potbardxdy(j,k) = d2potbardubardocaone*(dubardx(j)
     &                  *docaonedx(k)+dubardx(k)*docaonedx(j))
     &                  +d2potbardubardocatwo*(dubardx(j)
     &                  *docatwodx(k)+dubardx(k)*docatwodx(j))
     &                  +d2potbardocaonedocatwo*(docaonedx(j)
     &                  *docatwodx(k)+docaonedx(k)*docatwodx(j))
     &                  +dpotbardubar*d2ubardxdy(j,k)
     &                  +dpotbardocaone*d2ocaonedxdy(j,k)
     &                  +dpotbardocatwo*d2ocatwodxdy(j,k)
       ENDDO
      ENDDO

      DO j=1,nv-1
       d2potbardxdy(3,j) = d2potbardubardocaone*(dubardx(3)
     &                  *docaonedx(j)+dubardx(j)*docaonedx(3))
     &                  +d2potbardubardocatwo*dubardx(3)
     &                  *docatwodx(j)+d2potbardocaonedocatwo
     &                  *docaonedx(3)*docatwodx(j)
     &                  +dpotbardubar*d2ubardxdy(3,j)
```

```
     &                              +dpotbardocaone*d2ocaonedxdy(3,j)
       d2potbardxdy(j,3) = d2potbardxdy(3,j)
      ENDDO

      d2potbardxdy(3,3) = d2potbardubardocaone*(2.d0*dubardx(3)
     &                    *docaonedx(3))+dpotbardubar*d2ubardxdy(3,3)
     &                    +dpotbardocaone*d2ocaonedxdy(3,3)

      ELSE
       DO j=1,nv
        DO k=1,nv
         d2potbardxdy(j,k) = 0.d0
        ENDDO
      ENDDO
      ENDIF
```

****

Finally, we present the last section of the `variac` subroutine where we compute the linearized variational equations using the second derivatives of the potentials previously defined:

```
* Linearized variational equations (MWH2.0)

* Initialization

      DO j=1,n/2
       dax(j)=0.d0
      ENDDO

      DO j=1,nv
       DO k=1,nv
        d2potdxdy(j,k) = d2potsmbhdxdy(j,k)
     &                   +d2potbulgedxdy(j,k)
     &                   +d2potbardxdy(j,k)
     &                   +d2potarmsdxdy(j,k)
     &                   +d2potdiskmndxdy(j,k)
     &                   +d2potdisk1dxdy(j,k)
     &                   +d2potdisk2dxdy(j,k)
     &                   +d2potdisk3dxdy(j,k)
     &                   +d2potdisk1thkdxdy(j,k)
     &                   +d2potdisk2thkdxdy(j,k)
     &                   +d2potdisk3thkdxdy(j,k)
     &                   +d2potdmh1dxdy(j,k)
     &                   +d2potdmh2dxdy(j,k)
       ENDDO
      ENDDO
```

```
* Computation

      DO j=1,n/2
       DO k=1,n/2
        dax(j) = dax(j)-1.d0*d2potdxdy(j,k)*dx(k)
       ENDDO
      ENDDO
```

C.6 The `ADD-REM` parameters

The `ADD-REM` (short for adding/removing) parameters are used to eliminate the associated galactic components. They can be found in the preamble of the `milkywayhydra.pav` file and are the following:

```
**************************************************************************

* COMPONENT ADD-ONs
* The galactic components are treating separately, then the user can
* add/change as many as she/he wants, just copying/modifying the right
* blocks in the potinit, acelera and variac subroutines.
* In case of the spiral arms, the user can add/change modes by
* adding/changing the terms involved in the series.


* ADD-REM PARAMETERS
* Setting their values to zero, removes the associated component.
* Notice that in such cases, the value "zero" is always present as a
* comment.
* NUCLEAR REGION: gmsmbh.
* PEANUT-SHAPED BULGE: gmbulge [spheroid], alpha [bar].
* SPIRAL ARMS: armscoef.
* DISK:
* (1) gmdiskmn,
* (2) gmdisk(1,2,3) [thin disk], gmdiskthk(1,2,3) [thick disk].
* DARK MATTER HALO:
* (1) acoef,
* (2) vhalo.
* ADD-REM GROWTH FACTORS
* BAR AND SPIRAL ARMS: atime.


**************************************************************************
```

For instance, if the `gmsmbh` is set to zero, then the nuclear region component is discarded. If the `alpha` parameter is set to zero, the bar in the peanut–shaped bulge is discarded and we will only have a bulge made of a simple Hernquist spheroid. In case of the disk and DMH components, notice that there are two profiles for each component so one of those profiles should be set to zero. For example, if the user wants to have a NFW profile, the parameter `vhalo` corresponding to the logarithmic profile of the DMH should be set to zero in order to

discard that profile. The same happens with the disk, if the user wants to apply an exponential profile with a thin and a thick disks, then `gmdiskmn` should be set to zero in order to discard the MN option for the disk.

In case of these `ADD-REM` parameters, there is always two options in the `milkywayhydra.pav` file: the default option and the null option. If the user wants to discard one of the components, she/he has to comment the default value and uncomment the null value. Then, the selected component (potential, first and second derivatives) would be discarded from the computation.

C.7   The working units

The `milkywayhydra.pav` uses the following basic working units:

input file units:

- positions: `kpc`,

- velocities: `km/s`;

integration:

- positions: `kpc+km/s*[time]`,

- velocities: $\mathtt{km/s+(km/s)^2*(1/kpc)*[time]}$,

which implies that the time unit (u.t.) in the `milkywayhydra.pav` is:

- u.t.: `(kpc/gyr)*(s/km)*gyr`,

then $1\,[\text{u.t.}] \simeq 0.9778\,\text{Gyr}$;

physical quantities units:

- mass: $\mathrm{M}_\odot$,

- density: $\mathrm{M}_\odot/\mathtt{kpc}^3$,

- angles: $\mathtt{rad} \in [0 : 2\pi)$,

- angular velocity: `(km/s)/kpc`,

and the value for the gravitational constant G is: $4.30117 \times 10^{-6}\,(\text{km/s})^2 * (\text{kpc}/\mathrm{M}_\odot)$.

The derived quantities use the following working units:

1. `potinit` subroutine input units:

   - `gmsmbh:` $(\text{km/s})^2 * \text{kpc}$,
   - `epsmbh:`   kpc,
   - `atime:`   u.t.,

- `gmbulge`: $(\mathrm{km/s})^2 * \mathrm{kpc}$,
- `epsbulge`: kpc,
- `alpha`: adimensional,
- `barcoef`: $(\mathrm{km/s})^2 * \mathrm{kpc}^3$,
- `rbar`: kpc,
- `phibar`: rad,
- `bomegabar`: $\mathrm{km/s} * \mathrm{kpc}^{-1}$,
- `armscoef`: $(\mathrm{km/s})^2$,
- `narms`: adimensional,
- `nindex`: adimensional,
- `p`: rad,
- `rarms`: kpc,
- `rscarms`: kpc,
- `phiarms`: rad,
- `bomegarms`: $\mathrm{km/s} * \mathrm{kpc}^{-1}$,
- `hs`: kpc,
- `excoefarms`: kpc,
- `gmdiskmn`: $(\mathrm{km/s})^2 * \mathrm{kpc}$,
- `epscalemn`: kpc,
- `epsheightmn`: kpc,
- `gmdisk(i)`: $(\mathrm{km/s})^2 * \mathrm{kpc}$,
- `epscale(i)`: kpc,
- `epsheight(i)`: kpc,
- `acoef`: $\mathrm{kpc} * (\mathrm{km/s})^2$,
- `rs`: kpc,
- `scoefi(i)`: adimensional,
- `scoefe(i)`: adimensional,
- `vhalo`: $\mathrm{km/s}$,
- `d`: kpc[4],
- `ra`: kpc[5],
- `qcoef(i)`: adimensional,
- `qqcoef(i)`: adimensional,
- `ascoef(i)`: adimensional,
- `wcoef(i)`: adimensional;

---

[4] Actually, and formally speaking, all parameters and variables in the argument of the log function should be adimensional. However, this is not an issue here, so the number associated to the parameter should be thought as in the units shown.

[5] Idem `d`.

2. `pot` function output units:

   - `potential:` $(km/s)^2$;

3. `acelera` subroutine output units:

   - `acc(i):` $(km/s)^2 * kpc^{-1}$;

4. and finally, `variac` subroutine output units:

   - `dax(i):` $(km/s)^2 * kpc^{-1}$,
   - `d2potdxdy(i,j):` $(km/s)^2 * kpc^{-2}$,
   - `dx(j):`   kpc.

Appendix D

Validation

In the present appendix we are going to test numerically the validity of the pre–`SMART` flavour of the `milkywayhydra.pav`, comparing the results from both flavours, pre–`SMART` and `SMART` (which were computed in ways completely different) on the same test model.

The model chosen to test the validity of the `milkywayhydra.pav` is the *Hydra 2.0* introduced in Section 2.3 and consists of a nuclear region, a peanut–shaped bulge, two–armed spiral pattern (with super strong spirals, i.e. 200% density contrast, see Section 2.2.3 for further details), two–component exponential stellar disk and the option (1) for the DMH (Section 2.2.5). The latter has, indeed, a bi–triaxial shape for the experiments on individual orbits where we take our sample from the DMH, or a perfectly oblate shape in the inner regions while perfectly spherical in the outer parts for the experiments on big samples of orbits (i.e. a slightly modified *Hydra 2.0*), where our samples are taken from the thin disk instead. The rest of the values for the parameters are the ones for the default `MWH` 2.0 model (Section 2.2 for references).

D.1   Generating the initial conditions

In this section we present the setting of the experiments to validate the `milkywayhydra.pav`. We start applying the `MAGI` code [21][1] to generate the initial conditions following the distribution of the time independent (hereinafter TI) version of our *Hydra 2.0* Milky Way–type galactic potential under study (i.e. no bar or spiral pattern yet activated).

In the `run.sh` file we set the number of particles to be generated by the code in 33554432 (2^{25}), and the `problem ID` (as `MAGI` calls it) "6" that points to our TI model which reads as follows:

```
FILE=hydra
CONFIG=milkyway/hydra.cfg
EPS=1.5625e-2
ETA=0.5
FINISH=1575.0
```

---

[1] The code is provided as an open–source software and is publicly and freely available at https://bitbucket. org/ymiki/magi.

```
INTERVAL=25.0
```

Also, the unit system chosen to be used by `MAGI` during the computation is indicated by the number "1" which means "galactic scale": $M_\odot$, kpc and Myr being the corresponding astrophysical units, then $10^8\ M_\odot = 1$, $1\,\mathrm{kpc} = 1$ and $100\,\mathrm{Myr} = 1$ are the unit conversion parameters into computational units (C.U.). Finally, positions are returned by the code in units of kpc ($1\,\mathrm{kpc} = 1\,\mathrm{C.U.}$) but velocities need an intermediate unit conversion step because $1\,\mathrm{C.U.} = 9.777922\,\mathrm{km/s}$ in astrophysical units. Thus, in the latter case the unit conversion should take place before it can be read by the `LP-VIcode` which uses kpc and km/s as working units for positions and velocities, respectively (see further details on the unit system in Section C.7).

The input files for `MAGI` (further configuration details in the associated `README` file) are the following:

File name: `hydra.cfg`
File contents:

```
1
5
0  milkyway/hydra_nuclear.param 0 0
3  milkyway/hydra_bulge.param 0 0
4  milkyway/hydra_dmhalo.param 0 0
-1 milkyway/hydra_thindisk.param 0 0
-1 milkyway/hydra_thickdisk.param 0 0
```

where the numbering before the parameter files refers to:

- 0: Plummer sphere;

- 3: Hernsquist sphere;

- 4: NFW sphere;

- -1: Exponential disk;

The abovementioned parameter files for the nuclear region, the spherical component of the bulge, the two–component stellar disk and the DMH (respectively) are listed below:

File name: `hydra_nuclear.param`
File contents:

```
2.0e+8
0.03
1
0.3 0.03
```

File name: `hydra_bulge.param`
File contents:

```
4.74e+9
0.835
1
10.0 1.0
```

File name: `hydra_thindisk.param`
File contents:

```
5.276e+10
3.123
0.3
-1.0 0.1
0.0
1
30.0 3.0
```

File name: `hydra_thickdisk.param`
File contents:

```
0.686e+10
3.123
1
-1.0 0.1
0.0
1
30.0 3.0
```

File name: `hydra_dmhalo.param`
File contents:

```
14.564e+11
14.63
1
234.5 25.0
```

Finally, the last step in the configuration of `MAGI` is the `cmake` compilation flags. The following changes on the default flag values are used: `-DUSE_TIPSY_FORMAT=OFF` to avoid this format, `-DUSE_GALACTICS_FORMAT=ON` to output data in `ASCII` format and (optional) `-DQUICK_CHECK=ON` to have a smaller sample for an easy and fast checking.

A slightly modified `hydra.info.txt` is included below for references of the built system. This file is part of the `MAGI` documentation output files.

```
################################################################################
################################################################################
Fundamental information about the particle distribution
generated on Sat Jul 11 16:48:48 2020
Physical quantities in Astrophysical units is listed
################################################################################
################################################################################
```

```
Total mass of the system  Mtot is 1.520960e+12 Msun
Total number of particles Ntot is 33554432 (= 2^25)
Number of components      kind is 5
##############################################################################
Length of Plummer softening  is 1.953125e-03 kpc
Snapshot interval            is 2.500000e+01 Myr
Final time of the simulation is 1.575000e+03 Myr
##############################################################################
##############################################################################

##############################################################################
##############################################################################
0-th component: Plummer model
##############################################################################
Total number of particles Ntot is 4412 (about 2^12)
Range of idx for the component is [0, 4411]
Mass of each N-body particle m is 4.533092e+04 Msun
##############################################################################
Total mass of the component Mtot is 2.000000e+08 Msun
Scale radius of the component rs is 3.000000e-02 kpc
Scale density of the component rho0 is 1.216003e+01 E-20 g / cm3
##############################################################################
##############################################################################
Representative scales:
Half-mass radius          r_{1/2} is 3.859127e-02 kpc
Effective radius          R_{eff} is 1.712579e-02 kpc
#########
Representative quantities at the center:
Volume density              rho is 1.216003e+01 E-20 g / cm3
Column density            Sigma is 1.500800e+01 g / cm2
Velocity dispersion     sigma_r is 7.505508e+01 km / s
LoS velocity dispersion sig_los is 7.008284e+01 km / s
#########
Representative quantities at the scale radius:
Volume density              rho is 2.149610e+00 E-20 g / cm3
Column density            Sigma is 3.751419e+00 g / cm2
Enclosed mass of this component  is 7.184391e+07 Msun
Enclosed mass of  all components is 8.113377e+07 Msun
Velocity dispersion     sigma_r is 6.309609e+01 km / s
LoS velocity dispersion sig_los is 6.031318e+01 km / s
#########
Representative quantities at the half-mass radius:
Volume density              rho is 1.058938e+00 E-20 g / cm3
Column density            Sigma is 2.128883e+00 g / cm2
Enclosed mass of this component  is 1.000000e+08 Msun
Enclosed mass of  all components is 1.152773e+08 Msun
Velocity dispersion     sigma_r is 5.975230e+01 km / s
```

```
LoS velocity dispersion  sig_los is 5.738213e+01 km / s
#########
Representative quantities at the effective radius:
Volume density              rho is 6.007222e+00 E-20 g / cm3
Column density            Sigma is 8.536835e+00 g / cm2
Enclosed mass of this component  is 2.476088e+07 Msun
Enclosed mass of  all components is 2.778494e+07 Msun
Velocity dispersion       sigma_r is 6.892584e+01 km / s
LoS velocity dispersion  sig_los is 6.546126e+01 km / s
######################################################################
Cutoff radius of the component   is 3.000000e-01 kpc
Cutoff  width of the component   is 3.000000e-02 kpc
Cutoff radius over scale radius  is 1.000000e+01
Cutoff  width over scale radius  is 1.000000e+00
Cutoff energy of the component   is 2.695822e+05 E+10 erg / g
(= 9.402097e+00 G Mtot / rs)
######################################################################
Total number of particles within the scale length is      1.790000e+03
Enclosed mass of all components within the scale length is 8.113377e+07 Msun
Free-fall time at the scale length                 is 3.021021e-01 Myr
Two-body relaxation time at the scale length       is 6.186046e+00 Myr
######################################################################
Snapshot interval in the unit of free-fall time        is 8.275349e+01
Snapshot interval in the unit of two-body relaxation time is 4.041354e+00
######################################################################
Final time of the simulation in the unit of free-fall time       is 5.213470e+03
Final time of the simulation in the unit of two-body relaxation time is 2.546053e+02
######################################################################
######################################################################

######################################################################
######################################################################
1-th component: Hernquist model
######################################################################
Total number of particles Ntot is 104570 (about 2^16)
Range of idx for the component is [4412, 108981]
Mass of each N-body particle m is 4.532849e+04 Msun
######################################################################
Total mass of the component Mtot is 4.740000e+09 Msun
Scale radius of the component rs is 8.350000e-01 kpc
Scale density of the component rho0 is 1.032511e-02 E-20 g / cm3
######################################################################
######################################################################
Representative scales:
Half-mass radius          r_{1/2} is 1.562208e+00 kpc
Effective radius          R_{eff} is 5.150969e-01 kpc
#########
```

```
Representative quantities at the center:
Volume density            rho is 9.040235e+03 E-20 g / cm3
Column density          Sigma is 6.276181e+00 g / cm2
Velocity dispersion    sigma_r is 4.279501e+01 km / s
LoS velocity dispersion sig_los is 8.090217e+01 km / s
#########
Representative quantities at the scale radius:
Volume density            rho is 1.290639e-03 E-20 g / cm3
Column density          Sigma is 7.079408e-02 g / cm2
Enclosed mass of this component  is 1.395153e+09 Msun
Enclosed mass of  all components is 4.303589e+09 Msun
Velocity dispersion    sigma_r is 9.966850e+01 km / s
LoS velocity dispersion sig_los is 1.038131e+02 km / s
#########
Representative quantities at the half-mass radius:
Volume density            rho is 2.332300e-04 E-20 g / cm3
Column density          Sigma is 2.128270e-02 g / cm2
Enclosed mass of this component  is 2.370000e+09 Msun
Enclosed mass of  all components is 1.139864e+10 Msun
Velocity dispersion    sigma_r is 1.084882e+02 km / s
LoS velocity dispersion sig_los is 1.115300e+02 km / s
#########
Representative quantities at the effective radius:
Volume density            rho is 3.959651e-03 E-20 g / cm3
Column density          Sigma is 1.499972e-01 g / cm2
Enclosed mass of this component  is 8.123254e+08 Msun
Enclosed mass of  all components is 2.014898e+09 Msun
Velocity dispersion    sigma_r is 9.392771e+01 km / s
LoS velocity dispersion sig_los is 9.842555e+01 km / s
#############################################################################
Cutoff radius of the component   is 1.000000e+01 kpc
Cutoff  width of the component   is 1.000000e+00 kpc
Cutoff radius over scale radius  is 1.197605e+01
Cutoff  width over scale radius  is 1.197605e+00
Cutoff energy of the component   is 7.929909e+04 E+10 erg / g
(= 3.248020e+00 G Mtot / rs)
#############################################################################
Total number of particles within the scale length is    9.494200e+04
Enclosed mass of all components within the scale length is 4.303589e+09 Msun
Free-fall time at the scale length                is 6.090977e+00 Myr
Two-body relaxation time at the scale length      is 2.983088e+03 Myr
#############################################################################
Snapshot interval in the unit of free-fall time        is 4.104432e+00
Snapshot interval in the unit of two-body relaxation time is 8.380578e-03
#############################################################################
Final time of the simulation in the unit of free-fall time       is 2.585792e+02
Final time of the simulation in the unit of two-body relaxation time is 5.279764e-01
```

```
################################################################################
################################################################################

################################################################################
################################################################################
2-th component: NFW model
################################################################################
Total number of particles Ntot is 32130154 (about 2^24)
Range of idx for the component is [108982, 32239135]
Mass of each N-body particle m is 4.532814e+04 Msun
################################################################################
Total mass of the component Mtot is 1.456400e+12 Msun
Scale radius of the component rs is 1.463000e+01 kpc
Scale density of the component rho0 is 1.329217e-04 E-20 g / cm3
################################################################################
################################################################################
Representative scales:
Half-mass radius         r_{1/2} is 7.145874e+01 kpc
Effective radius         R_{eff} is 2.272094e+01 kpc
#########
Representative quantities at the center:
Volume density             rho is 2.039108e+03 E-20 g / cm3
Column density           Sigma is 1.509996e+00 g / cm2
Velocity dispersion      sigma_r is 4.593675e+01 km / s
LoS velocity dispersion  sig_los is 9.980669e+01 km / s
#########
Representative quantities at the scale radius:
Volume density             rho is 3.323043e-05 E-20 g / cm3
Column density           Sigma is 3.952033e-02 g / cm2
Enclosed mass of this component  is 1.492709e+11 Msun
Enclosed mass of  all components is 2.102915e+11 Msun
Velocity dispersion      sigma_r is 1.647067e+02 km / s
LoS velocity dispersion  sig_los is 1.546137e+02 km / s
#########
Representative quantities at the half-mass radius:
Volume density             rho is 7.859230e-07 E-20 g / cm3
Column density           Sigma is 3.514395e-03 g / cm2
Enclosed mass of this component  is 7.282000e+11 Msun
Enclosed mass of  all components is 7.927600e+11 Msun
Velocity dispersion      sigma_r is 1.221260e+02 km / s
LoS velocity dispersion  sig_los is 1.121341e+02 km / s
#########
Representative quantities at the effective radius:
Volume density             rho is 1.313105e-05 E-20 g / cm3
Column density           Sigma is 2.242102e-02 g / cm2
Enclosed mass of this component  is 2.542427e+11 Msun
Enclosed mass of  all components is 3.184481e+11 Msun
```

```
Velocity dispersion       sigma_r is 1.541847e+02 km / s
LoS velocity dispersion  sig_los is 1.442999e+02 km / s
####################################################################
Cutoff radius of the component   is 2.345000e+02 kpc
Cutoff  width of the component   is 2.500000e+01 kpc
Cutoff radius over scale radius  is 1.602871e+01
Cutoff  width over scale radius  is 1.708817e+00
Cutoff energy of the component   is 4.226321e+03 E+10 erg / g
(= 9.871166e-03 G Mtot / rs)
####################################################################
Total number of particles within the scale length is     4.639313e+06
Enclosed mass of all components within the scale length is 2.102915e+11 Msun
Free-fall time at the scale length                is 6.390403e+01 Myr
Two-body relaxation time at the scale length      is 1.038482e+06 Myr
####################################################################
Snapshot interval in the unit of free-fall time        is 3.912116e-01
Snapshot interval in the unit of two-body relaxation time is 2.407360e-05
####################################################################
Final time of the simulation in the unit of free-fall time      is 2.464633e+01
Final time of the simulation in the unit of two-body relaxation time is 1.516637e-03
####################################################################
####################################################################


####################################################################
####################################################################
3-th component: Exponential disk
####################################################################
Total number of particles Ntot is 1163956 (about 2^20)
Range of idx for the component is [32239136, 33403091]
Mass of each N-body particle m is 4.532817e+04 Msun
####################################################################
Total mass of the component Mtot is 5.276000e+10 Msun
Scale radius of the component rs is 3.123000e+00 kpc
####################################################################
Scale height of the component zd is 3.000000e-01 kpc
``ENABLE_VARIABLE_SCALE_HEIGHT'' is on.
Dimming height of the component is 16.000000 times zd
Retrograding fraction (input)    is 0.000000e+00
Retrograding fraction (output)   is 8.591390e-07
Central surface density   Sigma0 is 1.799453e-01 g / cm2
Circular speed at scale radius   is 2.895863e+02 km / s
Maximum circular speed           is 3.472355e+02 km / s
Circular speed is maximized      at 8.250000e+00 kpc
``ENFORCE_EPICYCLIC_APPROXIMATION'' is off.
Horizontal velocity dispersion   is 6.685713e+00 km / s
Vertical   velocity dispersion   is 8.972836e+01 km / s
Toomre's Q-value at scale radius is 1.332559e-01
```

```
Minimum of Toomre's Q-value      is 8.978121e-02 at R = 7.984375e+00 kpc,
when excluding central region (estimation from scale height profile)
Minimum of Toomre's Q-value      is 8.978121e-02 at R = 7.984375e+00 kpc
################################################################################
Representative scales:
Half-mass radius        r_{1/2} is 5.418332e+00 kpc
Effective radius        R_{eff} is 5.237401e+00 kpc
################################################################################
Cutoff radius of the component   is 3.000000e+01 kpc
Cutoff  width of the component   is 3.000000e+00 kpc
Cutoff radius over scale radius  is 9.606148e+00
Cutoff  width over scale radius  is 9.606148e-01
Cutoff energy of the component   is 1.920546e-137 E+10 erg / g
(= 2.643226e-142 G Mtot / rs)
################################################################################
Total number of particles within the scale length is      7.111970e+05
Enclosed mass of all components within the scale length is 3.223726e+10 Msun
Free-fall time at the scale length                 is 1.609724e+01 Myr
Rotation time scale at the scale length            is 6.625527e+01 Myr
Two-body relaxation time at the scale length       is 4.849586e+04 Myr
################################################################################
Snapshot interval in the unit of free-fall time          is 1.553061e+00
Snapshot interval in the unit of rotation time scale     is 3.773285e-01
Snapshot interval in the unit of two-body relaxation time is 5.155079e-04
################################################################################
Final time of the simulation in the unit of free-fall time       is 9.784284e+01
Final time of the simulation in the unit of rotation time scale    is 2.377169e+01
Final time of the simulation in the unit of two-body relaxation time is 3.247700e-02
################################################################################
################################################################################

################################################################################
################################################################################
4-th component: Exponential disk
################################################################################
Total number of particles Ntot is 151340 (about 2^17)
Range of idx for the component is [33403092, 33554431]
Mass of each N-body particle m is 4.532840e+04 Msun
################################################################################
Total mass of the component Mtot is 6.860000e+09 Msun
Scale radius of the component rs is 3.123000e+00 kpc
################################################################################
Scale height of the component zd is 1.000000e+00 kpc
''ENABLE_VARIABLE_SCALE_HEIGHT'' is on.
Dimming height of the component is 16.000000 times zd
Retrograding fraction (input)    is 0.000000e+00
Retrograding fraction (output)   is 0.000000e+00
```

```
Central surface density   Sigma0 is 2.339698e-02 g / cm2
Circular speed at scale radius  is 2.895863e+02 km / s
Maximum circular speed          is 3.472355e+02 km / s
Circular speed is maximized     at 8.250000e+00 kpc
''ENFORCE_EPICYCLIC_APPROXIMATION'' is off.
Horizontal velocity dispersion  is 8.692947e-01 km / s
Vertical   velocity dispersion  is 1.112269e+02 km / s
Toomre's Q-value at scale radius is 1.332559e-01
Minimum of Toomre's Q-value     is 8.978121e-02 at R = 7.984375e+00 kpc,
when excluding central region (estimation from scale height profile)
Minimum of Toomre's Q-value     is 8.978121e-02 at R = 7.984375e+00 kpc
################################################################################
Representative scales:
Half-mass radius        r_{1/2} is 5.374424e+00 kpc
Effective radius        R_{eff} is 5.237401e+00 kpc
################################################################################
Cutoff radius of the component   is 3.000000e+01 kpc
Cutoff  width of the component   is 3.000000e+00 kpc
Cutoff radius over scale radius  is 9.606148e+00
Cutoff  width over scale radius  is 9.606148e-01
Cutoff energy of the component   is 5.749344e-152 E+10 erg / g
(= 6.085671e-156 G Mtot / rs)
################################################################################
Total number of particles within the scale length is      7.111970e+05
Enclosed mass of all components within the scale length is 3.223726e+10 Msun
Free-fall time at the scale length                 is 1.609724e+01 Myr
Rotation time scale at the scale length            is 6.625527e+01 Myr
Two-body relaxation time at the scale length       is 4.849586e+04 Myr
################################################################################
Snapshot interval in the unit of free-fall time        is 1.553061e+00
Snapshot interval in the unit of rotation time scale   is 3.773285e-01
Snapshot interval in the unit of two-body relaxation time is 5.155079e-04
################################################################################
Final time of the simulation in the unit of free-fall time       is 9.784284e+01
Final time of the simulation in the unit of rotation time scale   is 2.377169e+01
Final time of the simulation in the unit of two-body relaxation time is 3.247700e-02
################################################################################
################################################################################
```

D.2   Experiment on individual orbits

As the reader may noticed, the DMH consider to generate the initial conditions is a classical
NFW sphere, then we have an axisymmetric system (nuclear region, bulge, double exponential
disk and DMH). In order to introduce a strong source of chaos in the DMH (2nd component in
the `hydra.info.txt` file, Section D.1), the integration with the `LP-VIcode` is done using the
`milkywayhydra.pav` file with the option 2 of the DMH selected, and given it a full bi–triaxial

shape.

As we are not interested in analysing a real system, but making the comparison on the computations of two code flavours on the same individual particles, we are not going to relax the system before doing the calculations. That is, we are going to integrate for 6.135 u.t. an axisymmetric distribution of initial conditions in a non-axisymmetric potential.

D.2.1   Using a TI model

We take 500 initial conditions randomly selected from the DMH sphere (`MAGI` returns 32130154 initial conditions for the DMH[2]) and integrate them for 6.135 u.t. (6 Gyr) using the *Hydra 2.0* TI version of our `milkywayhydra.pav` with all `LP-VIcode` flags activated, i.e. all quantities available are now `ON`.

After the integration is finished, we select three orbits with completely different behaviours: orbit labelled "1" seems to be a stable regular orbit, "2" an unstable regular orbit (sticky or may be mildly chaotic) and "3" is definitely a chaotic orbit (according to MEGNO criteria, middle right panel of Fig. D.2). On these three initial conditions, we have all the quantities that the `LP-VIcode` can offer applying both flavours of the `milkywayhydra.pav`: the pre–SMART flavour and the `SMART` flavour. In Fig. D.1 we present all the physical data for each orbit, while in Figs. D.2 and D.3 we show all the CIs that the `LP-VIcode` has available in its library.

Apart from the RLI, the coincidence between the results given by both flavours is total. There are differences in the RLI because such indicator uses two different orbits to be computed, and the selection of the shadow (second) orbit could differ. Then, the differences with the RLI are expected. However, the classification is the same for all the three orbits of the sample which is expected.

D.2.2   Using a PTD model

We integrate again the previously sample of 500 initial conditions, but using the *Hydra 2.0* periodic time dependent (PTD) version of the `milkywayhydra.pav`, i.e. we activate the bar and the spiral arms (but growth factor off, i.e. no cosmological evolution for such components, just periodic dependence). We select the same three orbits as before and the results are shown in Fig. D.4 where the $x(t)$, the projection of the three orbits on the plane as well as the projection for the chaotic orbit alone is shown on the top row, at the left, middle and right panels, respectively. Also, the time evolution of the energy and that of the CIs OFLI and MEGNO are presented on the bottom row, left, middle and right panels, respectively.

It is not our intention here to make a full dynamical analysis of the orbits considered in the experiment, but to make a couple of relevant observations. First, orbits one and two show no evident signs of differences in their computation of the phase space coordinates by both

---

[2]The complete distribution can be obtained from the `hydra.summary.txt` and it is the following: 4412 particles in the nuclear region, 104570 in the bulge, 32130154 in the DMH, 1163956 and 151340 in the thin and thick disks, respectively.
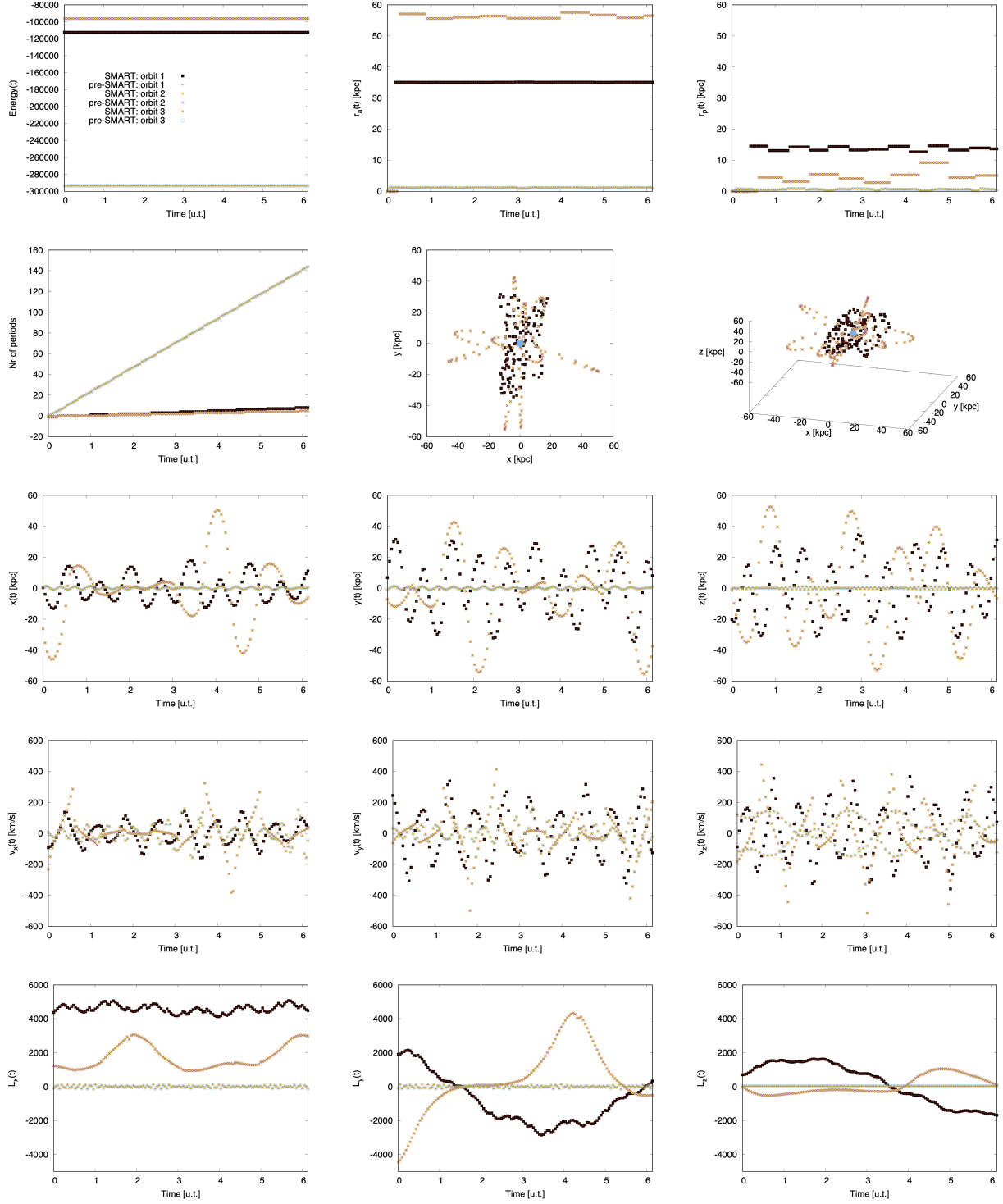
Figure D.1: Time evolution of the physical quantities. Top row: energy, last apocentre and pericentre of the orbit. Middle top row: number of periods, projection of the orbit on the xy–plane and its 3–dimensional representation. Middle row: positions, coordinates x, y and z. Middle bottom row: velocities, components x, y and z. Bottom row: angular momentum, components x, y and z.
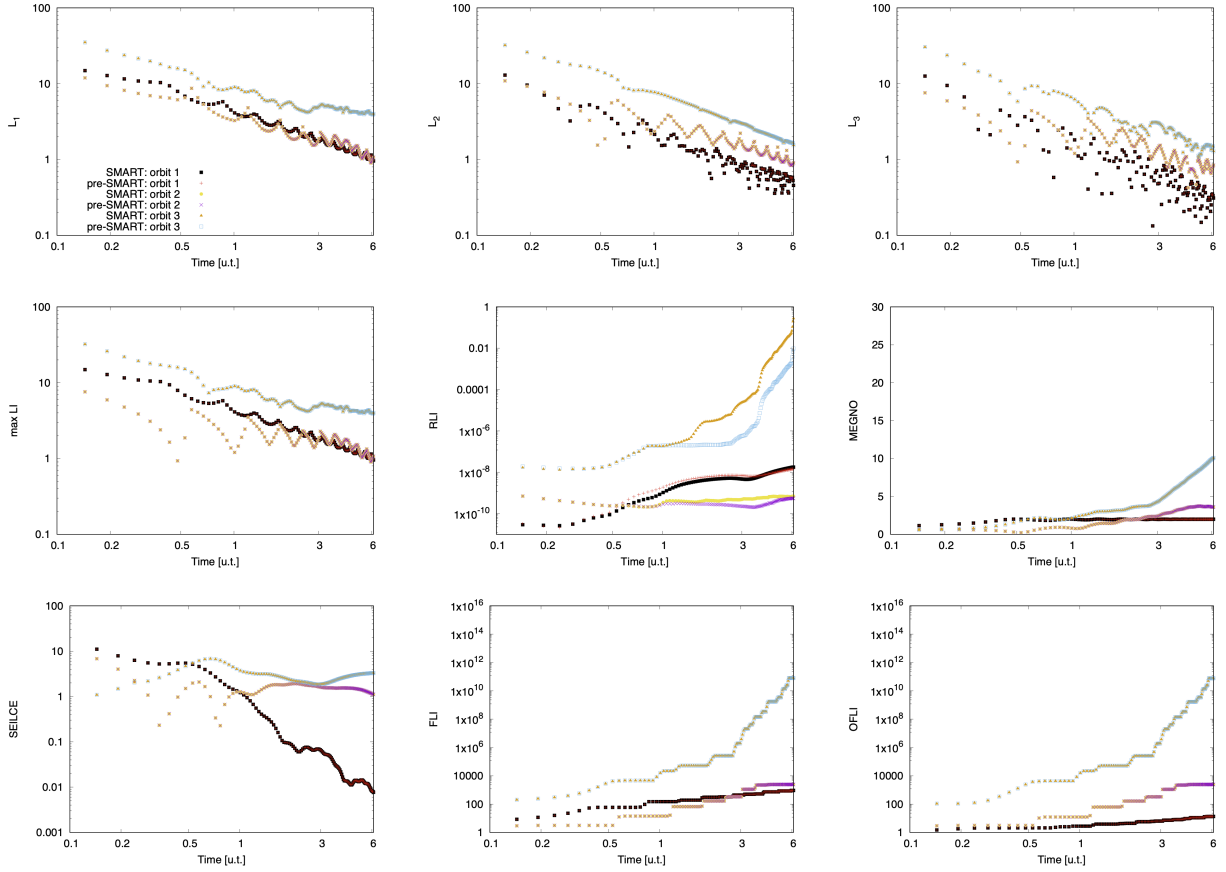
Figure D.2: Chaos indicators. Top row: the positive Lyapunov Indicators (L1, L2 and L3). Middle row: the maximum Lyapunov Indicador (maxLI), the Relative Lyapunov Indicator (RLI) and the Mean Exponential Growth factor of Nearby Orbits (MEGNO). Bottom row: the Slope Estimation of the largest Lyapunov Characteristic Exponent (SElLCE), the Fast Lyapunov Indicator (FLI) and the Orthogonal Fast Lyapunov Indicator (OFLI).
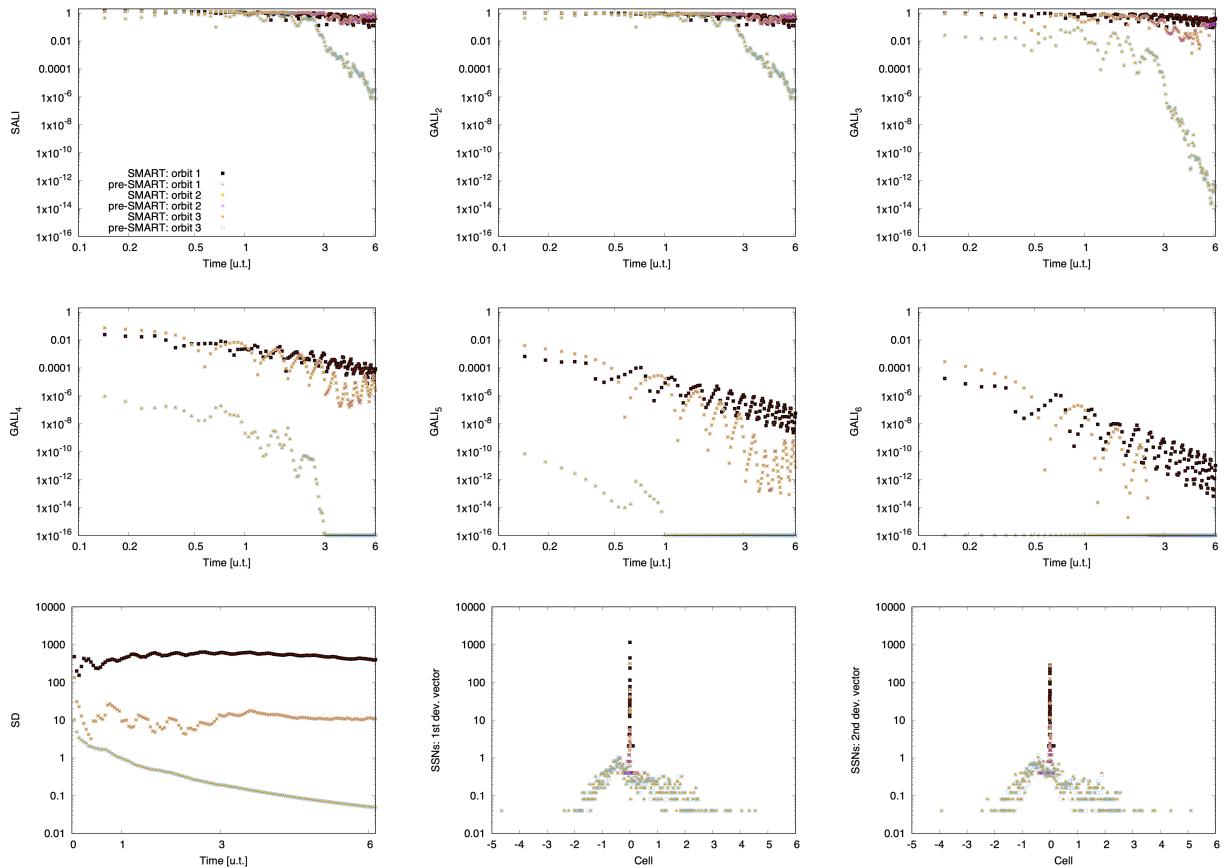
Figure D.3: Chaos indicators continuation. Top row: the Smaller ALignment Index (SALI) and the Generalized ALignment Index (GALI2 and GALI3). Middle row: GALI4, GALI5 and GALI6. Bottom row: the Spectral Distance (SD) and the dynamical Spectra of Stretching Numbers (SSN1 and SSN2).

flavours (top left and middle panels of Fig. D.4[3]). However, there is such sign at the end of the integration in some CIs (for instance, MEGNO, bottom right panel of Fig. D.4) while there is no clear sign on others (for instance, OFLI, bottom middle panel of same figure). Therefore, the reason for this somehow elusive discrepancy must lie on the evolution of the deviation vectors, which is expected when using two different programs to follow them on a TD potential: deviation vectors might evolve different even though base orbits are almost the same. The extreme case occurs with the third orbit (the one classified like chaotic in the TI model). Here we have clear signs of discrepancies right from the beginning: i.e. on their phase space coordinates (top right panel of Fig. D.4 shows the projection of the orbit on the plane). Also, the energy differs (bottom left panel of Fig. D.4) and thus, those differences between flavours are reflected on the CIs very easily, indeed. Again, this is totally expected, but in this case reinforced on the most probable chaotic nature of the orbit, i.e.: deviation vectors evolve different because base orbits are different.

Then, the first remark is that despite the fact that there are differences between the curves for both flavours, this is expected as they are not computed in the same way on a TD potential (where phase–space volumes are not conserved), and that difference increases with the chaotic character of the orbit. The second and more important remark is that the character of the orbits computed by both flavours seems to agree perfectly well. That is, all three orbits seem to have the same classification with all CIs independently of the flavour used to compute them, which is what really matters. For instance, notice that the probable chaotic orbit has an exponential profile with the OFLI and increases with time in case of the MEGNO (clear signs of chaotic behaviour in time independent potentials), and this happens using both flavours. Therefore, the characterization of the orbits do not vary from one flavour of the `milkywayhydra.pav` to another. In other words, the regular orbit (according to MEGNO in the TI model) is still regular for both flavours, the unstable regular or mildly chaotic seems to be characterized equally by both flavours and, last but not least, the aforementioned chaotic orbit remains clearly chaotic for both flavours of the `milkywayhydra.pav`.

D.2.3 Using a FTD model

We integrate one more time the sample of 500 initial conditions, but in this case using the *Hydra 2.0* full TD (FTD) version of the `milkywayhydra.pav`, i.e. not only we activate the bar and the spiral arms but we turn on the growth factor so the time dependent components are introduced in a more realistic way. Then, both components are not present from the beginning of the integration as in the PTD experiment, but they start to grow slowly until they reach their final amplitudes by 3.068 u.t. (i.e. 3 Gyr). The results for the same three orbits used with the TI and PTD models are shown in Fig. D.5 where the $x(t)$, the projection of the three orbits on the plane as well as the projection for the chaotic orbit alone is shown on the top row, at the left, middle and right panels, respectively. Also, the time evolution of the energy and that of the CIs OFLI and MEGNO are presented on the bottom row, left, middle and right panels, respectively.

The observations given in last section also applied in this experiment (see Fig. D.5 and compare with Fig. D.4). However, the differences are less evident, at least for the first part of

---

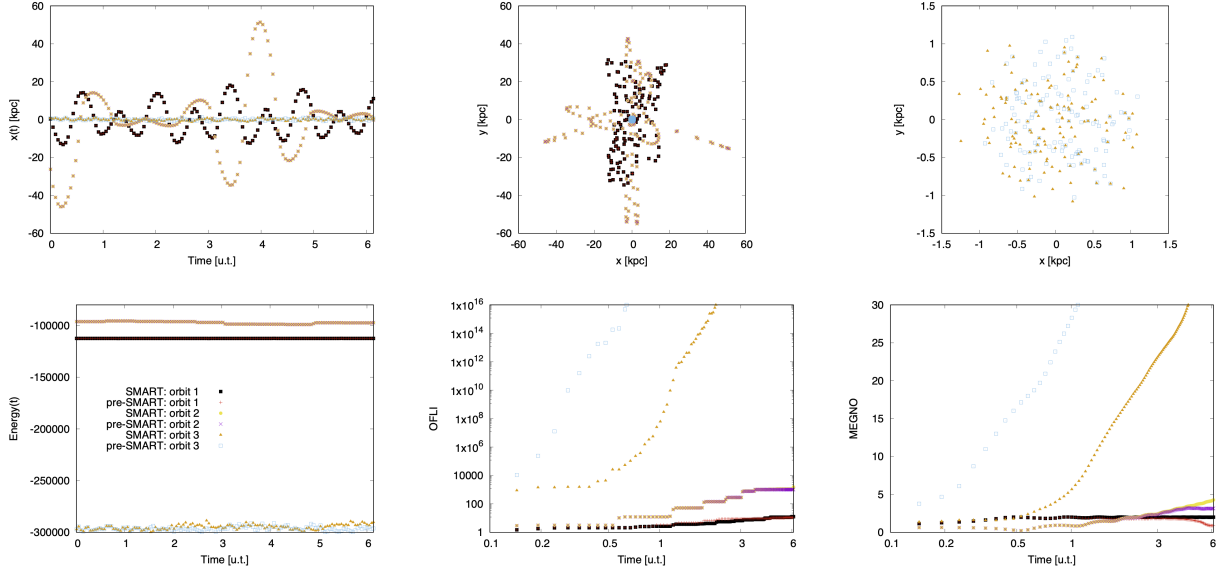[3]There are numerical differences, but they are rather small and thus, they are not evident in the plots.

Figure D.4: Experiment on the PTD model. Top row: $x(t)$ (left panel), (x, y) (middle panel) and (x, y) for the chaotic orbit alone (right panel). Bottom row: energy (left panel), OFLI (middle panel) and MEGNO (right panel).

the integration. The reason is that the time dependent components (bar and spiral arms) are now growing slowly and they are not present at full amplitude from the start, as in the previous experiment (PTD experiment). Then, at the beginning of the integration, the system resembles that of the TI model where both flavours matched completely. This can be seen very clearly from the behaviours of the CIs on the chaotic orbit, OFLI and MEGNO (bottom middle and right panels of Fig. D.5), where such orbit is depicted with equal curves with both flavours until ~ 0.7 u.t. Then, they start to be separated from each other, revealing that the effect of the bar and the spiral arms starts to be relevant on the computation of the evolution of the corresponding deviation vectors.

We are aware that the CIs should not be used so loosely to classify orbits in TD potentials, but inhere we are not interested in the precise classification of the orbits, but in the level of agreement of both flavours on plausible classifications. Then, these series of tests give evidence in favour of our main hypothesis: both flavours of the `milkywayhydra.pav` are fully compatible.

RESULT 0: this experiment on individual orbits allow us to confirm that the original `milkywayhydra.pav` file is now double–check: not only expression by expression with algebraic manipulators (Appendix B) but also as a whole with a completely separate automatic differentiation code.

In order to see if this result is or is not circunstancial due to the small size of the sample (visual inspection was only done on 3 orbits), we attempt to see if both flavours reach similar conclusions on statistical samples as well. Therefore, in the next section we make some further
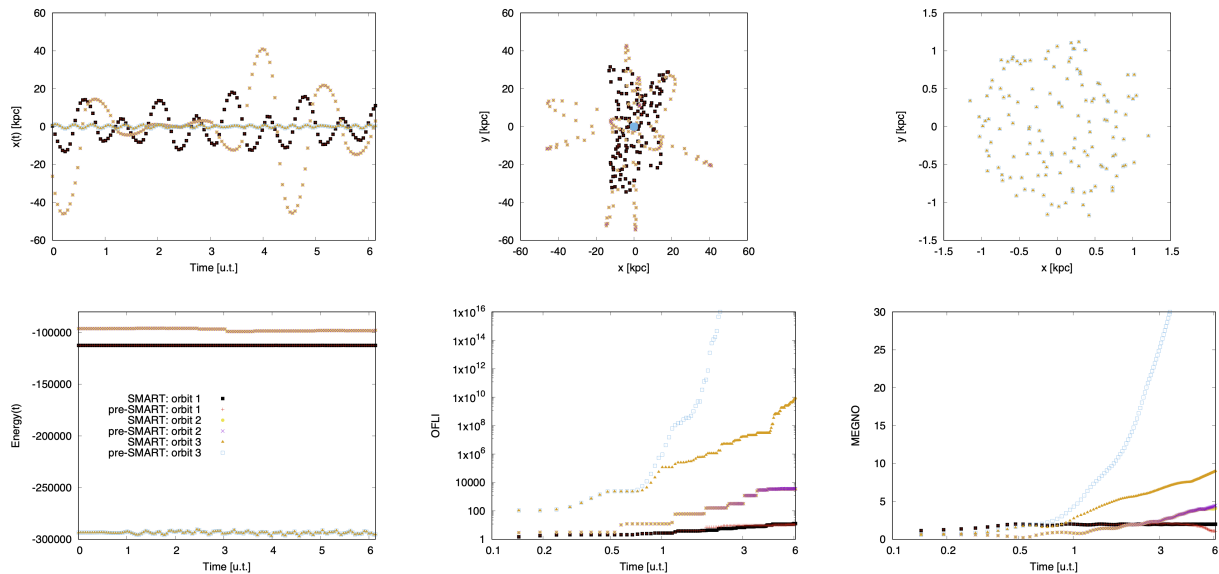
Figure D.5: Experiment on the FTD model. Top row: $x(t)$ (left panel), (x, y) (middle panel) and (x, y) for the chaotic orbit alone (right panel). Bottom row: energy (left panel), OFLI (middle panel) and MEGNO (right panel).

testing but considering a statistical meaningful sample of initial conditions.

D.3 Experiments on a statistical sample of orbits

D.3.1 First experiment: relaxing the thin disk component

In the next series of experiments we are going to focus our tests on the thin disk particles alone (3rd component in the `hydra.info.txt` file, Section D.1), which is a component full of rich dynamics. Then, `MAGI` returns 1163956 thin disk particles that are enough to have a good representation of such component.

As mentioned before, the initial distribution of the particles generated with `MAGI` does not follow exactly our (slightly modified) *Hydra 2.0* TI model, because they were not autoconsistently generated. For instance, our DMH for the following experiments is not completely spherical as the one used with `MAGI`, but oblate in the inner parts (parameter values are shown below). Hereinafter we will try to mimic a real study, thus we need to take good care of the details. Therefore, the next step before diving into the dynamics of the thin disk is to achieve a relaxed distribution by integrating the 1163956 thin disk particles for around 9.6 u.t. ($\sim 9.39\,\mathrm{Gyr}$) in the exact TI potential of the `milkywayhydra.pav` file (with the `LP-VIcode`).

After the unit conversion of the velocities from C.U. to km/s, we have the file with initial conditions for the `LP-VIcode`: `hydra.in`. We set up the configuration and parameter files for the latter code. In particular, the `LP-VIcode.in` reads:

```
# LP-VIcode version 2.0.2
```

```
# Initial conditions file (max. 50 characters)
hydra1.in
# Prefix for output files (max. 50 characters)
hydra1
# Step of integration
0.0048d0
# Initial time; final time of integration
0.d0 9.6d0
# Screen (0=no, 1=yes) & orbit (0=no output, 1=output, 2=output additionals)
1 1
# Indicators: 0=don't compute, 1=output for all t, 2=output only last value
# LIs, SALI, GALIs, SD & SSNs, RLI & LImax, MEGNO & SElLCE, FLI & OFLI
0 0 0 0 0 0 0
# Nr. of steps between outputs (when orbit or indicators are = 1)
400
# Initial dev. vectors (0 = at random, 1 = random orthonormal, 2=fixed)
1
# SALI & potential(t): normal saturation (=0) or restart dev. vectors (=1)
0
```

We are doing two parallel integrations, one with the LP-VIcode using the pre–SMART flavour of the TI model and the other using the SMART flavour of the same model. They have the following parameter values in the subroutine potinit:

```
**********************************************************************
* NUCLEAR REGION
**********************************************************************

* ADD-REM Parameter
* [SOURCE: Marinacci et al. 2014 (MNRAS, 437, 1750)]
* [COMMENT: M_nuclear = 2x10^8 M_sun]

      gmsmbh=8.60234d2
*      gmsmbh=0.d0

* [SOURCE: Launhardt et al. 2002 (A&A, 384, 112)]
      epsmbh=0.03d0


**********************************************************************
* GROWTH FACTOR
* BAR AND SPIRAL ARMS
**********************************************************************

* ADD-REM Parameter
* [SOURCE: Monari et al. 2016 (MNRAS, 461, 3835)]
*      atime=3.068d0
      atime=0.d0
```

```
**************************************************************************
* PEANUT-SHAPED BULGE
**************************************************************************


* Bulge spheroid
* ADD-REM Parameter
* [SOURCE: Marinacci et al. 2014 (MNRAS, 437, 1750)]
* [COMMENT: M_bulge = 4.74x10^9 M_sun]
      gmbulge=2.03875458d4
*      gmbulge=0.d0

      epsbulge=0.835d0


* Bar
* ADD-REM Parameter
* [SOURCE: Monari et al. 2016 (MNRAS, 461, 3835)]
*      alpha=0.01d0
      alpha=0.d0

      barcoef=8.331938927d6
      rbar=3.5d0
      phibar=5.65d0
* [COMMENT: bomegabar = -52.2 km s-1 kpc-1]
      bomegabar=-52.2d0


**************************************************************************
* SPIRAL ARMS
**************************************************************************


* ADD-REM Parameter
* [COMMENT: Super strong spirals 200 per cent density contrast]
*      armscoef=2279.d0
      armscoef=0.d0

* [SOURCE: Monari et al. 2016 (MNRAS, 461, 3835)]
      narms=2
      nindex=1
      p=0.17d0
      rarms=1.d0
      rscarms=3.124d0
      phiarms=3.31d0
* [COMMENT: bomegaarms = -18.9 km s-1 kpc-1]
      bomegarms=-18.9d0
* [COMMENT: scale height  of the thin disc]
      hs=0.3d0
* [COMMENT: Exclusion coefficient for inner spiral arms]
```

```
* [COMMENT: corrotation radius]
      excoefarms=4.08d0


*********************************************************************
* DISK
*********************************************************************

* (1) MN PROFILE
* ADD-REM Parameters
* [SOURCE: Marinacci et al. 2014 (MNRAS, 437, 1750), Model Aq-C-4/5]
* [COMMENT: M_disk = 5.961x10^10 M_sun]
* [COMMENT: e_s = 3.124 kpc]
* [COMMENT: e_h = 0.3 kpc]
*      gmdiskmn=25.63927437d4
      gmdiskmn=0.d0

      epscalemn=3.124d0
      epsheightmn=0.3d0

* (2) EXPONENTIAL PROFILE
* Thin disk
* ADD-REM Parameters
* [SOURCE: Binney J., Tremaine S., 2008, Galactic Dynamics: 2nd Ed.]
* [SOURCE: Monari et al. 2016 (MNRAS, 461, 3835)]
* [SOURCE: Smith et al. 2015 (MNRAS, 448, 2934)]
* [COMMENT: M^thin_disk = 5.276x10^10 M_sun (88.5% MN PROFILE)]
* [COMMENT: R^thin_d = 3.124 Gyr]
* [COMMENT: h^thin_z = 0.3 kpc]
      gmdisk(1)=3.65402813d4
      gmdisk(2)=-1.308919778d6
      gmdisk(3)=1.525374597d6
*      gmdisk(1)=0.d0
*      gmdisk(2)=0.d0
*      gmdisk(3)=0.d0

      epscale(1)=1.751620652d0
      epsheight(1)=0.357969749d0

      epscale(2)=8.045207335d0
      epsheight(2)=0.357969749d0

      epscale(3)=7.007698163d0
      epsheight(3)=0.357969749d0

* Thick disk
* ADD-REM Parameters
* [SOURCE: Binney J., Tremaine S., 2008, Galactic Dynamics: 2nd Ed.]
```

```
* [SOURCE: Monari et al. 2016 (MNRAS, 461, 3835)]
* [SOURCE: Smith et al. 2015 (MNRAS, 448, 2934)]
* [COMMENT: M^thick_disk = 0.686x10^10 M_sun (11.5% MN PROFILE)]
* [COMMENT: R^thick_d = 3.124 Gyr]
* [COMMENT: h^thick_z = 1 kpc]
      gmdiskthk(1)=3.9689420d3
      gmdiskthk(2)=-1.687186076d5
      gmdiskthk(3)=1.986529253d5
*      gmdiskthk(1)=0.d0
*      gmdiskthk(2)=0.d0
*      gmdiskthk(3)=0.d0

      epscalethk(1)=0.908485192d0
      epsheightthk(1)=1.41014739d0

      epscalethk(2)=7.026555501d0
      epsheightthk(2)=1.41014739d0

      epscalethk(3)=6.213630283d0
      epsheightthk(3)=1.41014739d0


***********************************************************************
* DARK MATTER HALO
***********************************************************************

* (1) BI-TRIAXIAL EXTENSION NFW MODEL
* ADD-REM Parameter
* [SOURCE: Marinacci et al. 2014 (MNRAS, 437, 1750), Model Aq-C-4/5]
* [COMMENT: M_200 = 145.64x10^10 M_sun]
* [COMMENT: c_nfw = 16.0287081]
      acoef=3308059.4167264947d0
*      acoef=0.d0

      rs=14.63d0

      scoefi(1)=1.02d0
      scoefi(2)=1.02d0
      scoefi(3)=0.958749185d0
      scoefe(1)=1.d0
      scoefe(2)=1.d0
      scoefe(3)=1.d0

* (2) MODIFIED LOGARITHMIC MODEL
* ADD-REM Parameter
* [COMMENT: v_halo = 166.258 km/s]
*      vhalo=166.258d0
      vhalo=0.d0
```

```
* [SOURCE: Vera-Ciro & Helmi 2013 (ApJL, 773:L4)]
      d=12.d0
      ra=30.d0
      qcoef(1)=1.d0
      qcoef(2)=1.d0
      qcoef(3)=0.9d0
      qqcoef(1)=1.38d0
      qqcoef(2)=1.d0
      qqcoef(3)=1.36d0
      ascoef(1)=0.121869343d0
      ascoef(2)=-0.992546152d0
      wcoef(1)=0.992946717d0
      wcoef(2)=0.532153052d0
      wcoef(3)=0.114888764d0
```

Notice the zero values for the `ADD-REM` parameters associated with the bar and the spiral arms (`alpha` and `armscoef`, respectively, in order to have the TI model), as well as for the MN disk (option 1, `gmdiskmn`) and the modified logarithmic DMH (option 2, `vhalo`) and the growth factor (`atime`, i.e. no cosmological evolution).

Using the pre–SMART version

Checking for errors, there were just one orbit that did not finish the integration.

Fig. D.6 presents the evolution of the distribution of thin disk initial conditions on the disk plane, showing the slow convergence to a new relaxed system. In Fig. D.7 we show such convergence of the initial particle distribution to a sufficiently relaxed system by 9.6 u.t., following the actual profile of the (slightly modified) *Hydra 2.0* TI version of the `milkywayhydra.pav`.

Using the SMART version

We compute the accelerations with `SMART`. No variational equations are computed because we only need to integrate the equations of motion.

Checking for errors, there were just one orbit that did not finish the integration (the same orbit as with the pre–SMART flavour).

On the left panel, Fig. D.8 shows the convergence curves of the initial particle distribution using the `SMART` flavour of the (slightly modified) *Hydra 2.0* TI version of the `milkywayhydra.pav` file. Compare with the distributions achieved by the pre–SMART flavour, left panel of Fig. D.7. They look exactly the same. Indeed, on the right panel (Fig. D.8) we plot the differences between both pre–SMART and SMART new relaxed distributions at 9.6 u.t. (linear scale in this case). The coincidence is clear, there is not a single particle difference with both versions of the `milkywayhydra.pav`.
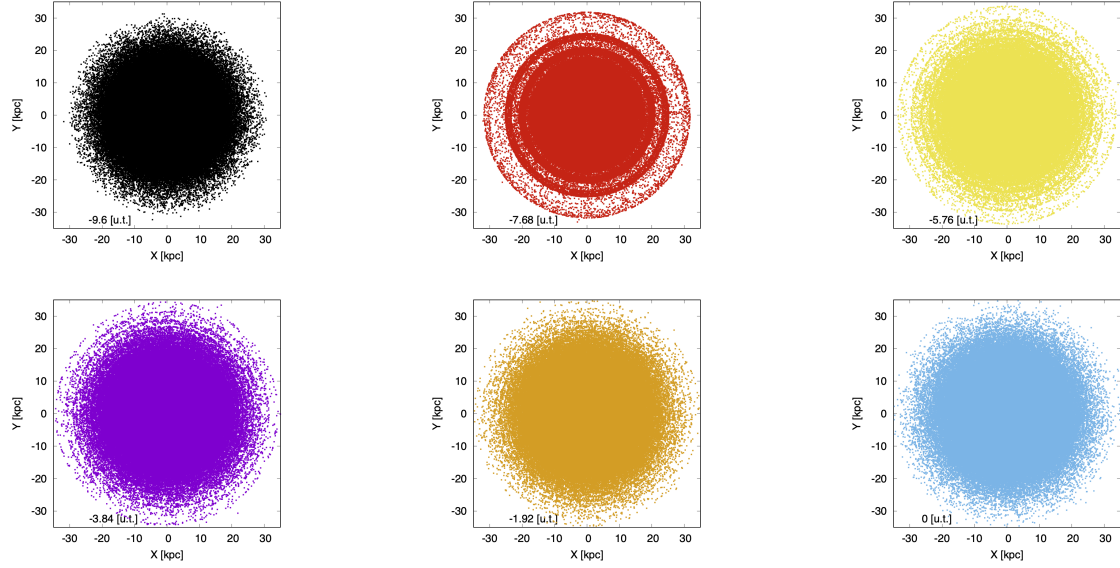
Figure D.6: Evolution of the distribution of thin disk initial conditions on the disk plane.
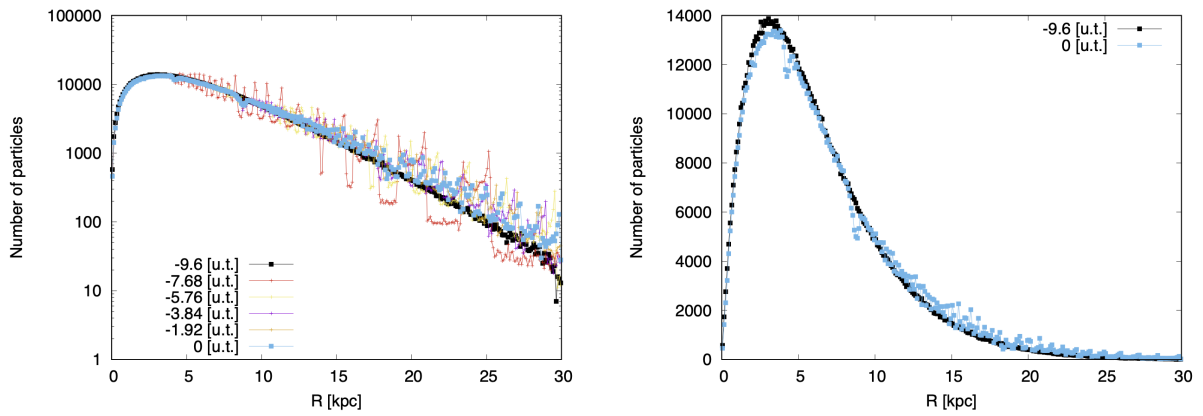

Figure D.7: Convergence of `MAGI` initial conditions to a new relaxed system after 9.6 u.t. using the pre–`SMART` `milkywayhydra.pav`. Left panel: logarithmic scale. Right panel: linear scale for −9.6 u.t. and 0 u.t. profiles alone.
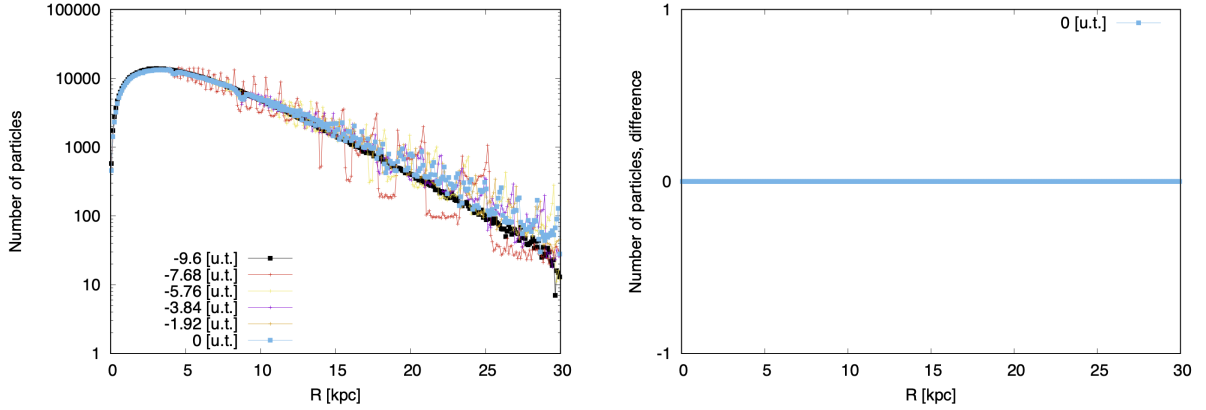
Figure D.8: Convergence of `MAGI` initial conditions to a new relaxed system after 9.6 u.t. using the `SMART` milkywayhydra.pav. Left panel: logarithmic scale. Right panel: linear scale for the differences between both flavours after 9.6 u.t. of evolution, they are exactly the same.

RESULT 1: this first experiment on a statistical sample of orbits shows that both flavours of the `milkywayhydra.pav` are compatible when `SMART` is only used to compute automatically the accelerations in a time independent model.

Now that we have reached convergence to our (slightly modified) *Hydra 2.0* TI model (after 9.6 u.t.), we can use the latter relaxed profile of new initial conditions to integrate it for an additonal 6.135 u.t. (6 Gyr) time interval, but in this case we are going to test two different configurations of the TD `milkywayhydra.pav` (i.e. bar and spiral pattern are now both activated). One will be using the so–called (slightly modified) *Hydra 2.0* PTD model (growth factor off, i.e. no cosmological evolution of bar or spiral arms) while the other will be the (slightly modified) *Hydra 2.0* FTD model (growth factor on).

D.3.2   Second experiment: computation of the equations of motion

Now that we have a new relaxed thin disk, we use the full `milkywayhydra.pav` file following two different (slightly modified) *Hydra 2.0* settings: (a) the PTD configuration where the bar and the spiral arms are activated at full strength right from the beginning and the integration is done for another 6.135 u.t. time interval, and (b) the FTD configuration where those time dependent components grow for the first 3.068 u.t. until they reach their maximum amplitudes, while keeping them at those values for the rest of the 6.135 u.t. time interval (Section 2.4 for further details).

We set up the configuration and parameter files for the `LP-VIcode`, particularly the `LP-VIcode.in` reads:

```
# LP-VIcode version 2.0.2
# Initial conditions file (max. 50 characters)
hydra2.in
# Prefix for output files (max. 50 characters)
```

```
hydra2
# Step of integration
0.004908d0
# Initial time; final time of integration
0.d0 6.135d0
# Screen (0=no, 1=yes) & orbit (0=no output, 1=output, 2=output additionals)
1 1
# Indicators: 0=don't compute, 1=output for all t, 2=output only last value
# LIs, SALI, GALIs, SD & SSNs, RLI & LImax, MEGNO & SElLCE, FLI & OFLI
0 0 0 0 0 0 0
# Nr. of steps between outputs (when orbit or indicators are = 1)
625
# Initial dev. vectors (0 = at random, 1 = random orthonormal, 2=fixed)
1
# SALI & potential(t): normal saturation (=0) or restart dev. vectors (=1)
0
```

With 625 steps between outputs we have an output file (for the orbits) made of blocks of 4 lines each, being those lines: (1) the initial condition (initial time 0 u.t.), (2) at ~ 3.068 u.t. (the moment when the bar and spiral arms reach their maximum and final amplitudes in case of the labelled "FTD" experiment), (3) at 6.135 u.t. (the final integration time) and (4) a blank line which divides the orbits.

Once again, we are doing two parallel integrations for each of both experiments, one with the LP-VIcode using a pre–SMART flavour (the initial conditions are those computed by the pre–SMART flavour in the first experiment after 9.6 u.t., i.e. the final integration time for the relaxing stage) and the other using its SMART counterpart (in this case, the initial conditions are those computed by the SMART flavour in the first experiment after 9.6 u.t.). The potinit subroutine section reads as follows for both PTD and FTD experiments:

```
**********************************************************************
* NUCLEAR REGION
**********************************************************************

* ADD-REM Parameter
* [SOURCE: Marinacci et al. 2014 (MNRAS, 437, 1750)]
* [COMMENT: M_nuclear = 2x10^8 M_sun]

      gmsmbh=8.60234d2
*       gmsmbh=0.d0

* [SOURCE: Launhardt et al. 2002 (A&A, 384, 112)]
      epsmbh=0.03d0


**********************************************************************
* PEANUT-SHAPED BULGE
**********************************************************************
```

```
* Bulge spheroid
* ADD-REM Parameter
* [SOURCE: Marinacci et al. 2014 (MNRAS, 437, 1750)]
* [COMMENT: M_bulge = 4.74x10^9 M_sun]
      gmbulge=2.03875458d4
*      gmbulge=0.d0

      epsbulge=0.835d0


* Bar
* ADD-REM Parameter
* [SOURCE: Monari et al. 2016 (MNRAS, 461, 3835)]
      alpha=0.01d0
*      alpha=0.d0

      barcoef=8.331938927d6
      rbar=3.5d0
      phibar=5.65d0
* [COMMENT: bomegabar = -52.2 km s-1 kpc-1]
      bomegabar=-52.2d0


*************************************************************************
* SPIRAL ARMS
*************************************************************************

* ADD-REM Parameter
* [COMMENT: Super strong spirals 200 per cent density contrast]
      armscoef=2279.d0
*      armscoef=0.d0

* [SOURCE: Monari et al. 2016 (MNRAS, 461, 3835)]
      narms=2
      nindex=1
      p=0.17d0
      rarms=1.d0
      rscarms=3.124d0
      phiarms=3.31d0
* [COMMENT: bomegaarms = -18.9 km s-1 kpc-1]
      bomegarms=-18.9d0
* [COMMENT: scale height  of the thin disc]
      hs=0.3d0
* [COMMENT: Exclusion coefficient for inner spiral arms]
* [COMMENT: corrotation radius]
      excoefarms=4.08d0


*************************************************************************
```

```
* DISK
*********************************************************************

* (1) MN PROFILE
* ADD-REM Parameters
* [SOURCE: Marinacci et al. 2014 (MNRAS, 437, 1750), Model Aq-C-4/5]
* [COMMENT: M_disk = 5.961x10^10 M_sun]
* [COMMENT: e_s = 3.124 kpc]
* [COMMENT: e_h = 0.3 kpc]
*      gmdiskmn=25.63927437d4
      gmdiskmn=0.d0

      epscalemn=3.124d0
      epsheightmn=0.3d0

* (2) EXPONENTIAL PROFILE
* Thin disk
* ADD-REM Parameters
* [SOURCE: Binney J., Tremaine S., 2008, Galactic Dynamics: 2nd Ed.]
* [SOURCE: Monari et al. 2016 (MNRAS, 461, 3835)]
* [SOURCE: Smith et al. 2015 (MNRAS, 448, 2934)]
* [COMMENT: M^thin_disk = 5.276x10^10 M_sun (88.5% MN PROFILE)]
* [COMMENT: R^thin_d = 3.124 Gyr]
* [COMMENT: h^thin_z = 0.3 kpc]
      gmdisk(1)=3.65402813d4
      gmdisk(2)=-1.308919778d6
      gmdisk(3)=1.525374597d6
*      gmdisk(1)=0.d0
*      gmdisk(2)=0.d0
*      gmdisk(3)=0.d0

      epscale(1)=1.751620652d0
      epsheight(1)=0.357969749d0

      epscale(2)=8.045207335d0
      epsheight(2)=0.357969749d0

      epscale(3)=7.007698163d0
      epsheight(3)=0.357969749d0

* Thick disk
* ADD-REM Parameters
* [SOURCE: Binney J., Tremaine S., 2008, Galactic Dynamics: 2nd Ed.]
* [SOURCE: Monari et al. 2016 (MNRAS, 461, 3835)]
* [SOURCE: Smith et al. 2015 (MNRAS, 448, 2934)]
* [COMMENT: M^thick_disk = 0.686x10^10 M_sun (11.5% MN PROFILE)]
* [COMMENT: R^thick_d = 3.124 Gyr]
```

```
* [COMMENT: h^thick_z = 1 kpc]
      gmdiskthk(1)=3.9689420d3
      gmdiskthk(2)=-1.687186076d5
      gmdiskthk(3)=1.986529253d5
*      gmdiskthk(1)=0.d0
*      gmdiskthk(2)=0.d0
*      gmdiskthk(3)=0.d0

      epscalethk(1)=0.908485192d0
      epsheightthk(1)=1.41014739d0

      epscalethk(2)=7.026555501d0
      epsheightthk(2)=1.41014739d0

      epscalethk(3)=6.213630283d0
      epsheightthk(3)=1.41014739d0


***********************************************************************
* DARK MATTER HALO
***********************************************************************

* (1) BI-TRIAXIAL EXTENSION NFW MODEL
* ADD-REM Parameter
* [SOURCE: Marinacci et al. 2014 (MNRAS, 437, 1750), Model Aq-C-4/5]
* [COMMENT: M_200 = 145.64x10^10 M_sun]
* [COMMENT: c_nfw = 16.0287081]
      acoef=3308059.4167264947d0
*      acoef=0.d0

      rs=14.63d0

      scoefi(1)=1.02d0
      scoefi(2)=1.02d0
      scoefi(3)=0.958749185d0
      scoefe(1)=1.d0
      scoefe(2)=1.d0
      scoefe(3)=1.d0

* (2) MODIFIED LOGARITHMIC MODEL
* ADD-REM Parameter
* [COMMENT: v_halo = 166.258 km/s]
*      vhalo=166.258d0
      vhalo=0.d0

* [SOURCE: Vera-Ciro & Helmi 2013 (ApJL, 773:L4)]
      d=12.d0
      ra=30.d0
```

```
          qcoef(1)=1.d0
          qcoef(2)=1.d0
          qcoef(3)=0.9d0
          qqcoef(1)=1.38d0
          qqcoef(2)=1.d0
          qqcoef(3)=1.36d0
          ascoef(1)=0.121869343d0
          ascoef(2)=-0.992546152d0
          wcoef(1)=0.992946717d0
          wcoef(2)=0.532153052d0
          wcoef(3)=0.114888764d0
```

Notice in this case (compare with the setting for the first experiment, Section D.3.1), the non–zero values for the `ADD-REM` parameters associated with the bar and the spiral arms (`alpha` and `armscoef`, respectively) in order to have the TD model.

The bar and spiral arms growth section for the PTD experiment is:

```
*************************************************************************
* GROWTH FACTOR
* BAR AND SPIRAL ARMS
*************************************************************************

* ADD-REM Parameter
* [SOURCE: Monari et al. 2016 (MNRAS, 461, 3835)]
*       atime=3.068d0
        atime=0.d0
```

while for the FTD experiment, the growth factor must be non–zero and equal to the time when the time dependent components reach they final amplitudes (3.068 u.t. for the present set of simulations):

```
*************************************************************************
* GROWTH FACTOR
* BAR AND SPIRAL ARMS
*************************************************************************

* ADD-REM Parameter
* [SOURCE: Monari et al. 2016 (MNRAS, 461, 3835)]
        atime=3.068d0
*        atime=0.d0
```

Using the pre–SMART version

First, we check all the initial conditions that did not finish the integration.

PTD model. Initial conditions (0 u.t., initial time): 1163955. By ~ 3.068 u.t.: 1163933 and by the final integration time, 6.135 u.t.: 1163907, which means that 48 initial conditions have
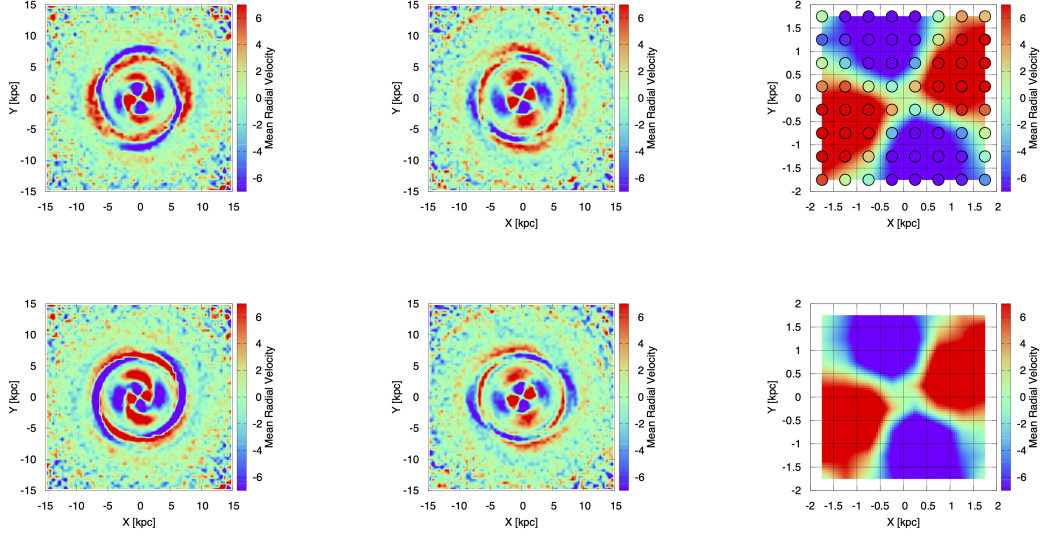
Figure D.9: Mean radial velocity maps. Left panels: full maps at ~ 3.068 u.t. Middle panels: full maps at 6.135 u.t. Right panels: zoom–in region at 6.135 u.t. (details in the text). Top panels show the mean radial velocity maps for the PTD experiment. Bottom panels show the same maps as before but for the FTD experiment.

not finished.

FTD model. Initial conditions (0 u.t., initial time): 1163955. By ~ 3.068 u.t.: 1163940 and by the final integration time, 6.135 u.t.: 1163904, which means that 51 initial conditions have not finished.

In Fig. D.9 we show the distribution on the plane of the mean radial velocity of thin disk particles using the pre–SMART `milkywayhydra.pav`. Full maps are presented on the left and middle panels (at ~ 3.068 and 6.135 u.t., respectively) while a selected zoom–in region (at 6.135 u.t.) is presented on the right panels. The zoom–in region on the top, shows also the procedure of making these plots: each circle represent the mean radial velocity inside the square cell of 0.5 kpc of side where it is calculated, and the background is then filled with an interpolation scheme by the plotting program, `gnuplot`. Top panels show the mean radial velocity maps for the PTD experiment, i.e. when the bar and the spiral arms are at full strength from the beginning to the end of the simulation. Bottom panels show the same maps as before but when the bar and the spiral arms grow slowly until they reach full strength at 3.068 u.t., which amplitudes are kept until the end of the simulation (FTD experiment). Notice that the color scale highlights differences up to 1 km/s.

Using the SMART version

We compute the accelerations with the SMART code. No variational equations are computed because we only need to integrate the equations of motion.
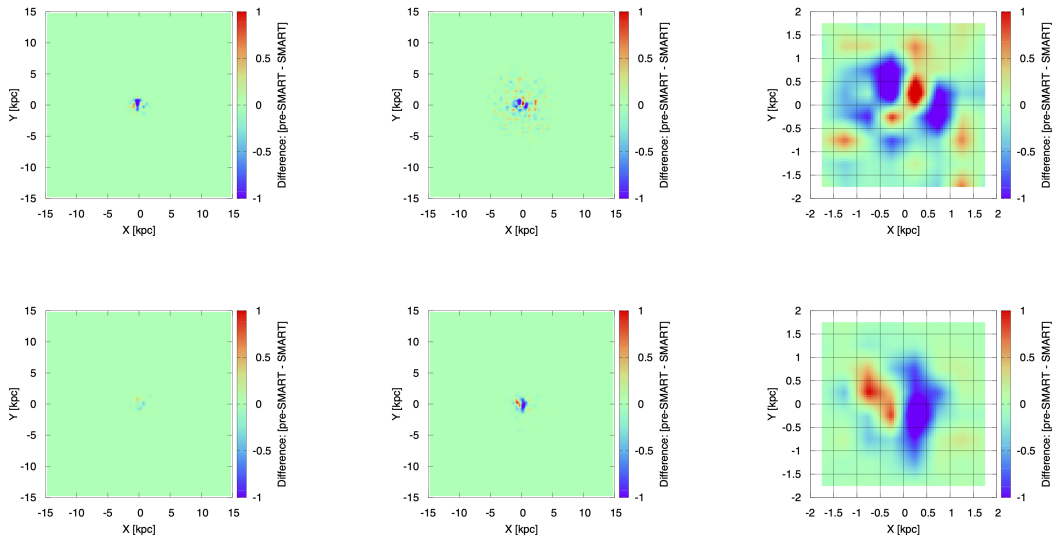
Figure D.10: Differences in mean radial velocity maps. Left panels: full maps at 3.068 u.t. Middle panels: full maps at 6.135 u.t. Right panels: zoom–in region at 6.135 u.t. Top panels show the differences in mean radial velocity maps for the PTD model experiment. Bottom panels show the same difference maps as before but for the FTD model experiment.

First we check all the initial conditions that did not finish the integration.

PTD model. Initial conditions (0 u.t., initial time): 1163955. By ~ 3.068 u.t.: 1163934 and by the final integration time, 6.135 u.t.: 1163896, which means that 59 initial conditions have not finished.

FTD model. Initial conditions (0 u.t., initial time): 1163955. By ~ 3.068 u.t.: 1163947 and by the final integration time, 6.135 u.t.: 1163907, which means that 48 initial conditions have not finished.

Fig. D.9 is recreated here but using automatic differentiation to build the `pav` file. Then, in Fig D.10 we show the differences between the mean radial velocity maps using the pre–SMART (Fig. D.9) and SMART flavours of the `milkywayhydra.pav` file. Notice that in this case, we need to use a color scale that highlights differences up to a fraction of a km/s to reveal the distribution of the discrepancies, otherwise they are all wash out.

Once again, the small difference between both sets of maps supports the initial hypothesis of a clear agreement between both versions.

Finally, we repeat the computation with the pre–SMART version but on the samples previously computed with the SMART version. That is, now the initial conditions are *exactly* the same. On the second experiment, the initial conditions were slightly different due to the fact that the files by 9.6 u.t. on the first experiment (i.e. the initial conditions on the current

second experiment) were not exactly the same after the computation using both flavours of the `milkywayhydra.pav` (there were differences below the 5/6th decimal, as much).

`SMART` **PTD model: checking with pre–`SMART`**. Initial conditions (0 u.t.): 1163955. By 3.068 u.t.: 1163936 and by the final integration time, 6.135 u.t.: 1163895, which means that 60 initial conditions have not finished.

`SMART` **FTD model: checking with pre–`SMART`**. Initial conditions (0 u.t.): 1163955. By 3.068 u.t.: 1163945 and by the final integration time, 6.135 u.t.: 1163912, which means that 43 initial conditions have not finished.

Now, as mentioned before, the initial conditions are chosen to be exactly the same and the results do improve in case of the FTD model, but not on the PTD model: in Fig. D.11 we recreate Fig. D.10. Although there are still signs of discrepancies for the FTD model (bottom panels, specially bottom right panel), they are less evident than in Fig. D.10 (compare the bottom panels) which means that the small differences seen in bottom panels of Fig. D.10 are mainly a consequence of the effect of the slightly differences in the initial conditions rather than on a mismatch between both flavours. On the other hand, we see the same level of discrepancies in the PTD model, see top panels of Figs. D.10 and D.11, which means that there is still a chance of a potential disagreement between flavours, but very small indeed (notice the color scale) which make it for most situations, irrelevant. Nevertheless, see next section for more probable reasons for the missmatch.

RESULT 2: this second experiment on a statistical sample of orbits shows that both flavours of the `milkywayhydra.pav` are compatible when `SMART` is also used to compute automatically the accelerations in a full time dependent model.

D.3.3 Third experiment: computation of the first variational equations

In order to test the computation of the CIs over volumes that should share, statistically, similar dynamics, we select the initial conditions within the same region of the FTD model where most of the discrepancies between flavours appeared (bottom right panel of Fig. D.10). Then, the region is $[-2\,\mathrm{kpc}, 2\,\mathrm{kpc}]$ on the plane and has 180336 initial conditions for both pre–`SMART` and `SMART` flavours of the `milkywayhydra.pav` file. The initial conditions are those obtained in the first experiment, after 9.6 u.t. of evolution computed with each flavour (Section D.3.1) and thus, there are slightly differences between initial conditions for each flavour.

We set up the configuration and parameter files for the `LP-VIcode`, particularly the `LP-VIcode.in` reads:

```
# LP-VIcode version 2.0.2
# Initial conditions file (max. 50 characters)
hydra3.in
# Prefix for output files (max. 50 characters)
hydra3
# Step of integration
0.004908d0
```
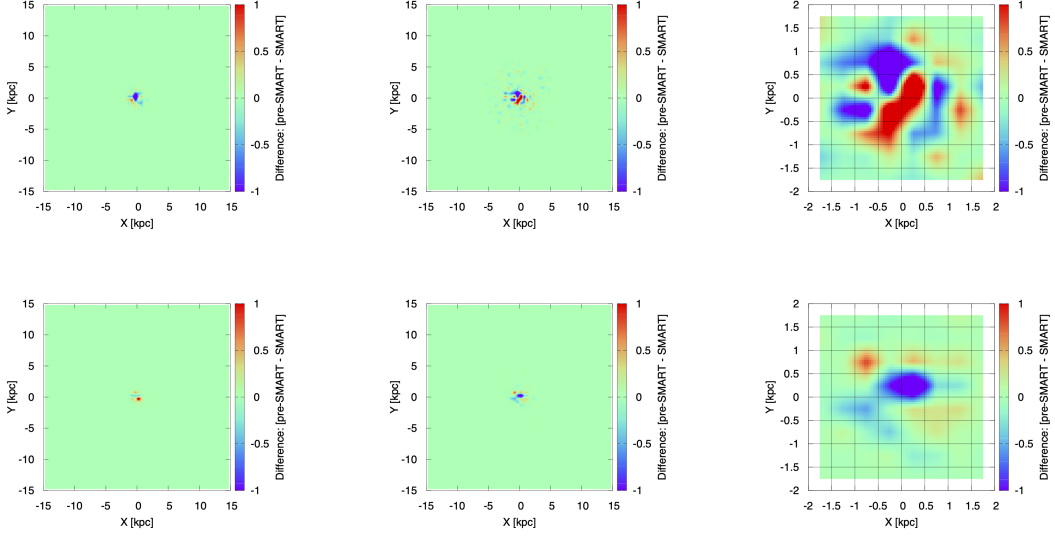
Figure D.11: Differences in mean radial velocity maps using exactly the same initial conditions. Left panels: full maps at 3.068 u.t. Middle panels: full maps at 6.135 u.t. Right panels: zoom–in region at 6.135 u.t. (details in the text). Top panels show the differences in mean radial velocity maps for the PTD model experiment. Bottom panels show the same difference maps as before but for the FTD model experiment.

```
# Initial time; final time of integration
0.d0 6.135d0
# Screen (0=no, 1=yes) & orbit (0=no output, 1=output, 2=output additionals)
1 0
# Indicators: 0=don't compute, 1=output for all t, 2=output only last value
# LIs, SALI, GALIs, SD & SSNs, RLI & LImax, MEGNO & SElLCE, FLI & OFLI
0 0 0 0 0 2 2
# Nr. of steps between outputs (when orbit or indicators are = 1)
625
# Initial dev. vectors (0 = at random, 1 = random orthonormal, 2=fixed)
1
# SALI & potential(t): normal saturation (=0) or restart dev. vectors (=1)
0
```

Then, only the MEGNO & SElLCE and FLI & OFLI are activated in order to limit the computing time (see Section D.4). All the quantities provided by the LP-VIcode were tested in Section D.2. Now, we are interested in comparing both flavours over the computation of the first variational equations, so we proceed with only a small subset of the CIs provided by the main code.
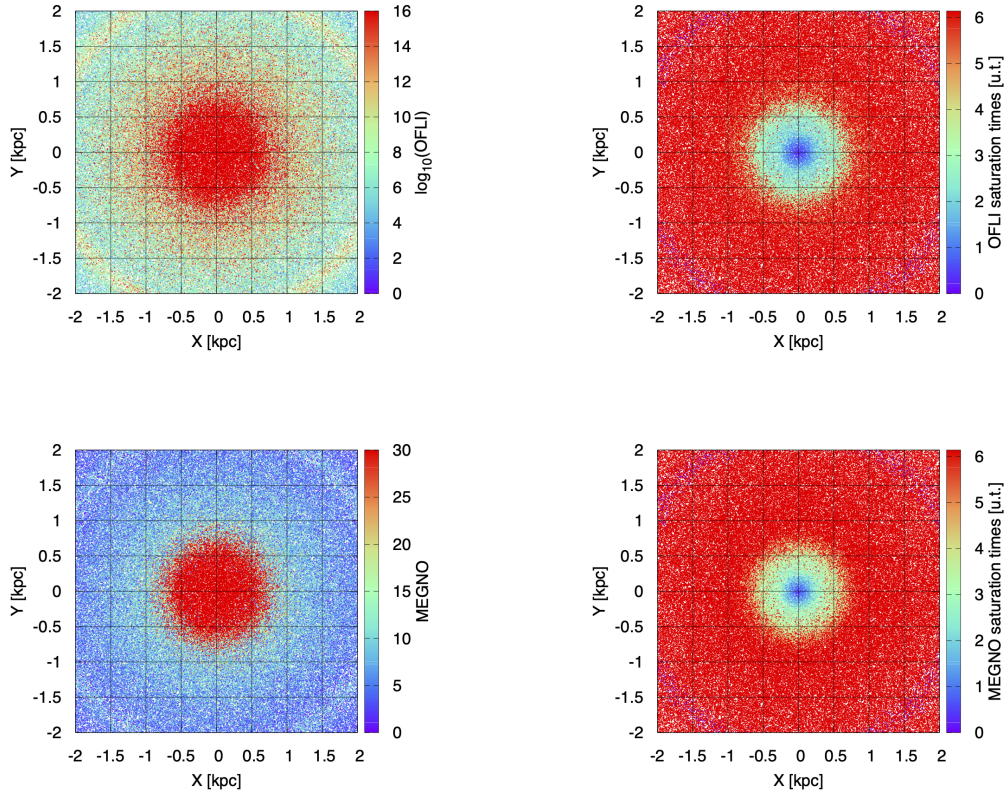
Figure D.12: CIs maps computed with the pre-SMART flavour: OFLI and OFLI saturation times (top left and right panels, respectively). MEGNO and MEGNO saturation times (bottom left and right panels, respectively).

Using the pre–SMART version

In Fig D.12 we show maps according to the final values of a small set of CIs (OFLI and MEGNO and their saturation times[4]) from the LP-VIcode's library, and for the volume under study.

Using the SMART version

We compute the accelerations and first variational equations with SMART.

In Fig D.13 we show maps according to the final values of a small set of CIs (OFLI and MEGNO and their saturation times) from the LP-VIcode's library, and for the volume under study.

---

[4]The saturation time is defined as the time the associated chaos indicator reaches its saturation value (saturates and it is stopped). In case of the OFLI the saturation value is 10^{16} and in case of the MEGNO, that value is 30. The saturation time is a complementary quantity defined to recover structure beyond saturation due to strong chaotic behaviour (further references in [16]).
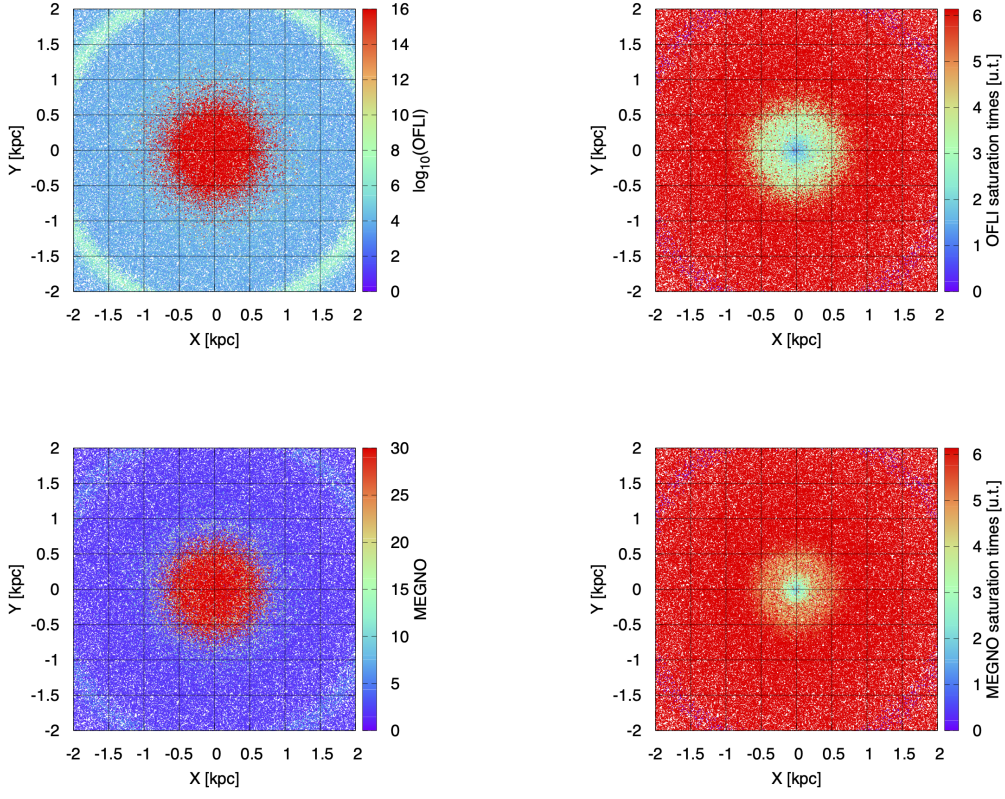
Figure D.13: CIs maps computed with the `SMART` flavour: OFLI and OFLI saturation times (top left and right panels, respectively). MEGNO and MEGNO saturation times (bottom left and right panels, respectively).

Despite the fact that the indicators are computed on slightly different initial conditions because the latter are the result of a 9.6 u.t. integration interval using different programs, the final maps for both flavours (Fig. D.12 and Fig. D.13 for the pre–`SMART` and `SMART` flavours, respectively) preserve the same characteristics as expected.

Notice also that the central region is the most chaotic one, thus supporting the idea that the small discrepancies seen in the central part of the bottom right panel of Fig. D.10 (Section D.3.2) might be caused by the chaotic nature exhibit inside such region, rather than some numerical missmatch between flavours.

RESULT 3: this third experiment on a statistical sample of orbits shows that both flavours of the `milkywayhydra.pav` are compatible when `SMART` is used to compute automatically not only the accelerations (first and second experiments) but also the first variational equations (third experiment) in a full time dependent model.

D.4   Computing times

We use an Intel(R) Core(TM) i7–4790K CPU (4 cores, 8 threads) @ 4.00GHz with 8 GB RAM[5], Windows 7 Ultimate Service Pack 1, 64 bits, running a virtual machine Oracle VM VirtualBox using Ubuntu 18.04 64 bits wth 4 GB RAM. The computing times are an average among the four threads running simultaneously, if not stated otherwise. "With optimization" means `O3` flag on.

D.4.1   Experiment on individual orbits: with and without optimization

In the following experiment the computing times are not an average, but the time used by one single core to do the calculations.

TI model

500 initial conditions **with optimization**. pre–`SMART` flavour: 6 min 27.711 s. `SMART` flavour: 9 min 26.413 s.

500 initial conditions **without optimization**. pre–`SMART` flavour: 15 min 37.402 s. `SMART` flavour: 54 min 55.131 s.

Then, the optimized pre–`SMART` flavour needs 68.45% the time of its counterpart `SMART` flavour on this experiment on individual orbits (TI model, equations of motion, variational equations and all `LP-VIcode` quantities activated), while the non–optimized pre–`SMART` flavour needs 28.45% the time of its counterpart `SMART` flavour on the same experiment.

PTD model

500 initial conditions **with optimization**. pre–`SMART` flavour: 9 min 5.009 s (302, 88%). `SMART` flavour: 14 min 12.281 s.

500 initial conditions **without optimization**. pre–`SMART` flavour: 21 min 56.270 s (302, 88%). `SMART` flavour: 76 min 45.029 s.

FTD model

500 initial conditions **with optimization**. pre–`SMART` flavour: 8 min 55.107 s (420, 41%). `SMART` flavour: 14 min 10.894 s (128, 85%; 225, 67%).

500 initial conditions **without optimization**. pre–`SMART` flavour: 21 min 24.395 s (245, 32%; 420, 41%). `SMART` flavour: 77 min 26.369 s (225, 67%; 245, 67%).

Then, the optimized pre–`SMART` flavour needs 62.89% the time of its counterpart `SMART` flavour on this experiment on individual orbits (FTD model, equations of motion, variational equations and all `LP-VIcode` quantities activated), while the non–optimized pre–`SMART` flavour

---

[5]Further   details   at   https://ark.intel.com/content/www/us/en/ark/products/80807/intel-core-i7-4790k-processor-8m-cache-up-to-4-40-ghz.html.

needs 27.64% the time of its counterpart `SMART` flavour on the same experiment.

The compilation with the optimization flag activated takes just a few seconds more than the non–optimized compilation. Therefore, there is no justification to drop it, and there is no further need to continue the comparison using non–optimized flavours. In the next section and due to the large sample of initial conditions that must be processed, we are going to use optimized flavours alone.

D.4.2 Experiments on a statistical sample of orbits: with optimization

D.4.2.1 First experiment

pre–`SMART` flavour: [average time] 573 min 35.113 s. 1163956 initial conditions from `MAGI`: 1 error (run4, id 108490, 0%) during the first 9.6 u.t. → 1163955 valid initial conditions for the rest of the experiments.

`SMART` flavour: [average time] 616 min 59.741 s. 1163956 initial conditions from `MAGI`: 1 error (run4, id 108490, 0%) during the first 9.6 u.t. → 1163955 valid initial conditions for the rest of the experiments.

Then, the optimized pre–`SMART` flavour needs 92.96% the time of its counterpart `SMART` flavour on this first experiment (TI model and only equations of motion) on a big sample of initial conditions (1163956).

D.4.2.2 Second experiment

pre–`SMART` flavour. PTD model: [average time] 513 min 40.954 s. 1163955 initial conditions from `LP-VIcode`: 13, 14, 16 and 5 errors (run 1, run 2, run 3 and run 4, respectively) during the 6.135 u.t. → 1163907 valid initial conditions.

pre–`SMART` flavour. FTD model: [average time] 487 min 44.172 s. 1163955 initial conditions from `LP-VIcode`: 17, 14, 11 and 9 errors (run 1, run 2, run 3 and run 4, respectively) during the 6.135 u.t. → 1163904 valid initial conditions.

`SMART` **flavour.** PTD model: [average time] 567 min 25.765 s. 1163955 initial conditions from `LP-VIcode`: 15, 14, 15 and 15 errors (run 1, run 2, run 3 and run 4, respectively) during the 6.135 u.t. → 1163896 valid initial conditions.

`SMART` **flavour.** FTD model: [average time] 552 min 5.518 s. 1163955 initial conditions from `LP-VIcode`: 10, 14, 11 and 13 errors (run 1, run 2, run 3 and run 4, respectively) during the 6.135 u.t. → 1163907 valid initial conditions.

Then, the optimized pre–`SMART` flavour needs ∼ 90%, and ∼ 88% the time of its counterpart `SMART` flavour for the PTD and FTD models, respectively, on this second experiment (TD model and only equations of motion) on a big sample of initial conditions (1163955).

D.4.2.3   Third experiment

Only the MEGNO & SElLCE and FLI & OFLI were computed.

pre–`SMART` flavour. FTD model: [average time] 718 min 44.940 s. 180336 initial conditions from `LP-VIcode`: 457, 447, 438 and 430 errors (run 1, run 2, run 3 and run 4, respectively) during the 6.135 u.t. → 178564 valid initial conditions.

`SMART` flavour. FTD model: [average time] 885 min 21.579 s. 180336 initial conditions from `LP-VIcode`: 405, 458, 416 and 428 errors (run 1, run 2, run 3 and run 4, respectively) during the 6.135 u.t. → 178629 valid initial conditions.

Then, the optimized pre–`SMART` flavour needs $\sim 81\%$ the time of its counterpart `SMART` flavour on this third experiment (TD model, equations of motion and variational equations with MEGNO & SElLCE and FLI & OFLI flags activated) on a big sample of initial conditions (180336).

D.5   Conclusions

FINAL RESULT: the set of experiments presented in the previous sections supports the initial hypothesis that both flavours of the tested `milkywayhydra.pav` are clearly compatible, which means that:

1. the original or pre–`SMART` flavour of the `milkywayhydra.pav` is, indeed, working as expected and it can be used with confidence;

2. the automatic differentiation pre-processing slave program `SMART` is also working as expected and it can be also used with confidence.

Finally, the original flavour of the `milkywayhydra.pav` file speeds up the computation with regards to the automatic flavour, due to its more efficient coding. However, such difference in speed is only large when the computation of variational equations is involved: between $\sim 20\%$ and $\sim 40\%$ time reduction (with optimization on full time dependent models), depending on the number of chaos indicators computed. **Therefore, when chaos indicators need to be computed on big samples of initial conditions, the original "handcrafted' version of the `milkywayhydra.pav` is worth using it over the automatic differentiation flavour provided by `SMART`. In all other cases, `SMART` seems to be the right choice due to the almost none effort from the user to set things up.**